Project no.: 101022587

Project full title: Sustainable energy system for achieving novel carbon neutral energy communities

Project Acronym: SUSTENANCE

Deliverable number:	**D2.4**
Deliverable title:	**Report on Developed Models and Control Schemes for Smart Integration of Energy Carriers**
Work package:	**WP2**
Due date of deliverable:	**M26**
Actual submission date:	**M27 - 28/09/2023**
Start date of project:	**01/07/2021**
Duration:	**42 months**
Reviewer(s):	**Birgitte Bak Jensen (AAU), Richard van Leeuwen (SAX)**
Author/editor:	**Zakir Rather, Soudipan Maity (IITB)**
Contributing partners:	**Indian Institute of Technology Bombay (IITB), Motilal Nehru National Institute of Technology (MNNIT), Aalborg University (AAU), University of Twenty (UT)**
Dissemination level of this deliverable	**PU**
Nature of deliverable	R

This project has received funding from the European Union's Horizon 2020 research and innovation programme under grant agreement No 101022587, and the Department of Science and Technology (DST), Government of India under the SUSTENANCE project. Any results of this project reflect only this consortium's view and the funding agencies and the European Commission are not responsible for any use that may be made of the information it contains.

Document history

Version no.	Date	Authors	Changes
0.1	20.06.23	Gerwin Hoogsteen	General chapter outline.
0.2	02.08.23	Gerwin Hoogsteen	Draft for UT inputs.
0.3	21.08.23	Zakir Rather	1st full draft.
0.4	28.08.23	Birgitte Bak Jensen	Reviewed with comments.
0.5	21.09.23	Richard van Leeuwen	Additional review and further comments.
0.6	27.09.23	Zakir Rather	Revised version based on reviews comments.
1.0	28.09.23	Zakir Rather	Final version completed.

Contributors

Partner no.	Partner short name	Name of the Contributor	E-mail
1	AAU	Rakesh Sinha	rsi@energy.aau.dk
	UT	Aditya Pappu	a.pappu@utwente.nl
		Bahman Ahmadi	b.ahmadi@utwente.nl
		Gerwin Hoogsteen	g.hoogsteen@utwente.nl
-	IITB	Zakir Rather	zakir.rather@iitb.ac.in
		Soudipan Maity	soudipan.maity@iitb.ac.in
		Pijush Kanti Dhara	pijush92.dhara@iitb.ac.in
		Angshu Nath	194170008@iitb.ac.in
		Payal Dahiwale	194170009@iitb.ac.in
		Manorath Prasad	manorath.prasad@iitb.ac.in
-	MNNIT	Manohar Yadav	ssmyadav@mnnit.ac.in
		Nyenshu Seb Rengma	nyneshu@gmail.com

Contents

Executive Summary

This report covers modelling and analysis aspects of different energy carriers in sector coupled carbon neutral energy system. The main focus areas of this report include electrification of transportation system (EVs), distributed control of DERs and flexibility from such resources, solar PV powered water pumping system for domestic applications in remote rural areas, grid support from RE sources and distribution-transmission system coordination.

The report addresses the challenge posed by the growing penetration of RE resources, which displaces synchronous generators and leads to diminished grid inertia. This reduction in grid inertia can result in a high rate-of-change-of-frequency and deteriorating frequency nadir, potentially breaching limits for less severe contingencies. To address this, the report presents a disturbance-based approach for estimating system inertia that improves upon earlier approaches by considering the size, location, and timing of frequency disturbances in a power system and takes into account the inertia contribution of RE generators.

The other focus point of this report is on flexibility support that distribution system operators can potentially utilize to manage the grid better, for example for congestion management. A transactive approach consisting of flexibility frameworks that quantify flexibility into a quantity that can be traded has been discussed followed by describing an optimization approach that rely on using demand side management (DSM) techniques to optimize the order of activation of devices. Furthermore, the application of transactive and optimization approaches for congestion management frameworks has been discussed in this report. A new concept of Energy Modii is then described followed by its evaluation with a simulation of the Dutch demonstrator site.

Uncontrolled charging of electric vehicles (EVs) can give rise to a range of technical issues within distribution networks. These issues encompass voltage instability, phase imbalance, heightened peak loads, overloading, power loss, and power quality problems. Distribution grids, characterized by high resistance-to-inductance ratios, are particularly susceptible to voltage sags when subjected to substantial power consumption, which can lead to deviations of voltages from nominal levels. The proliferation of EV usage exacerbates this vulnerability due to the significant power demand associated with EV charging. Furthermore, EV charging often coincides with evening peak demand, further intensifying the challenges related to voltage stability.

To address these challenges stemming from uncontrolled charging, one potential solution is the integration of EVs through smart charging control for EVs that is responsive to both the demand from EVs and the network conditions. This approach ensures that the charging load does not compromise network stability, including voltage and thermal loading. Smart charging strategies take into account temporal and spatial characteristics of EV loads, travel patterns, and charging behaviors when determining the charging schedule. In this context, a centralized charging strategy has been developed to address multiple challenges associated with uncontrolled EV charging. This strategy aims to minimize charging costs for EV users, level the load on the grid, and reduce peak-to-average ratios for system operators. Additionally, maintaining an adequate reserve of reactive power is essential for voltage stability of the network. Traditionally, network operators invest significantly in devices such as capacitor banks and synchronous condensers to provide reactive power compensation. However, DC EV chargers offer an alternative solution. These chargers can operate in all four quadrants, making them capable of providing reactive

support to the network. The versatility of four-quadrant operation allows DC chargers to contribute to reactive power compensation regardless of whether they are actively charging EVs.

Further, the report explores a novel practical approach for creating a reduced real-time steady-state model of active distribution networks (ADNs) using synchrophasor measurements. Such models prove advantageous for conducting co-simulations involving the bulk power system and multiple ADNs, particularly for grid support applications. Additionally, the report delves into sector coupling of different energy domains, an innovative concept gaining global recognition, which involves linking various sectors to enhance the utilization of RE. The primary goal of sector coupling is to facilitate the integration of RE sources and electrify various end-use domains.

This report also delves into the strategic deployment of solar photovoltaic water pumping systems (SPVWPS) to ensure reliable and cost-effective access to clean water for disadvantaged communities. By developing an optimal methodology that considers factors such as water consumption patterns, solar availability, system efficiency, and community needs, the study aims to provide a standardized approach for SPVWPS deployment. A user-friendly software tool has been designed to guide users in sizing the system efficiently while emphasizing cost-effectiveness. This tool's effectiveness has been rigorously tested through a case study in economically disadvantaged remote areas with complex terrains. The results align with real-world data, offering valuable insights into system design and deployment. This endeavour contributes to existing knowledge and provides practical insights, serving as a comprehensive guide applicable on a global scale. Through a scientific and methodical approach, it seeks to address water access challenges and promote sustainable solutions for the benefit of communities worldwide.

1. Optimal operation of multi-carrier energy systems and provision of grid support services from local integrated energy systems

1.1. Optimal operation of sector-coupled multi-energy system

The impact of relying on conventional energy sources to meet our energy requirements is evident, seen through resource depletion and the emergence of global warming. To lessen our reliance on fossil fuels, RE sources emerge as a favorable option, promoting both reduced dependence and environmentally friendly power. These sustainable sources hold the promise of satisfying our growing electricity demands with minimal drawbacks. The enthusiastic reception of RE has spurred increased research and development efforts aimed at mitigating their inherent limitations. This aligns with the push to incorporate RE systems, marking a significant stride in this direction. As RE sources become more integrated, there is an opportunity to combine diverse energy sources to curtail emissions and achieve decarbonization. In this scenario, the sector coupled energy systems are adopted by the system operators. Sector coupling, a novel concept pioneered in Europe and progressively gaining global recognition, involves linking various sectors to enhance the utilization of RE. Its primary objective is to amplify the integration of RE sources and electrify end-use domains. By electrifying sectors such as heating, transportation, and culinary practices, mechanisms for stabilizing the power sector become imperative.

The European Commission has extended the scope of sector coupling beyond its initial definition. It views sector coupling to achieve cost-effective decarbonization by introducing adaptability into the energy system. Essentially, sector coupling aligns with the integration of energy systems, as depicted in Figure 1.1. The broader interpretation encompasses the coordinated operation and planning of the energy system across different channels and geographical scales, with the aim of delivering reliable, affordable energy services while minimizing environmental repercussions [1]. Several factors promote energy system integration or sector coupling, ranging from climate effect mitigation and economics to social and regulatory considerations. Energy systems include several sectors: electricity, heat, gas, and transportation. These sectors are independent till now except for their coupling via combined heat and power (CHP) system. When integrating energy systems, some sectors may offer flexibility to other sectors, while other sectors will need flexibility when connecting with other sectors [2].

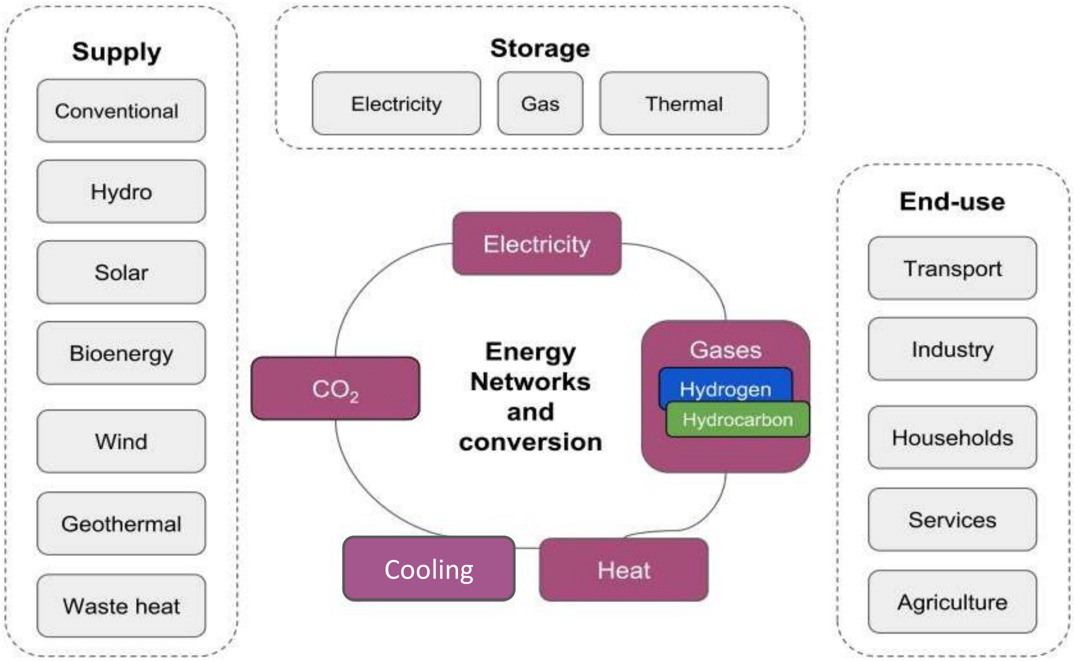

Figure 1.1: Sector coupling in energy system [3]

To support these sector synergies, it is critical to investigate and quantify mutual interactions, as well as seek examples of how these integrations might bring flexibility and other benefits. According to the perspective of the electrical sector, the interconnected systems must have

sufficient flexibility to support decarbonization targets, such as those set forth in the Paris Agreement, while maintaining operational reliability [4].

The current power system in India is centralized, relying on a utility grid to meet electricity demand. Population growth and development needs have led to challenges like higher electricity costs, increased global emissions from conventional power plants, and strain on the existing system. To tackle these issues, restructuring the centralized generation is necessary. Distributed energy sources (DERs) such as solar PV, wind, biogas generators, and batteries offer a solution by curbing carbon emissions and reducing generation costs. DERs, predominantly solar PV due to ample solar insolation, range from kW to MW capacity. Microgrids, functioning as small-scale electricity sectors, incorporate DERs, electrical loads, and control systems. They can operate in islanded or grid-connected modes based on grid availability. Advanced communication technologies enable bi-directional data flow between producers and consumers, allowing decisions to be informed by generator and load information [5].

The sector coupled energy systems can increase the flexibility and security of the energy system by providing frequency and voltage supports whenever required. Linking the end-use sectors also promotes the utilization of intermittent RE sources, contributing to the decarbonization of the energy sector.

1.1.1. Division of sector-coupled energy

Sector coupling can be classified into two types:

- *End-use sector coupling* - Energy demand electrification while enhancing the relationship between electricity supply and end-use.
- *Cross-vector coupling* - The integrated use of various energy infrastructures and vectors, particularly electricity, heat, and gas, either on the supply side, e.g., by converting (surplus) electricity to hydrogen, or on the demand side, for instance, by using waste heat from industrial processes or power generation for district heating

1.1.2. Opportunities and challenges in sector coupling of energy system

While sector-coupled energy systems offer several benefits, it's essential for the technology to reach a level of maturity suitable for widespread adoption. The present state of sector-coupled systems presents both opportunities and challenges for their implementation, as outlined below.

Opportunities –

1. One of the key tactics for decarbonizing the energy industry will be electrification.
2. End-use sector coupling - Increased deployment of intermittent RE sources.
3. Integration of electricity, gas, and heat across vectors - Flexibility and security of the energy system.
4. The combination of end-use sector coupling and cross-vector integration – Reduced transition cost to a low-carbon energy system

Challenges -

Techno economic barriers

1. Resource availability
2. Markets
3. Technology
4. Infrastructure

Policy and regulatory barriers

1. Integrated planning and operation
2. Climate and energy policy
3. Market design including grid tariffs.

1.1.3. Distributed energy resources

Various sources can be integrated into the coupled system, but DERs are accessible on a more compact scale, primarily relying on renewable forms. As a result, this contributes to the mitigation of carbon emissions. This document entails an elucidation of energy sources based on solar PV [6], wind [7], and biogas [8].

1.1.4. Modelling of loads

Within a power system, approximately 60% to 70% of the total power usage can be attributed to induction motor loads. The remaining fraction of power consumption is allocated to lighting loads, loads regulated by thermostats, the effects of transformer saturation, and shunt capacitors. To facilitate dynamic studies, the entirety of these loads has been represented in models that account for their respective voltage and frequency dependencies. The aggregated load of an area or system is generally modelled as a combination of constant impedance, constant current, and constant power loads (ZIP) in terms of their voltage dependency. ZIP modelling is effective and widely used in steady-state and dynamic studies. The formula for the ZIP model is shown in X and Y. The equations represent the active and reactive power demands by the modelled load:

$$P_L = P_0[a_0 + a_1\left(\frac{V}{V_0}\right) + a_2\left(\frac{V}{V_0}\right)^2 \quad (1.1)$$

$$Q_L = Q_0[b_0 + b_1\left(\frac{V}{V_0}\right) + b_2\left(\frac{V}{V_0}\right)^2 \quad (1.2)$$

Where the scalars a_0, a_1, a_2, and b_0, $b_1, and\ b_2$ are the specified coefficients of the ZIP loads. Different factors have been taken into account to find the ZIP values of different load components and the behaviour by ZIP load matched with the behaviour by actual load. Motor loads can be taken as a ZIP model, or its characteristics can be used for modelling the load.

1.1.5. Voltage and frequency controls by the coupled system

Coupled electrical sector or microgrids can operate in grid connected as well as islanded mode. The stable, safe, and economic operation depends on the design of control system.

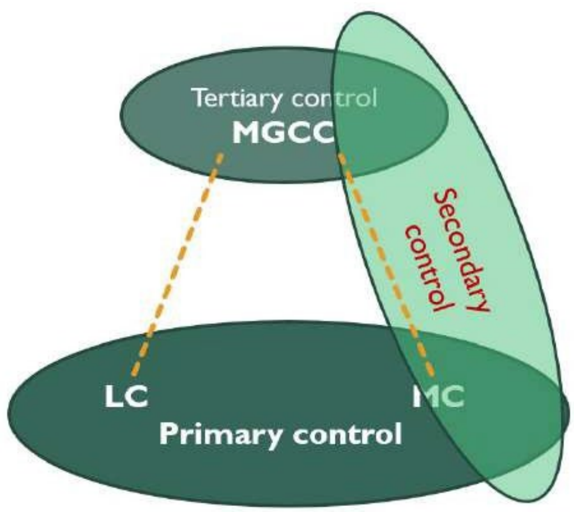

Figure 1.2: Different levels of control

In the case of islanded mode, the hierarchical approach is used to enhance the flexibility and controllability of the microgrid system. There are three levels of frequency and voltage control services in the microgrid as well as in power system: primary, secondary, and tertiary control. The relation between the levels of controls is depicted in Figure 1.2 where MGCC, LC, and MC stand for Microgrid Central Controller, Load controller and Microsource controller respectively.

Primary controls of the coupled system

Primary control, also known as local control, represents the initial tier in a hierarchical control system. It boasts the quickest response time and is employed to maintain stable voltage and frequency within the Microgrid by ensuring proper load distribution among the Distributed Generation (DG) units. It is classified into two methods of control, communication-based and without communication-based. The classification of the primary control categories for an islanded Microgrid is shown in Figure 1.3.

a. **Communication-based controls** - Communication-based primary control methods give an excellent voltage regulation. It has good transient response, accurate power sharing, high-power quality and circulating current elimination. In contrast to droop-based methods, the output voltage and frequency are close to their nominal values without using a secondary control. However, the method is limited due to higher cost and high bandwidth communication link. Complexity will also increase as the number of sources and loads increases. Some typical communication-based primary control methods are the centralized control, distributed control, Master-slave control, and Angle droop control.
b. **Without communication-based controls (Droop-based control):** This method provides the feature of plug and play, thus addition or removal, replacement of new, faulted units is straightforward.

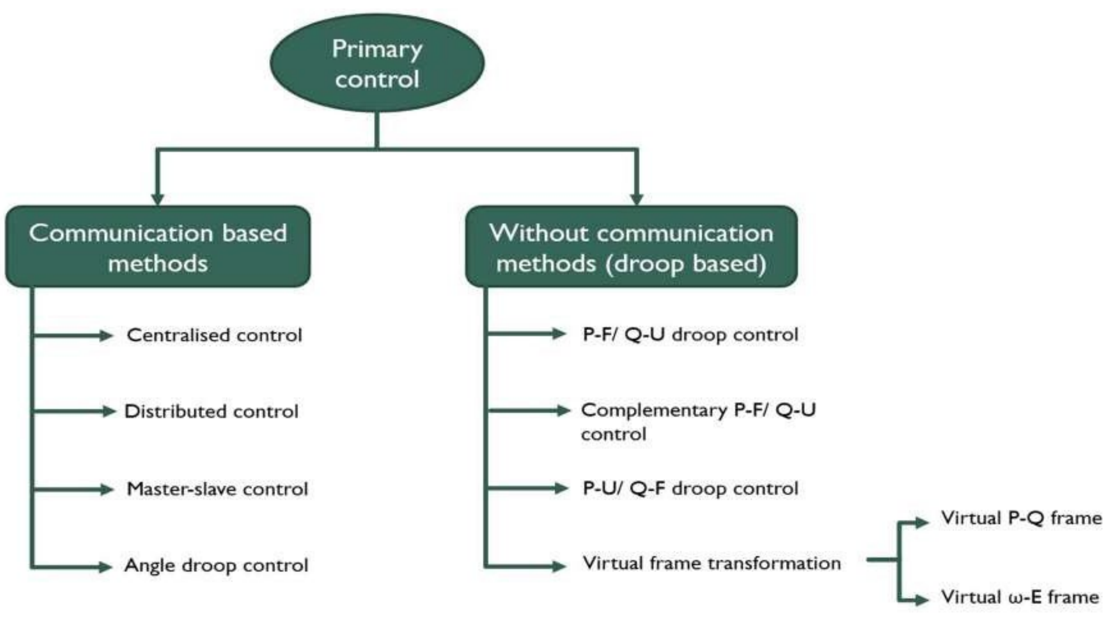

Figure 1.3: Primary level control in coupled system

Droop-based primary control

The described control techniques rely on the droop concept, enabling power sharing without the need for communication. This communication-free operation is essential for remote inverter connection. Additionally, the plug-and-play nature of modules allows faulted units to be swapped out seamlessly, ensuring uninterrupted system functioning. As a result, communication lines are typically omitted, particularly for longer distances to reduce investment costs. The subsequent subsections delve into the specifics of droop-based methods.

P-F/Q-U droop control

Considering high voltage lines, the value of X>>R and thus, R is ignored. Also, for small power angle, cos δ = 1 and sin δ = 0, where δ is the power angle. The approximations prove that the active power is controlled by power angle δ and reactive power is controlledby the voltage. Power angle is controlled by frequency control and thus the overall P/F- Q/U droop equation is given by:

$$\omega = \omega_{ref} - K_p P \quad (1.3)$$

$$U = U_{ref} - K_q Q \quad (1.4)$$

where, ω_{ref} and U_{ref} are the nominal frequency and voltage of the grid. In above equations, K_p, K_q are static droop gains. The conventional droop-based technique comes with certain limitations. These limitations include reliance on power line parameters, imprecise regulation of active and reactive power due to their interconnected nature, and the inability to distribute harmonics effectively among nonlinear loads. As a result, enhancements have been made to the conventional control approach. These enhancements encompass implementing filters to reduce power harmonics, introducing a derivative term to enhance the system's dynamic behavior, incorporating virtual impedance to mitigate the interaction between active and reactive power, and other modifications aimed at boosting responsiveness. In the context of medium or low voltage lines, the earlier approximation in the mentioned control strategy becomes invalid. Given that low voltage lines typically have a considerable R/X ratio of about 7.7, it becomes necessary to consider the new approximation where R significantly exceeds X. Moreover, a relationship between voltage difference and active power, as well as power angle and reactive power, becomes evident. This leads to the introduction of new equations for controlling active and reactive power, as illustrated by (1.5) and (1.6).

$$\omega = \omega_{ref} - K_q Q \quad (1.5)$$

$$U = U_{ref} - K_p P \quad (1.6)$$

Virtual frame transformation

Cross coupling of active and reactive power in medium voltage and low voltage lines is the biggest issue in control implementation. Thus, a virtual P-Q frame and virtual ω− frame is used. Every control has its own limitations and advantages, different hybrid controls (communication+ droop based) can be implemented for robust and flexible operation of microgrid system.

1.1.6. Optimization techniques

In sector coupled energy systems, in order to fulfill the projected energy demand, establishing a dispatch strategy is crucial, but this becomes challenging due to the unpredictable nature of RE sources such as solar and wind. Dealing with uncertainties in optimization complicates the task of satisfying constraints. The issue of resource allocation follows a hierarchical structure, progressing from unit commitment to economic dispatch and then optimal power flow. Numerous studies have concentrated on minimizing energy costs by treating it as a sole objective [9]. For instance, an approach employing mixed-integer linear programming (MILP) has been developed to optimize the energy cost from both the grid and natural gas sources while catering to loads [10]. To enhance accuracy and efficiency, the literature has turned to multi-objective optimization techniques. These techniques are more effective as they incorporate objectives such as emission reduction, resulting in a more comprehensive approach [11].

In [12], an investigation into optimizing the Levelized Cost of Energy (LCOE) is carried out to ascertain the optimal quantities of necessary batteries and solar PVs. Similarly, studies conducted in [11]–[13] also delve into LCOE-driven optimization aimed at minimizing energy-related expenses and devising plans. LCOE optimization is applied for strategic planning purposes, while optimization based on operational costs focuses on determining component sizes. For systems that have already been designed, optimization seeks to achieve daily optimal operational costs [10], [14]. The integration of battery energy storage systems adds intricacy to optimization due to the introduction of various constraints such as State of Charge (SOC) and maximum/minimum charging and discharging currents.

As the number of sources or the complexity of optimization increases, the computational time likewise escalates, demanding higher-power GPUs. To attain forecasted optimal dispatch within specific intervals, it becomes essential to simplify the optimization problem's complexity. Traditional optimization techniques like mixed integer linear programming (MILP), quadratic programming, and non-linear programming (NLP) necessitate significant computational resources. Moreover, these techniques have their own limitations. To overcome these challenges, heuristic optimization methods like Genetic Algorithm (GA) and Artificial Neural Network (ANN) are increasingly adopted in research efforts [15].

1.1.7. Demand response in coupled system

Demand side management, also known as demand response, involves utility strategies aimed at influencing electricity consumers by adjusting the size and timing of their loads. The primary goal is to lower load demand during peak periods and relocate this demand to off-peak times. This results in a decrease in peak power necessity, leading to reduced reliance on peak power plants and a decrease in the need for load shedding.

Types of demand response:

1. *Price-driven demand response:* Consumers voluntarily alter their electricity usage patterns due to varying rates throughout the day, affecting overall electricity costs.
2. *Incentive-driven demand response:* Grid operators initiate these, incentivizing customers for load reduction through real-time, time-of-use, and critical peak pricing mechanisms.
3. *Direct load control:* Utility remotely manages loads, with customers compensated for this service. After customer enrolment, utilities install control devices for flexible loads like air conditioners and water heaters. This suit residential or small commercial users.
4. *Interruptible load:* Customers manage their demand via sources like CHP, battery storage, or solar power. They receive discounts for load interruptions.

5. *Capacity market programs:* Consumers contract with the utility grid to reduce loads to predetermined levels. Incentives are granted for compliance, while penalties apply for non-compliance.
6. *Ancillary service market programs:* Customers can bid for load reduction, receiving incentives for curtailing loads as requested by the utility.

In [16], a heuristic optimization technique is employed to shift loads within demand side management. This optimization aims to align the load curve as closely as possible with the desired demand curve, although this approach may result in a loss of consumer comfort due to the shift of flexible loads. Heuristic optimization is chosen due to the large number of controllable devices that linear and dynamic programming cannot effectively manage. Demand response (DR) from sources like EVs can be adjusted when power from RE resources is abundant. EVs can also contribute to Vehicle-to-Home services, storing excess power from RE sources for utilization during high-demand, low-generation periods. In [17], a dual-auction electricity market concept is explored. Transaction controllers submit bids to the electricity market, and upon price clearance, these controllers schedule loads, and generators according to the bids.

The application of various DR strategies has increased customer engagement and bolstered microgrid system reliability through participation from retailers and consumers. The consumer's motivation emerges as a pivotal factor, alongside infrastructure, for the successful implementation of demand side management.

1.1.8. Reliability indices assessment

Reliability indices are calculated to assess the performance of the system, the reliability indices are taken for a microgrid system in different modes and conditions. It is per- formed to check the need to conduct the maintenance and planning tasks to improve the reliability. A few of the reliability metrics are given below [18].

Operation reliability index:

$$Island\ loss\ of\ load\ probability\ (ILOLP) = \frac{(Islanded\ hours\ with\ demand\ not\ fully\ met)}{(Total\ microgrid\ island\ hours)} \tag{1.7}$$

Microgrid economic index:

$$Purchase\ probability\ (PP) = \frac{\sum(hours\ when\ microgrid\ purchase\ energy)}{(Total\ microgrid - grid\ connected\ hours)} \tag{1.8}$$

Index reflecting DGs and load characteristics:

$$Expected\ energy\ not\ supplied\ (EENS) = \frac{Amount\ of\ energy\ not\ supplied}{Total\ period\ of\ operation\ (Week)} \tag{1.9}$$

1.1.9. Test system modelling for dynamic analysis

A small-scale electrical system based on an AC/DC busbar distribution is simulated using PowerFactory. Different components are modeled based on their predefined ratings. The model incorporates various residential loads connected to the AC bus alongside the utility grid and a biogas generator. The DC bus features diverse sources linked through converters. A Woodward governor with automatic voltage regulation (AVR) and power system stabilization (PSS) serves as the biogas generator's governor. The generator connects to the AC bus via a transformer.

The AC/DC bus connection is facilitated by an appropriate converter for bidirectional power flow. However, the battery can only charge through solar PV and wind sources, making AC to DC power conversion unnecessary. Solar PV integration employs a boost converter for the DC bus, while a Type-4 wind turbine connects via a rectifier, converting wind turbine AC power to DC for the DC bus.

The model includes various household loads simulated as ZIP loads. Household devices like fans, lighting, water pumps, refrigerators, and EVs are taken into account in the simulation. The block diagram of the test system is shown in Figure 1.4.

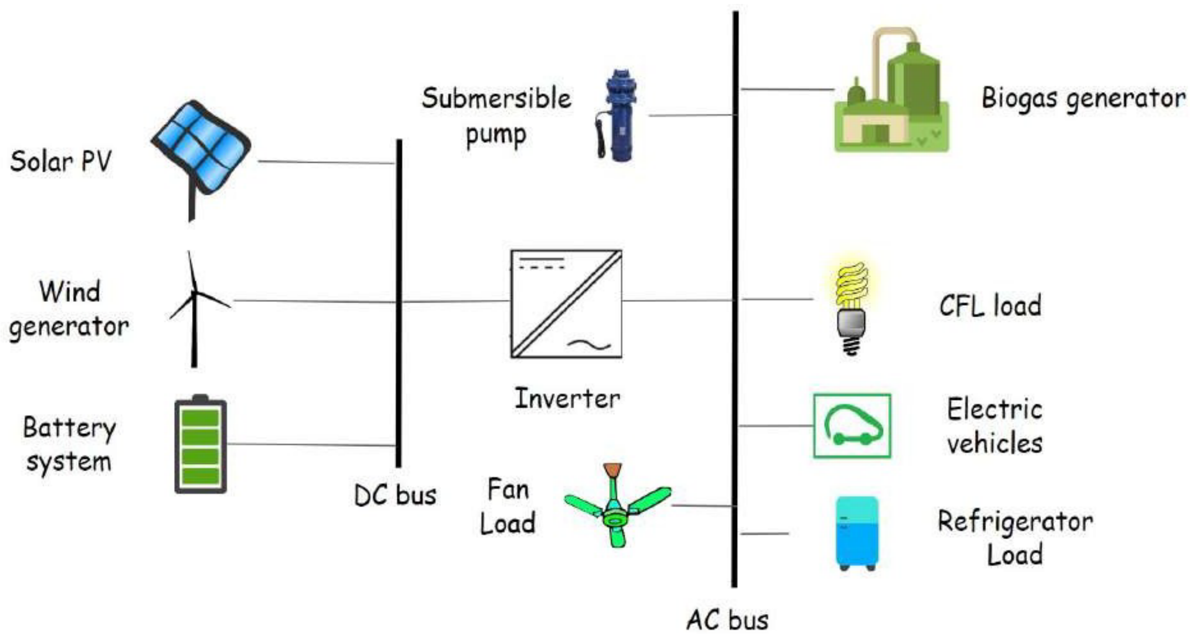

Figure 1.4: Schematic of the developed system

Test system

The overall generation capacity of the power plant is rated at 56 kW while the overall loads are rated at 49.58 kW. The household loads are distributed among 60 houses. The ratings of the different loads and sources are given in Table 1.1.

Table 1.1: Ratings of different components of the system

Component	Rating
Solar PV plant	34 kW
Wind power plant	10 kW
Biogas generator	12 kW
Battery capacity	256 kWh
Water pumping system	2×5 hp = 7.355 kW
Fan load	60 × (0.09+0.06) = 9 kW
Refrigerator load	10×0.15 = 1.5 kW
CFL load	60× (0.009+0.018) = 1.62 kW
EV load	7×2.5 kW

Regarding EV loads, the simulation includes 5 two-wheelers and 2 three-wheelers, each connected to a 2.5 kW socket. The model incorporates two variations of Compact Fluorescent Lamps (CFLs) for lighting, with power ratings of 9 W and 18 W. Additionally, two different fan load sizes are considered: 60 W and 90 W. The water pumping system is powered by two 5 hp motors. The simulation accounts for 60 households, with each having fan and lighting loads.

The AC busbar links up with all the loads and the biogas generator, while the DC busbar is connected to a hybrid power plant incorporating a VRLA-based battery system, solar PV, and wind turbine setup. The power distribution between the inverter and the biogas generator employs a droop-based method. The biogas generator operates in a constant voltage-controlled mode with a 4.5 kW/Hz drop rate, whereas the interconnecting inverter functions in a P-Vac control model with a 5 kW/Hz droop.

Loads like EVs, fans, and the water pumping system are linked to the 3-phase low voltage (LV) busbar. Refrigerators and CFLs, on the other hand, are connected to the LV busbar through a transformer.

Dynamic analysis of the test system

The microgrid system's control responses are examined by analyzing the dynamic responses of different components when faced with abrupt load and source changes or contingencies. This examination encompasses scenarios such as sudden load changes, immediate generator connections or disconnections, transitions between grid-connected and islanded modes, and occurrences of 3-phase faults.

The dynamic analysis is specifically focused on the islanded mode of operation. This is because the presence of the grid eliminates dynamic behavior originating from microgrid sources and loads. The utility grid, being an adaptable source, can either absorb or supply varying levels of active and reactive power during contingencies.

Sudden changes in load: 20% step change in EV load

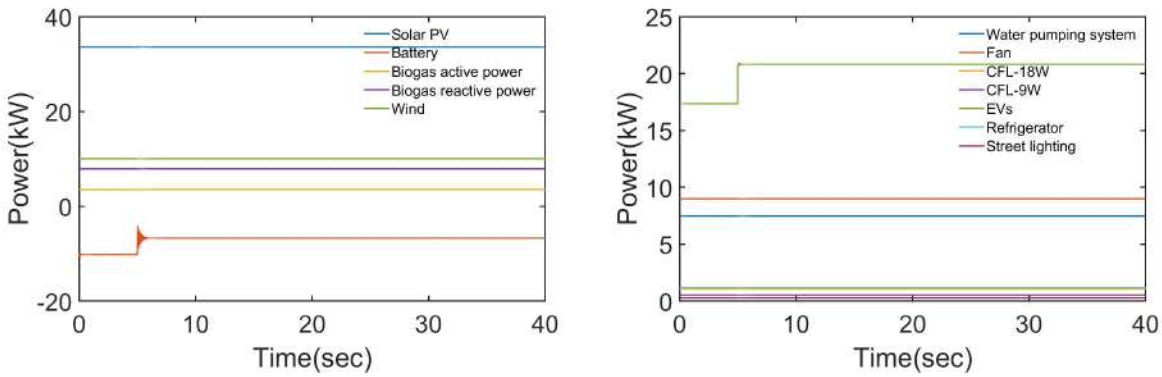

Figure 1.5: Contribution from source and loads

A 20% step change in EV load signifies a load alteration of 5 kW within the system. The entire power adjustment comes from the battery system, as the biogas generator and other sources are operating at their specified capacity. This can be observed in Figure 1.5.

Because of the presence of motor, fan loads and biogas generator, the sudden change in the load is countered by their inertia and the change in frequency and voltage of AC busbar is seen in Figure 1.6.

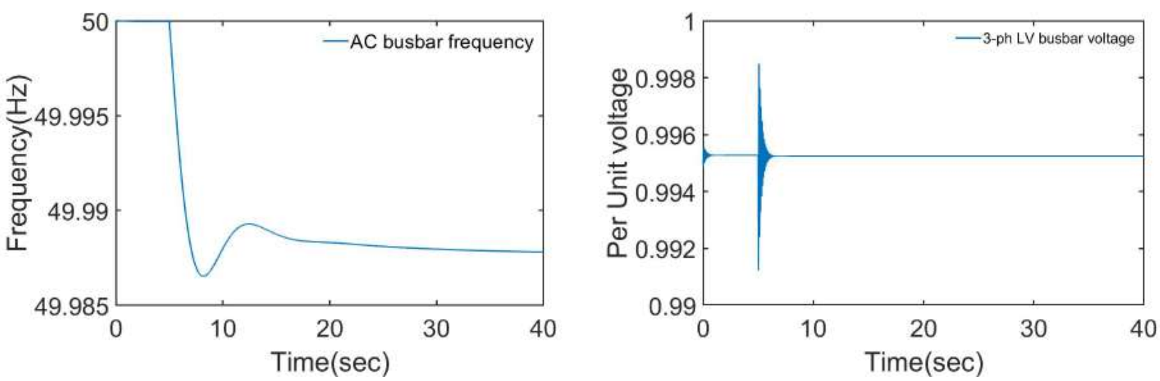

Figure 1.6: 3-Φ LV busbar values

Generator event: Sudden disconnection of bio-gas generator

The changes in the active and reactive power that occurred during biogas generator disconnection are contributed by the inverter and battery, providing most of the contribution, as shown in Figure 1.7.

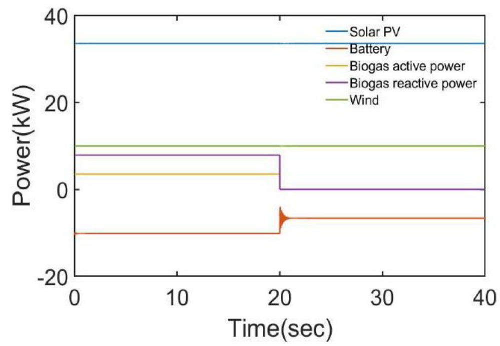

Figure 1.7: Changes in power contribution from all the sources

Changes in the frequency and voltage are shown in Figure 1.8. The change is very minimum, and the frequency is settled at 50 Hz due to fast acting behavior of inverter.

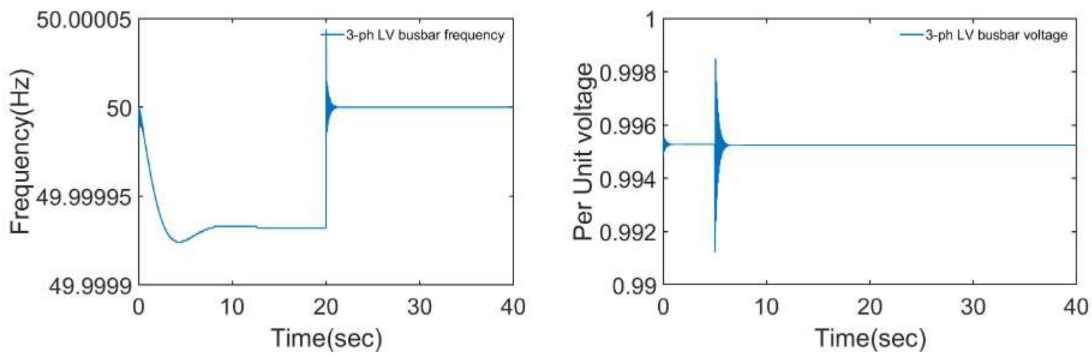

Figure 1.8: 3-Φ LV busbar values

Grid event: Islanded to grid-connected and vice versa.

The system is started without the grid, and the grid is connected by closing the switch at 5 sec, and the grid is disconnected again at 15 seconds, as shown in Figure 1.9. The changes in the active and reactive power through the sources occurred because of the changes in grid contribution. Busbar voltage increased suddenly during the grid connection to 1 pu and suddenly came back to the value when the grid was disconnected, as shown in Figure 1.10. It shows that the voltage support is less from the microgrid side. It is unable to maintain voltage. Similarly, frequency changes when the grid is disconnected, indicating the absence of inertia in the microgrid.

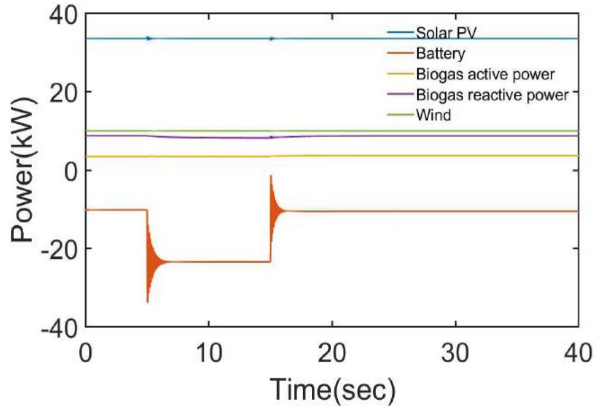

Figure 1.9: Changes in power contribution from all the sources

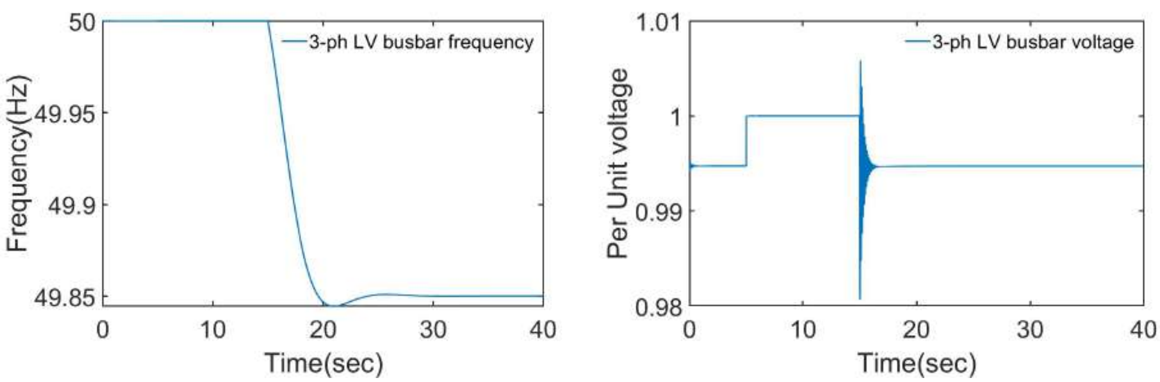

Figure 1.10: 3-Φ LV busbar values

A dynamic system model is created to ensure durability in the face of load, source, or grid events. The biogas generator operating in conjunction with a synchronous generator presents a challenge due to rapid inverter switching. The inverter's model maintains a constant frequency of 50 Hz and a voltage of 1 per unit. All simulations are conducted within an islanded system since any impacts of changes can be swiftly addressed with grid assistance.

1.1.10. Implementation of operation cost optimization using demand response

Optimization is necessary within multi-energy systems as it enables the enhancement of different system aspects while adhering to diverse constraints. Planning necessitates LCOE-driven optimization, while operational scheduling exclusively relies on cost-based optimization. The operational cost values are drawn from NREL's provided data [19].

Problem formulation

Objective function

A linearization of all the cost curves gave the flexibility to perform low-level computation with similar accuracy levels. The proposed optimization strategy generates a schedule for the forecasted solar, wind, and load data and provides the minimum cost of operation. The proposed objective function is as follows:

$$MinC = \sum (C_{pv}P_{pv}(i) + C_{wind}P_{wind}(i) + C_{bio}P_{bio}(i) + C_{bat}P_{bat}(i) + C_{grid}P_{grid}(i)) \tag{1.10}$$

Where, i = 1 to 24 for a single-day analysis and 1 to 168 for a weekly analysis

Constraints –

- $P_{pv} + P_{wind} + P_{bat} + P_{bio} + P_{grid} = P_{load}$
- $0.5 \leq SOC(i) \leq 0.95$
- Upper and lower bounds of all the sources, $P_{lb} \leq P_{gen} \leq P_{ub}$
- Solved using LP-based solver in MATLAB programming

Conditions –

- Battery cannot discharge to the grid.
- Only RE is used to charge the battery.
- Biogas generator is available for 2-3 hours a day

Solar and wind data

Solar irradiance and wind speed data is captured for the Barubeda village of Jharkhand. The data for the past 15 years is taken and averaged into monthly and seasonal data. The variation in data is captured as shown in Figure 1.11 and in Figure 1.12.

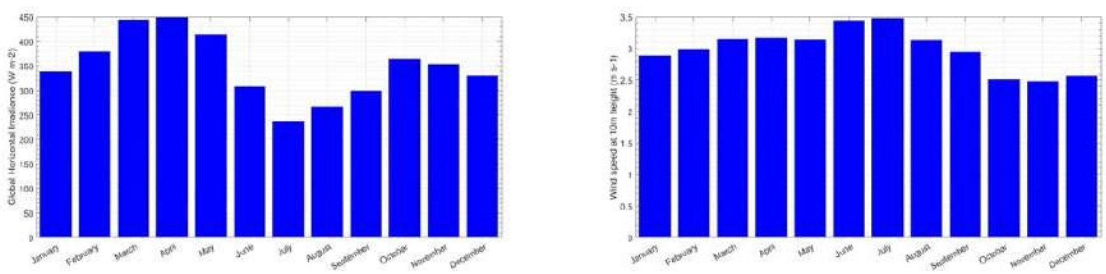

Figure 1.11: Monthly data: Monthly averaged global horizontal irradiance (w-m^2) (Left side), Monthly averaged wind speed (m/s)

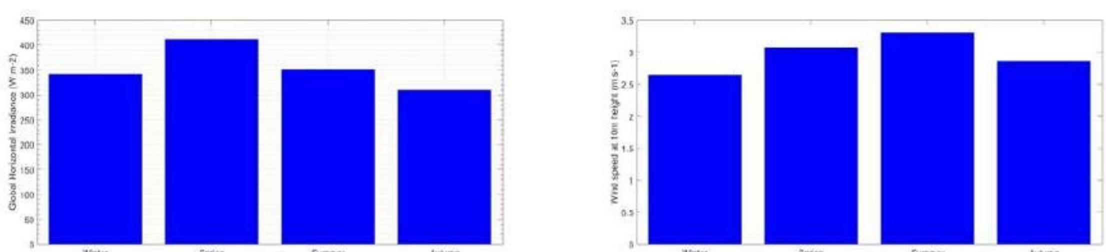

Figure 1.12: Seasonal data: Seasonal averaged global horizontal irradiance (w-m^2) (Left side), Seasonal averaged wind speed (m/s)

Load distribution and overall load curve

The load curve and overall load distribution pattern are given in Figure 1.13 and Figure 1.14. respectively.

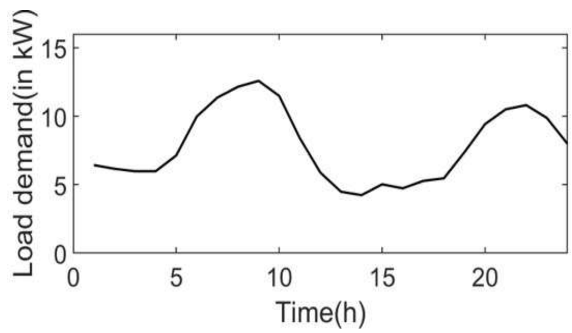

Figure 1.13: Load curve for Barubeda village

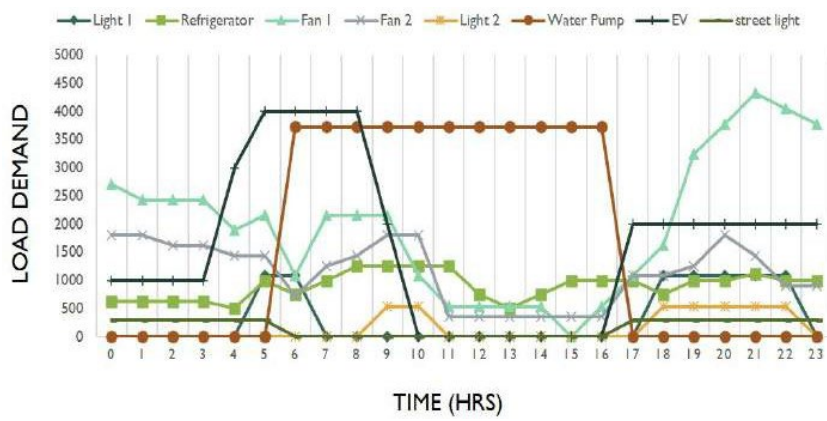

Figure 1.14: Load distribution pattern

Demand response

DR or Demand Side Management (DSM) involves regulating electricity consumption or production within a community or household. DR utilizes adjustable loads like EVs, HVAC systems, and washing machines. In this context, water-pumping loads and EVs are identified as controllable and flexible loads. The primary aim of DR is to adjust the timing of these loads to minimize operational costs. Notably, this study does not utilize heat energy for storage purposes. To implement DR, loads are categorized as flexible, critical, or base loads. Initial optimization is performed to establish the cost of the operation curve. Flexible loads, along with their timings and daily energy consumption, are inputted. Energy consumption is divided into predefined iterations and scheduled during intervals with the lowest operational costs.

EV loads are assigned random charging patterns using a random number generator. All EVs are positioned based on the highest random number within an interval where the cost is at its lowest. In contrast, water pumping loads lack random number assignment and must be placed in the interval with minimal cost as determined by the value of parameter 'a' specified in the algorithm. The flowchart is depicted in Figure 1.15.

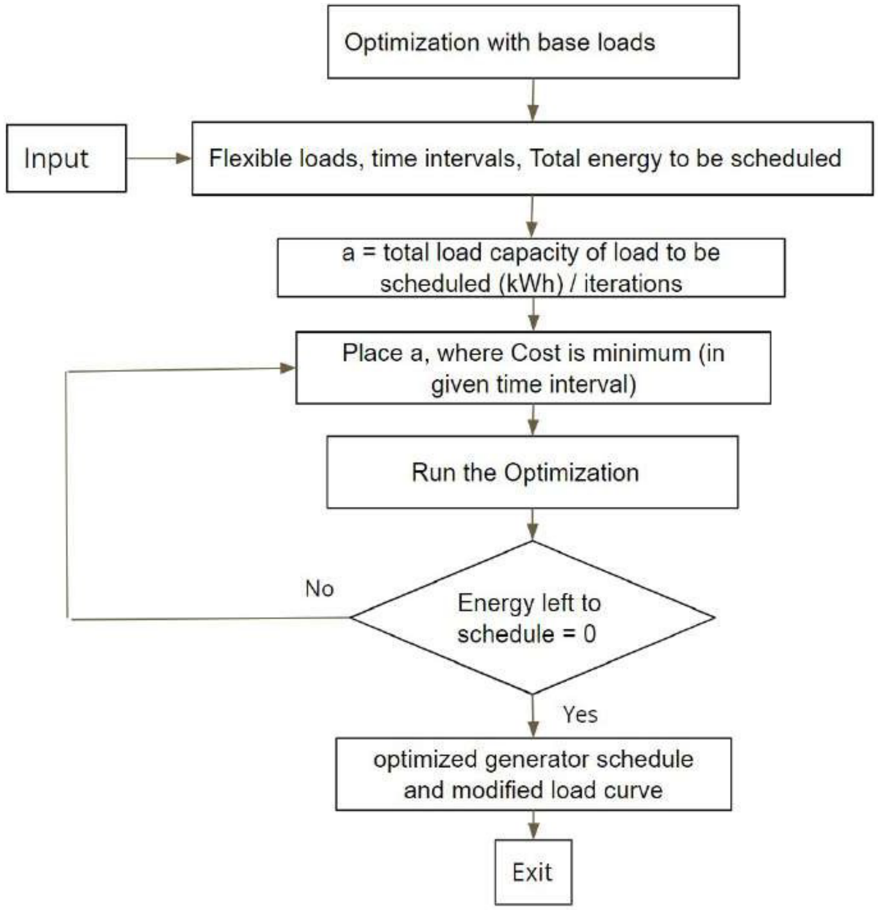

Figure 1.15: Algorithm for DR

Cost of operation

Obtaining the cost of operation values for various sources is challenging due to their reliance on multiple variables such as geographical location, environmental conditions, economic factors, and labour expenses. The operating cost data is sourced from the National Energy Modelling System (NEMS) established by the Energy Information Agency (EIA). This data is provided in Table 1.2.

Table 1.2: Operational cost of sources

Generator	Fixed cost ($/kWh)	Variable cost ($/kWh)	Total ($/kWh)
Biomass	18.10	30.07	48.17
Solar PV	6.38	0	6.38
Wind	7.7	0	7.7
VRLA battery	29.64	24.83	54.47

Single day analysis for all seasons in islanded system

The data for the different seasons is taken from the dataset generated after contributing the losses in solar plant for the Barubeda village of Jharkhand. The months are classified into four seasons and the data is taken as the average of the first week of each month. The initial value of battery SOC is taken as 0.8.

Power scheduling of generators

Figure 1.16 shows the power curve from all the generators participating in the scheduling. The optimization algorithm schedules the generators as per their availability and cost of operation. Biogas generator is operated for 3 hours each day thus, it is considered to give 36 kWh of energy (12 kW x 3 hrs) each day.

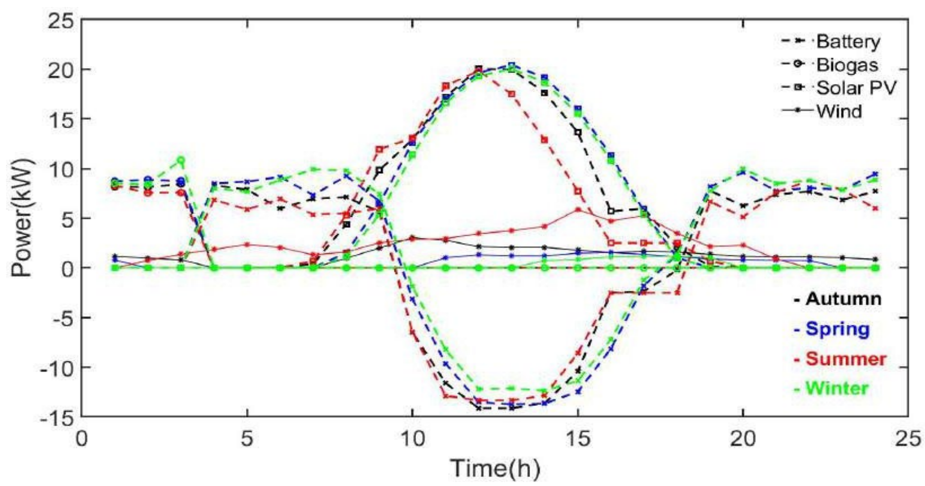

Figure 1.16: Generator scheduling

Cost curve and DR based load scheduling

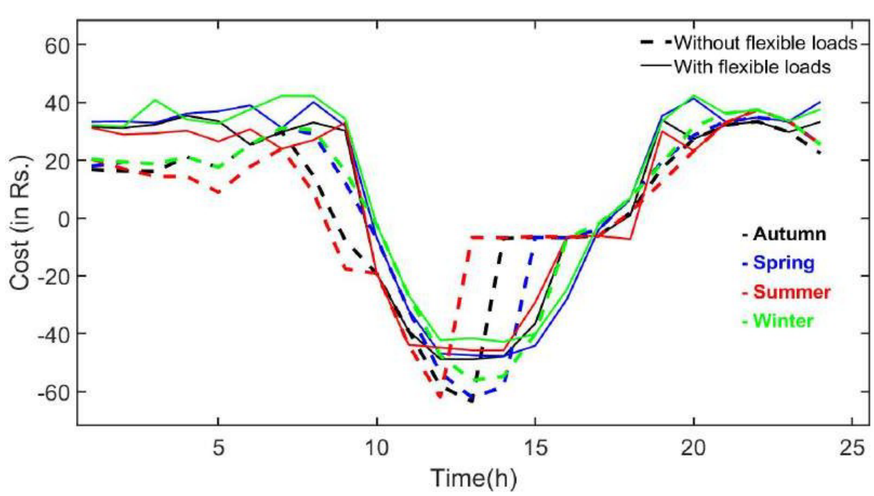

Figure 1.17: Cost of operation

The figure below shows the DR based approach to schedule the flexible loads such that the cost of operation is minimum, and it can be seen as a modified valley filling approach taken while load shifting as seen in Figure 1.17. The average cost per hour comes to around 14.24 for all the seasons.

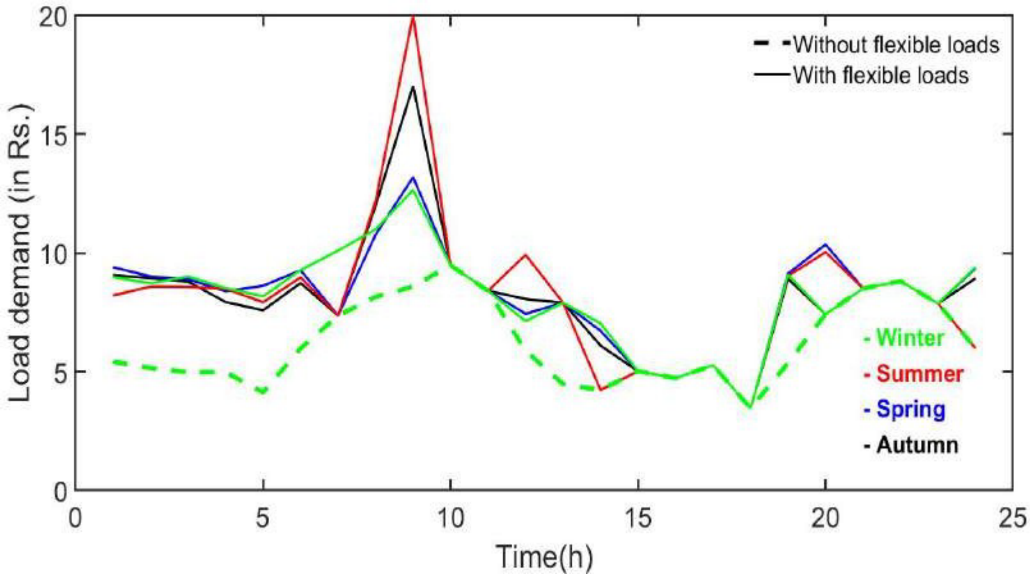

Figure 1.18: Load demand curve

Base load curve and load curve after adding flexible loads.

The base load curve is taken from [20]. The load curve is obtained by measuring the residential demand for 90 households for one year. The flexible loads are shifted to places where the cost is minimum. Here, the conventional idea of reducing the peak demand isnot applicable and thus, the increase in the peak load demand in the morning period hasbeen seen in Figure 1.18.

Scenario without solar PV for two days in islanded system

The effect of solar PV plant is shown in the overall load demand met by the developed system. The load shedding is performed when the load demand is not met by battery and solar PV. The critical loads are satisfied at each interval. After two days of operation without solar PV, the energy system started operating in normal condition with improved reliability and reduced load shedding. Figure 1.19 - Figure 1.22 shows the behavior of generators and loads.

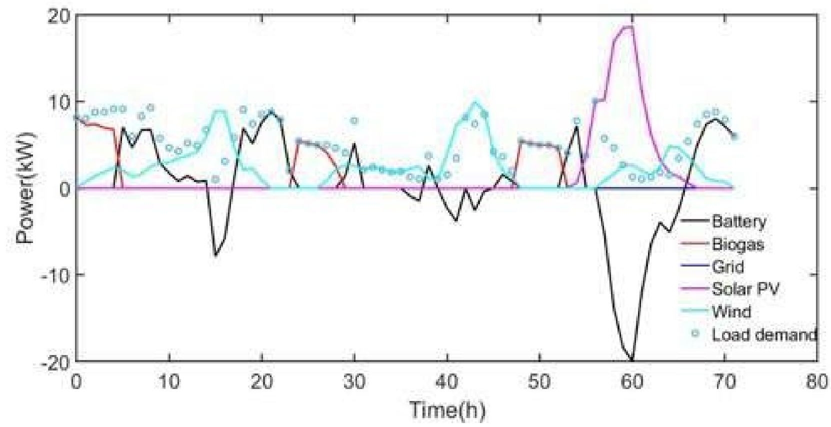

Figure 1.19: Scheduling of generators without solar for two days

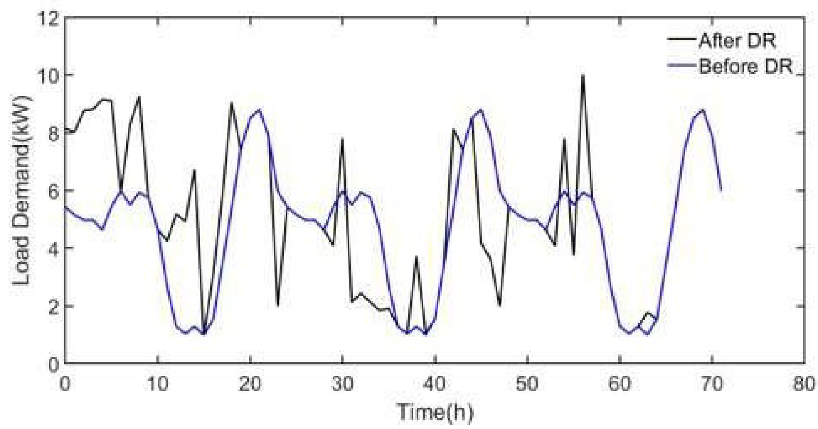

Figure 1.20: Load demand met in the scenario

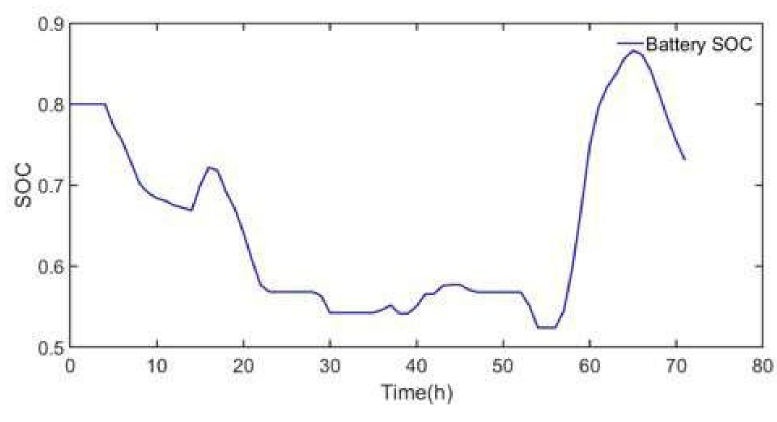

Figure 1.21: Variation in the SOC

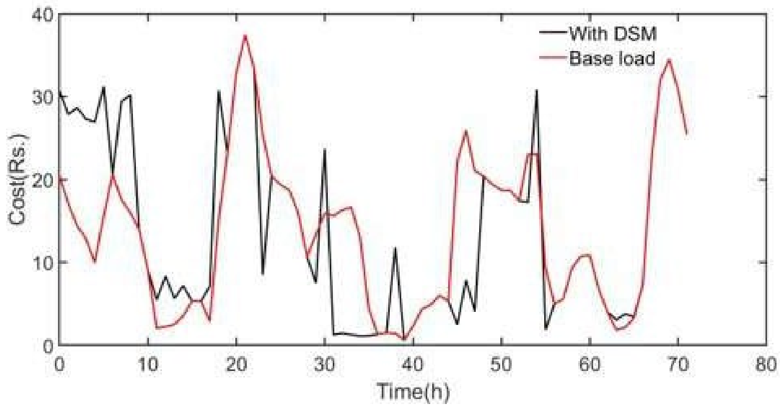

Figure 1.22: Cost of operation

Demand response on approach of load curve valley filling

On of the conventional approaches used for DR involves the approach based on valley filling of the load curve as there is need of lowering the peak demand. The approach is not exactly suitable in RE based multi-energy system, which is highly uncertain in nature. This section shows the dispatch based in load curve valley filling in the Barubeda energy management system. The load curve is taken from already generated load profile from DR program. The initial battery SOC is taken to be 0.8. The dispatch results are shown in Figure 1.23 – Figure 1.26. The hourly cost of operation comes to Rs. 24.33.

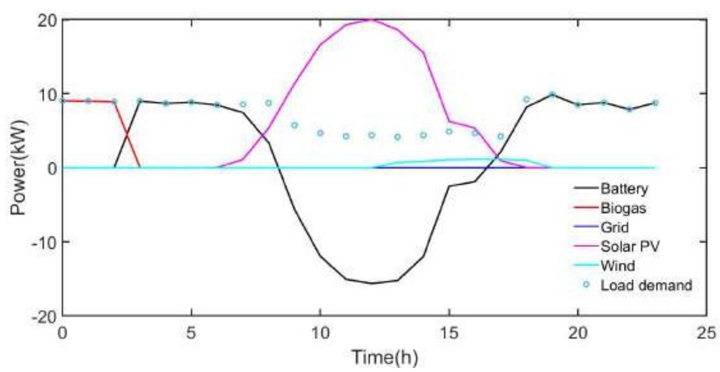

Figure 1.23: Generator power dispatch

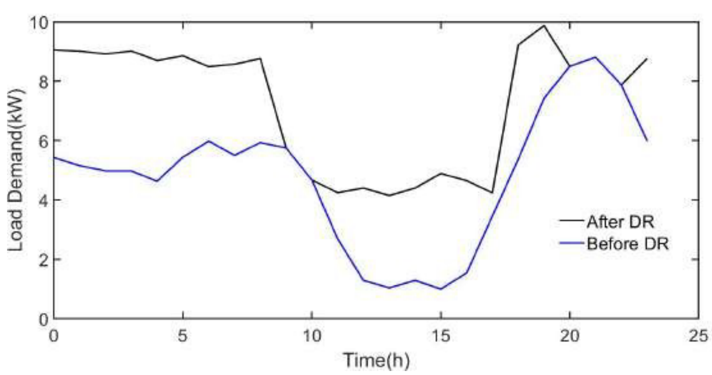

Figure 1.24: Load curve

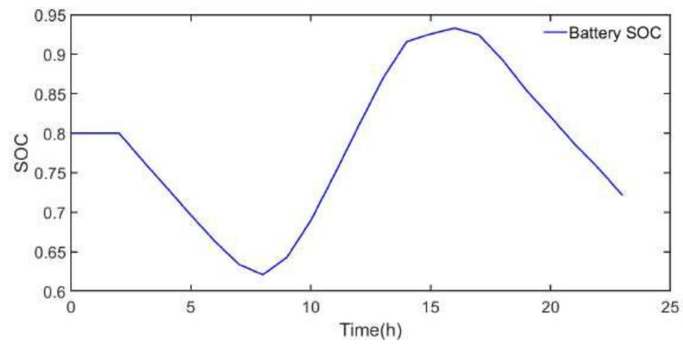

Figure 1.25: Battery SOC

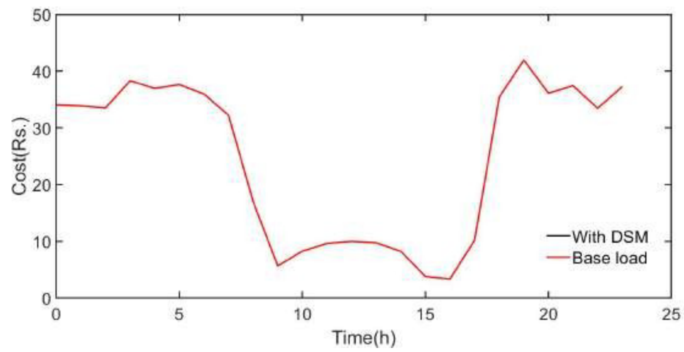

Figure 1.26: Hourly cost of operation

Power management for a rule-based dispatch:

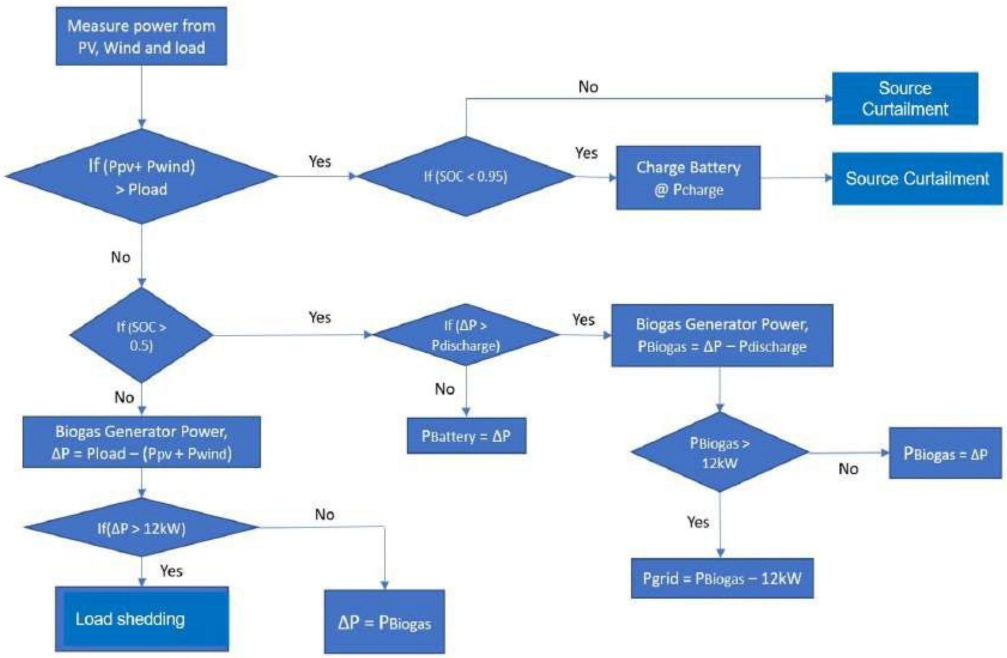

Figure 1.27: Algorithm for rule-based dispatch

The Figure 1.27 illustrates a heuristic planning method, executed according to a designed algorithm. The rule-driven dispatch relies on priority scheduling, with the biogas generator having the lowest priority as it functions to supply load during periods of uncharged battery. Priority determination hinges on generator capacity and operational costs. The source wise power output and the load profile are presented in Figure 1.28.

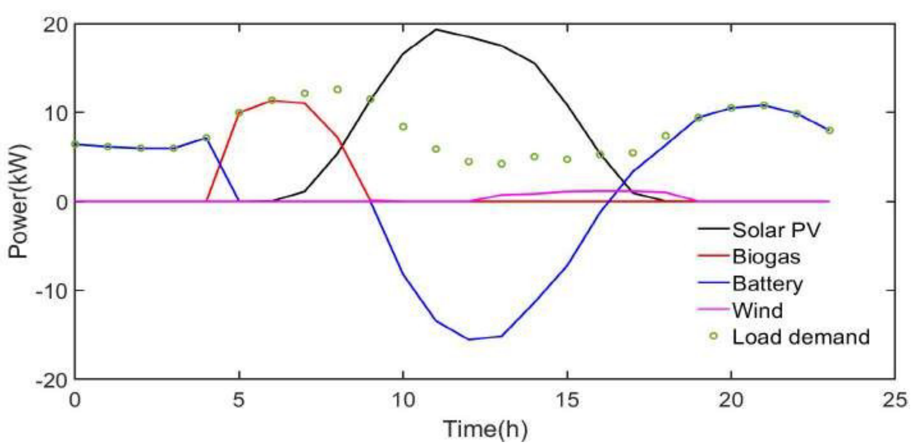

Figure 1.28: Power flow

The load curve is taken from already generated load profile from DR program. The initial battery SOC is taken to be 0.6. The dispatch from Figure 1.29 shows that the biogas generator is not scheduled, and the algorithm will wait for the SOC of battery to be exhausted. Hourly cost of operation comes at Rs. 24.67 for rule-based optimization.

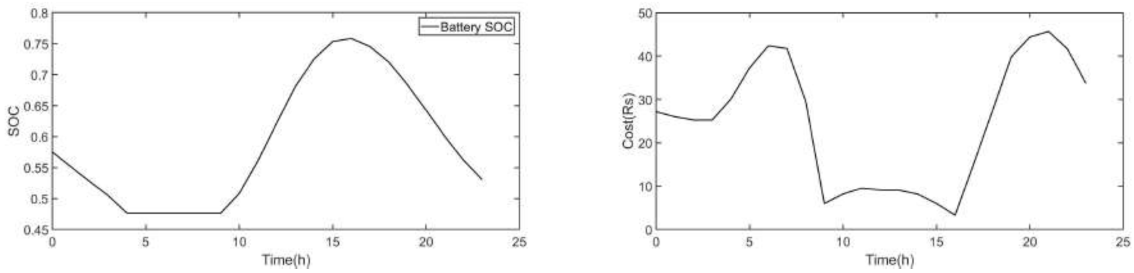

Figure 1.29: SOC and cost curve for the rule-based dispatch

Conducting operational cost optimization offers a comprehensive understanding of the energy system's performance on a daily basis. Employing a rule-based algorithm for dispatch results in an operational cost of Rs. 24.67 per hour. Among various strategies, the rule-based dispatch yields the highest hourly operational cost.

1.1.11. Summary

The multi-energy system designed for Barubeda village undergoes both dynamic and steady-state assessments. Dynamic analysis reveals the system's transient behavior during contingencies like load, generator, and grid events, highlighting the inverter's robustness in maintaining frequency and voltage. Steady-state analysis facilitates generator scheduling based on the lowest operating cost. Solar and wind variations impact power generation, as evident in the cost curves for different seasons. Table 1.3 shows the comparison of different strategies used in applying the demand side management and shows the operational cost comparison. The cost of operation for the proposed strategy is the lowest. Introducing flexible residential loads enhances DR, reducing costs through techniques like load shedding and battery charge control. The optimized dispatch results in an average hourly operating cost of Rs. 17.67.

Table 1.3: Operating costs of various strategies

S. No.	Strategy	Operating cost (Rs/hr)
1	No flexible load/ with DSM	20.33
2	Flexible load/ With DSM	17.67
3	Approach for load curve valley filling	24.33
4	Rule based dispatch	25.46

Reliability indices-

- Island loss of load probability (ILOLP) - 11.19 %
- Purchase probability (PP) - 3.48 %
- Expected energy not supplied (EENS) - 3839.9 kWh = 5.97 %

1.2. Inertia and its relevance in converter-interfaced power system[1]

The rapid incorporation of RE into traditional power systems has become a global trend, driven by concerns over high carbon emission and dwindling reserves of fossil fuels. While RE integration offers several advantages, it also puts some challenges related to power system planning and operational aspects. Among these challenges, frequency instability emerges as a significant issue due to the reduction in system inertia [21]. This diminished inertia leads to an increased rate of change of frequency (RoCoF) and a decline in frequency levels, which can potentially breach limits during otherwise less critical contingencies. Consequently, situations characterized by reduced inertia make the system more prone to tripping of RoCoF and frequency deviation-based relays, such as under-frequency load shedding (UFLS) [22], and even system collapse under worst-case scenarios. In the realm of inertia sources, assistance for maintaining inertia can be generally categorized into three primary groups: synchronous inertia (originating exclusively from synchronous generators), load inertia (arising from voltage and frequency-sensitive loads), and non-synchronous inertia (emulated from inverter interfaced resources, known as IBRs). The inherent and instantaneous inertial support provided by the rotational mass of synchronous generators is significant. It is regulated by the electro-mechanical swing equation within the first few seconds after a contingency event, even in the absence of turbine governor intervention. However, the inertial response from frequency and voltage-dependent loads, while instantaneous, does not adhere to the swing equation-based pattern observed in synchronous machines.

Historically, studies have often overlooked the contribution of load-end inertial response in inertia estimation, mainly due to practical challenges associated with estimating and monitoring this aspect. When dealing with non-synchronous inertia, like inertia from IBRs, the reaction is impacted by additional inertial control configurations and controller settings. Unlike the inherent and immediate synchronous inertial response, the start of inertial response from IBRs experiences a delay of at least 100 milliseconds from the initiation of the disturbance [23].

Given the decline in synchronous inertia driven by RE, estimating synchronous, load, and non-synchronous inertia becomes crucial for system operators to ensure a secure and stable grid.

1.2.1. Challenges in power system operation under low Inertia

As RE displaces traditional generation, leading to an anticipated reduction in inertia, it becomes crucial to evaluate how this diminished inertia impacts power system dynamics and the role of inertia in power system stability, reliability, and operation. The timescale for power system dynamics spans from microseconds to seconds, encompassing both rapid and slower electromagnetic phenomena. Inertia becomes significant within seconds, particularly in electromechanical events following disturbances. This

[1] Contents from this chapter are a part of the following articles published/to be published under the SUSTENANCE project:
P. K. Dhara and Z. H. Rather, "Non-synchronous Inertia Estimation in a Renewable Energy Integrated Power System with Reduced Number of Monitoring Nodes," in *IEEE Transactions on Sustainable Energy*, vol. 14, no. 2, pp. 864-875, April 2023, doi: 10.1109/TSTE.2022.3227603

section addresses the key challenges associated with various forms of power system stability concerns linked to decreased synchronous machine presence in the grid.

Impact on frequency stability: Reducing synchronous inertia results in an increased RoCoF following credible contingencies, creating challenges in maintaining RoCoF and frequency within acceptable limits. Furthermore, the overall system governor response weakens due to greater RE integration, potentially affecting primary frequency control. Although inverters connected to RE sources can technically aid during over frequency incidents by reducing their output, proactive curtailment is required for frequency support during underfrequency events. Such underfrequency support might not be practically viable due to economic, policy, and regulatory factors, except for cases involving forced curtailment of RE generation due to network issues like congestion or stability problems. Grid standards define the permissible frequency range within which generators should remain connected to the transmission grid. In the Indian power system, the Central Electricity Authority's regulations specify that generating units must operate within the frequency range of 47.5 to 52 Hz and deliver their rated output between 49.5 Hz and 50.5 Hz. Distributed energy sources are designed to trip if the frequency falls below 47.5 Hz or rises above 50.5 Hz for 200 milliseconds. Prolonged frequency excursions can trigger a cascading effect of tripping throughout the system.

Impact on transient stability: Decreasing power system inertia hampers its capacity to attenuate oscillations, particularly evident during substantial disturbances in system equilibrium. The Critical Clearing Time (CCT) for faults also diminishes, contributing to cascading disconnections and insecure power system conditions. Yet, transient stability relies on Inverter-Based Resources (IBR) control strategies and grid code regulations. Previous research suggests that effective system planning, and adaptive grid operation practices can address transient stability concerns.

Impact on power system protection: The reliability of the power system heavily depends on proper power system protection functioning. Diminished inertia contributes to elevated RoCoF after contingencies. Power system protection strategies are designed to manage extreme low-frequency events. UFLS schemes activate when frequency drops below a set threshold. However, the time taken for frequency measurement and relay activation introduces delays, potentially leading to UFLS inaccuracies or system collapse if high RoCoF values cause delays in measurement.

Effect on short circuit capacity of the power system: Synchronous machines swiftly inject approximately 7-8 times their nominal current during severe network short circuits, aiding voltage recovery and enhancing transient stability. Transitioning to power electronics-based devices considerably diminishes this ability. The applied power system protection relies on robust short-circuit current injection, yet declining capability necessitates constant monitoring and evaluation of the scheme to prevent protection malfunctions.

Effect on small signal stability: The power system hosts numerous inherent oscillatory modes resulting from component interactions, with many modes tied to generator rotor mass oscillations. Ensuring reliable system operation mandates adequate damping for all modes across different conditions. Damping relies on system parameters and can be compromised by decreased inertia. Reduced power system inertia leads to diminished frequency and damping of these modes.

Considering the aforementioned points, it's evident that diminishing system inertia adversely impacts power system stability, leading to elevated RoCoF and worsened frequency nadir during identical power imbalances. The minimum required inertia for secure operation heavily relies on the system's ability to withstand RoCoF. A surge in maximum RoCoF subsequent to an event heightens the chance of system frequency nearing load-shedding thresholds. Consequently, system inertia, coupled with primary frequency control, plays a crucial role in defining the permissible time delay for governor and prime mover responses to counteract frequency decline.

1.2.2. Classification of inertia estimation methods

In recent years, considerable attention has been given to accurately determine system inertia, primarily due to its decrease resulting from the integration of RE. The methods for estimating inertia, as documented in existing literature, can be categorized into different groups based on the timeframe of estimation and the intended level of inertia. Depending on the timeframe, these methods are divided into offline, online or real-time, and forecasting techniques. In terms of the intended level of inertia, these estimation methods encompass system-level, regional-level, synchronous generator inertia, power electronics interfaced source (or embedded generation) inertia, and demand-level inertia. The classification of inertia estimation methods is illustrated in Figure 1.30.

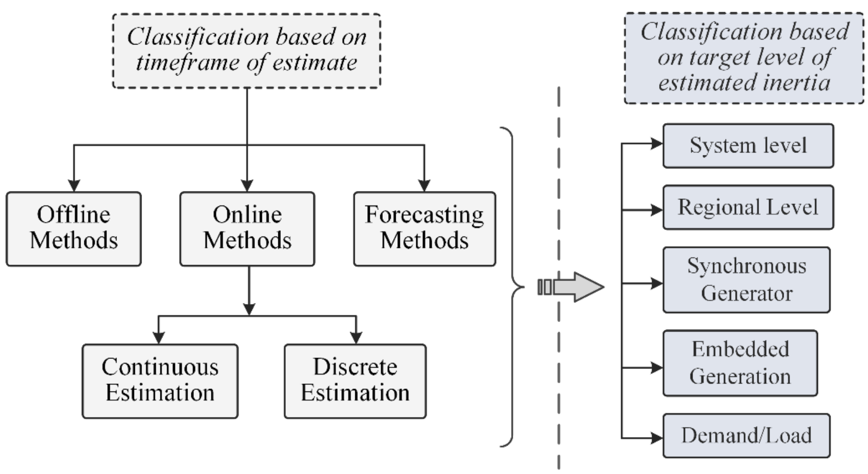

Figure 1.30: Classification of inertia estimation methods [24]

Offline inertia estimation: Inertia estimation involves utilizing historical frequency and power response data collected during major disruptions in the power system. The approach employs the swing equation, using disturbance size and initial RoCoF derived from measured frequency, to estimate system inertia. The offline post-mortem method was initially proposed by Inoue et al. to estimate Japan's power system inertia [25], subsequently prompting similar studies in the field. These methods can be categorized into system-level, regional-level, synchronous generator, converter interfaced generation, and demand-side/load estimation.

Challenges in offline inertia estimation include handling the disturbance's active power size, timing, and location, addressing frequency measurement discrepancies across the power system, and filtering measured frequency data to accurately calculate RoCoF while eliminating unwanted oscillations. A limitation of this approach is its lack of real-time and continuous value, making it unsuitable for immediate decision-making due to its changing nature influenced by synchronous generator count and load conditions. The accuracy of estimates also depends on the selected time window for RoCoF calculation in offline methods. Furthermore, the reliability of the method diminishes when power electronics (PE)-based sources with virtual inertia provision are integrated into the system, as their inertial responses differ from synchronous generators.

Online inertia estimation: Differing from post-mortem analysis that relies on historical data, online estimation strategies determine inertia in real-time utilizing live measurements. These online estimation techniques can be further divided into discrete and continuous methods. Categorizing these estimation techniques can also be based on the domain in which inertia is assessed: time-series, Laplace domain, and modal-domain oriented approaches. Time-series methods involve utilizing recorded time series data and employing a simplified swing equation for inertia estimation. Conversely, the Laplace domain approach employs transfer function models to identify inertia through a system-identification-based method. Lastly, modal domain methods estimate inertia by analyzing inter-area oscillations captured during active power disturbances.

Inertia forecasting: To ensure readiness for potential contingencies and facilitate appropriate allocation of rapid frequency reserves, the prediction of system inertia is crucial. The required time resolution for inertia forecasting varies based on operational practices for generation re-dispatch. In instances like the Great Britain system, a fixed 30-minute contractual interval for online generators determines the forecasting duration. The forthcoming availability of inertia can be estimated using the equation:

$$KE_{t+k|t} = \sum_{i} K_{t+k|t,i} * H_i * P_i^g \tag{1.11}$$

where $K_{t+k|t,i}$ represents the status of the $i'th$ generator online at time t for a duration of $t+k$, and H_i and P_i^g denote the inertia constant and generating capacity of the $i'th$ generator, respectively. Although ERCOT and Nordic TSOs have applied this approach, it tends to underestimate inertia due to its failure to consider contributions from demand and other potential sources. To address this limitation, the National Grid includes the inertia contribution from demand-side and embedded generations by incorporating load forecast data. This leads to a modified equation:

$$KE_{t+k|t} = \sum_{i} K_{t+k|t,i} * H_i * P_i^g + a * P_{t+k|t}^D \tag{1.12}$$

where $P_{t+k|t}^D$ signifies the system demand forecast at time t for a duration of t+k, and a is a constant regression factor applicable to the entire system. The precision of inertia forecast models diminishes with higher integration of PE-based sources into the system. The variable and uncertain nature of RE sources introduces unpredictability in reported statuses, affecting day-ahead predictions. Moreover, the model doesn't incorporate the contribution of virtual inertia in anticipating future inertia.

1.2.3. Proposed methodology of inertia estimation

An inertia estimation method based on large disturbance is proposed. This method assumes knowledge of sudden frequency disturbances' size, location, and time in a power system. The disturbance data can be obtained from historical records or through real-time detection using PMU measurements. The research presumes complete visibility into synchronous generators, limited visibility into grid-connected loads, and an absence of visibility into IBRs because of financial constraints associated with PMU placement. PMUs in the system are synchronized, collecting data at 30-60 samples per second. The proposed approach is categorized as either offline or close-to-real-time based on how disturbance details are obtained. Offline methods offer high accuracy but may not reflect current system conditions, while online methods provide faster estimates but can be less accurate due to limited detection and processing time. The proposed approach combines advantages of both offline and close-to-real-time methods to estimate system inertia effectively.

Estimation of the synchronous inertial response: PMUs are positioned at synchronous generator buses to directly measure dynamic power and frequency, but these measurements might include additional transients affecting accurate inertia estimation. To address this, a moving average filter with a 200 ms window is applied to the active power signal, ensuring a transient-free signal. The method calculates all synchronous generators' inertial response following a disturbance as shown below:

$$\Delta P_{sg}(t) = \left|\sum_{i=1}^{n} \Delta P_i(t)\right| \tag{1.13}$$

where $\Delta P_{sg}(t)$ is the total inertial power response from the synchronous generators and $\Delta P_i(t)$ is an individual generator's inertial response at a specific time instant t.

Estimation of load inertial response: The frequency-sensitive loads resist changes in frequency by generating damping power, determined by their damping constant. The initial calculation of the Center of Inertia (COI) frequency is explained using (1.14), incorporating measurements from synchronous generator buses and their MVA ratings. Then, the change in COI frequency (Δf) is calculated relative to its pre-disturbance value. Dynamic load operation is modelled based on dependencies on voltage and frequency. The system assumes knowledge of the proportion of frequency-dependent loads, enabling the calculation of inertial response using a specified equation:

$$\Delta P_f(t) = a_f \left|P_{prod}(t) * (\Delta f(t))\right| \tag{1.14}$$

Here, $\Delta P_f(t)$ represents the alteration in active power for the loads affected by frequency changes at the specific time t following a disturbance is the net change in active power in the frequency-dependent loads at time instant t after the disturbance, $P_{prod}(t)$ signifies the total power consumed by connected loads just before the disturbance occurred. Meanwhile, is the net power drawn by the connected loads immediately prior to the disturbance, and a_f signifies the proportion of frequency-dependent loads within the system, where 0 indicates the absence of frequency-dependent loads, and 1 signifies that the entire system consists of only frequency-dependent loads the share of frequency-dependent loads in the system, with 0 indicating no frequency-dependent load and 1 indicating only a frequency-dependent load in the system.

Voltage-dependent loads, like frequency-dependent loads, react to power deviations by adjusting their active power consumption in response to voltage fluctuations at their terminal buses. When power generation experiences an outage, the decrease in reactive power generation can disrupt the voltage profile at various buses. This disturbance causes voltage-dependent loads to alter their power consumption. The calculation for the change in active power consumption caused by voltage variations involves rearranging (1.15), substituting total load with total power generation($P_{prod}(t)$):

$$\Delta P_v(t) = \left|P_v(t) - P_{prod}\right| \tag{1.15}$$

Similarly, $P_v(t)$ is calculated using the modified Equation (4.12) presented below:

$$P_v(t) = P_{prod}\left\{k_1\left(\frac{V_{li}(t)}{V_{li0}}\right)^2 + k_2\left(\frac{V_{li}(t)}{V_{li0}}\right)^1 + k_3\right\} \tag{1.16}$$

The average voltage technique, as introduced in a prior investigation [134], was initially employed to collect voltage measurement data.

Non-synchronous inertia estimation: The inertial power and energy response from the IBRs are considered as non-synchronous inertia in the proposed method. The non-synchronous inertial response differs from synchronous inertia because it cannot be accurately represented as an inertia constant or stored kinetic energy. This response varies for the same frequency event based on factors like fast frequency reserve, RE source converter rating, virtual controller gains, and the type of inertial response. Additionally, there is an intentional 100 ms delay in non-synchronous inertia, unlike synchronous response, which mimics its real-world behavior. In the initial 2 seconds when synchronous machine governors begin responding, the total imbalance is compensated by synchronous, load, and non-synchronous inertial responses. To estimate the non-synchronous inertial response, one can calculate the difference between the active power imbalance caused by the sudden disturbance and the inertial responses from synchronous generators and loads within a predetermined time window, using the provided equation.

$$P_v(t) = P_{prod}\left\{k_1\left(\frac{V_{li}(t)}{V_{li0}}\right)^2 + k_2\left(\frac{V_{li}(t)}{V_{li0}}\right)^1 + k_3\right\} \tag{1.17}$$

where $\Delta P_{Non-SI}(t)$, $P_{dist}(t)$, $\Delta P_{sg}(t)$, $\Delta P_f(t)$ and $\Delta P_v(t)$ are the inertial support from the non-synchronous sources, the disturbance size, the synchronous generators' inertial response, frequency-sensitive and voltage-sensitive load inertial response, respectively. The proposed methodology is summarized in a flowchart as shown in Figure 1.31.

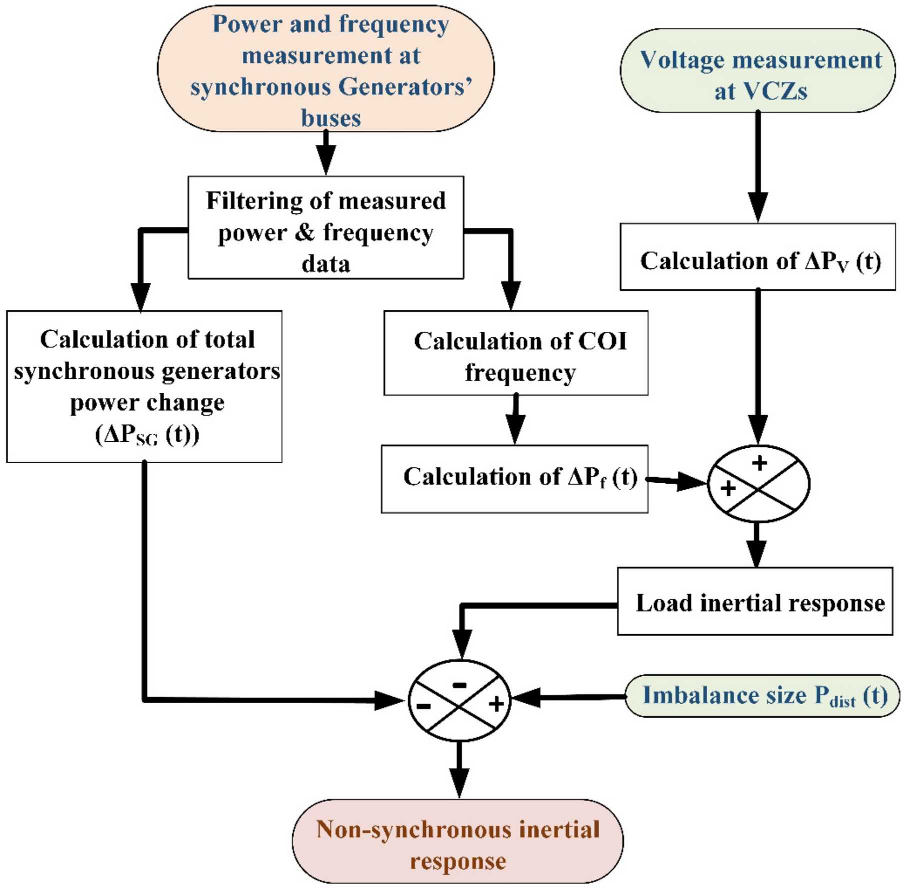

Figure 1.31: Proposed non-synchronous inertia estimation method [26]

1.2.4. Results and Discussions

The devised approach to calculate inertia has undergone validation testing using the adapted IEEE 39 bus New England grid. This standard system comprises ten synchronous generators supplying a combined demand of 6,147 MW. Various operational scenarios were taken into account while applying this method, and the alterations in inertial responses from diverse sources of inertia were examined. Various scenarios of operation have been considered, encompassing two distinct levels of RE integration, defined in relation to the overall power generation percentage. Additionally, three separate frequency disturbance situations have been examined for each level of RE integration. Furthermore, two distinct case studies involving load modeling have been explored, as outlined in. In the proposed study, the wind turbine generators (WTGs) simulated are modelled based on the IEC-type IV(B) dynamic WTG model. These WTGs incorporate a two-loop-based inertial controller that adjusts proportionally to both the rate RoCoF and frequency variation. To simulate the latency inherent in measurement and control responses, a 100 ms delay has been incorporated into the controller. The PV power plant is modeled using the WECC solar PV model, and the identical virtual inertial controller used in WTGs has been employed for this purpose. All the inverter-based resources (IBRs) are linked through grid-following inverters. The modified IEEE-39 bus system, which includes RE plants, three frequency events, and 7 Voltage Control Zones (VCZs) along with their respective pilot buses for voltage measurement, is depicted in Figure 1.32.

Table 1.4: Different Operating Conditions Used in the Proposed Study

RE penetration levels	24% - G_{10} and G_6 of the IEEE- 39 bus system are replaced with WG_1 and WG_3, respectively, and G_7 is replaced with solar PV plant (PV_1)	34% - G_{10}, G_4, and G_6 of the IEEE-39 bus system are replaced with WG_1, WG_2 and WG_3, respectively and G_7 is replaced with solar PV plant (PV_1)
Scenarios	Scenario 1: Generation outage ($G_8 = 540$ MW) at Bus-37 at $t = 5s$ Scenario 2: Load outage (247.5 MW) at Bus-23 at $t = 5$ s Scenario 3: Load increase (540 MW) at Bus-15 at $t = 5$ s	
Case studies	Case Study 1: Frequency influences 60% of the active power load. Regarding voltage sensitivity, the active power load is divided into constant impedance (20%), constant current (40%), and constant power (40%) components. It's important to mention that the reactive power load is comprised of 70% constant impedance and 30% constant power components	Case Study 2: In terms of frequency sensitivity, 60% of the active power load is frequency dependent. In relation to voltage sensitivity, the active power load is distributed as follows: constant impedance (30%), constant current (50%), and constant power (20%). It's worth highlighting that the reactive power load consists of 70% constant impedance and 30% constant power components.

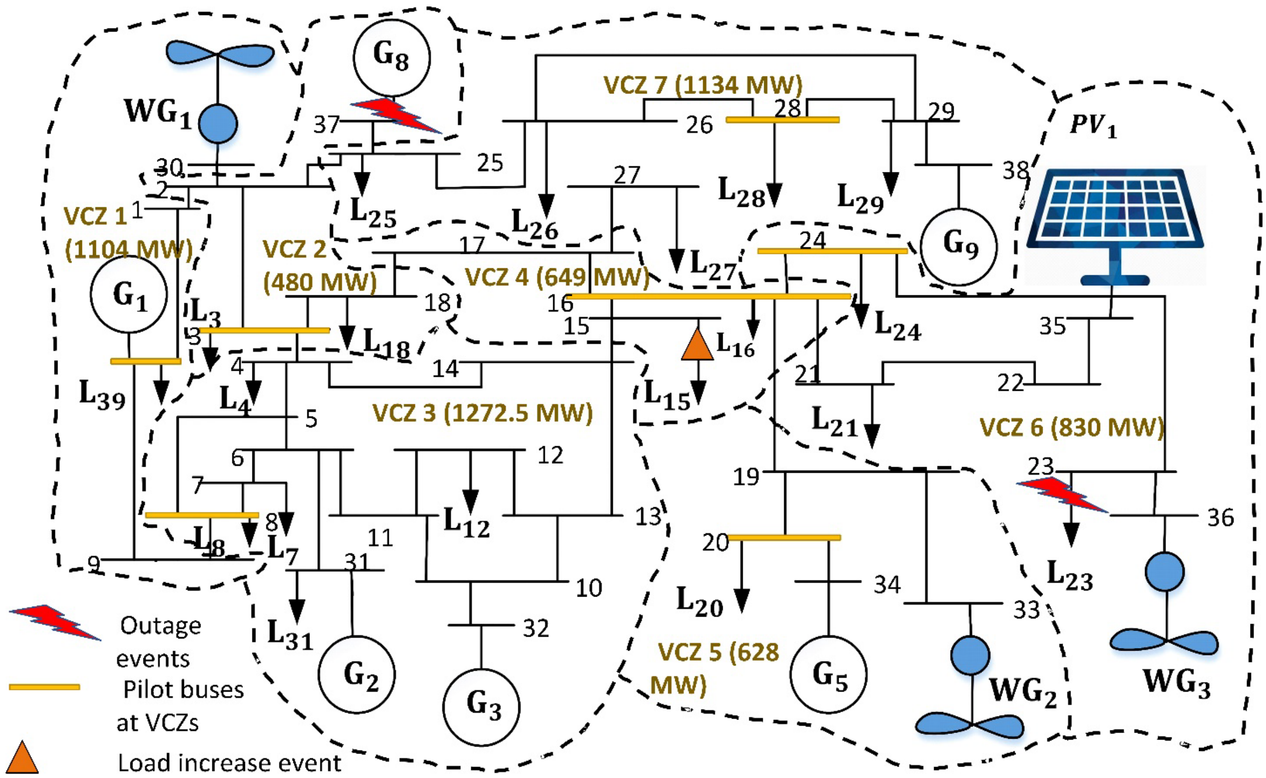

Figure 1.32: Modified IEEE 39 bus system

Estimation of synchronous inertia:

The existing PMUs at each generator bus are employed to measure the change in combined output power of synchronous generators after executing different scenarios. In the instance of a 24% penetration of RE, the deviation in aggregate synchronous power following Scenario 1 in Case Study 1 is depicted in Figure 1.33. During the disturbance's onset, the measured power response displays transients and exhibits a significantly higher peak value (463.6 MW) compared to the actual value (414.4 MW). This actual value is derived by applying a 200 ms moving average filter to the measured power response.

Moreover, the estimated synchronous inertial response, derived through the swing equation using available high minimum-voltage angle (HMVA) data from the generators and RoCoF derived from frequency measurements at each generator bus, is contrasted with the filtered power response, as shown in Figure 1.33. The comparison underscores the need for filtering the power response, as the filtered response closely matches the estimated inertial response for approximately 2 seconds post-disturbance. Beyond this period, the power response deviates due to the engagement of governors. Consequently, the filtered power response within the initial 2 seconds reflects the generators' inertial response.

Furthermore, the utilization of a 200 ms moving average filter on the power response introduces a delay of 178 ms. As a result, the inertial response (measured in MWs) is computed over a 2-second interval, commencing from t=5.178 seconds to t=7.178 seconds, by calculating the area under the filtered power response throughout this duration. This procedure is similarly applied across all operational conditions and is illustrated in Figure 1.34(a).

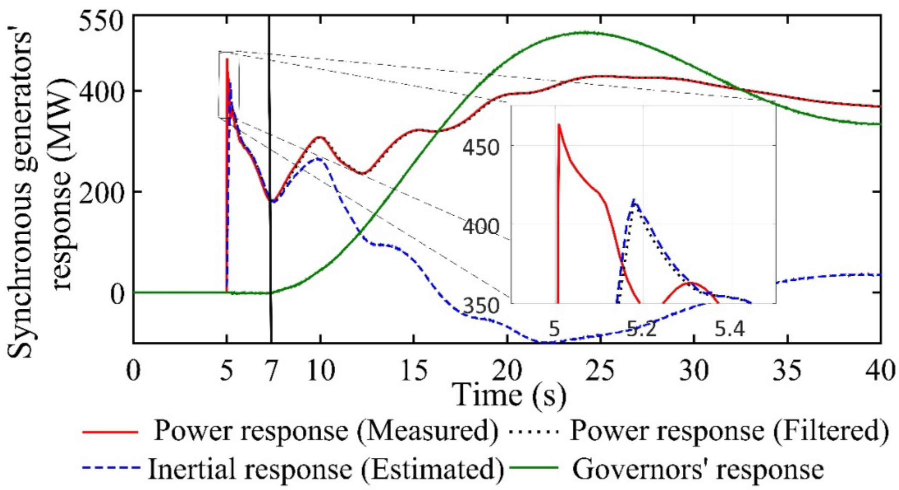

Figure 1.33: Power response of synchronous generators (Scenario I) where 'Measured' refers to power signals directly observed from the simulation and 'Estimated' pertains to the calculated power response.

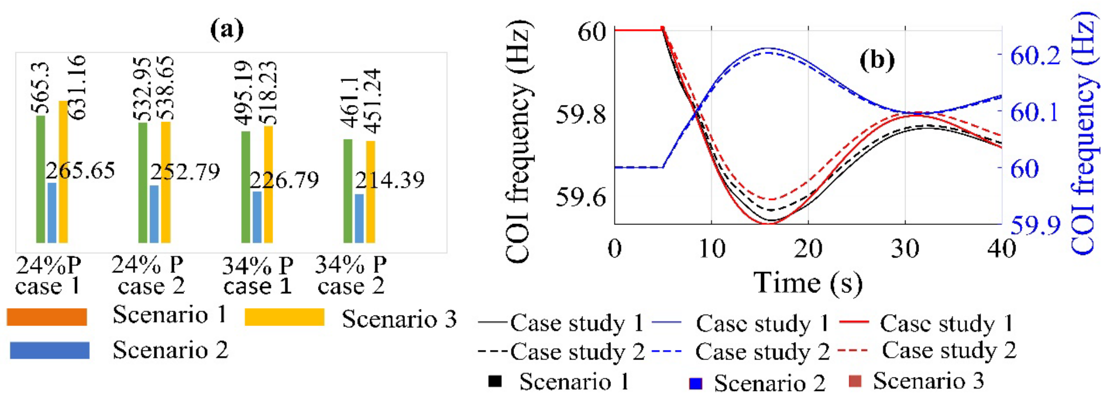

Figure 1.34: The inertial energy reaction of synchronous generators under varying operational circumstances, (b) COI frequency: Scenario 1 (left Y-axis) and Scenario 2 (right Y-axis)

Estimation of load inertial response:

The inertial response arising from loads encompasses the cumulative contributions of both frequency and voltage-dependent loads. To accurately determine the inertial response of loads following a disturbance, it's essential to precisely measure changes in dynamic frequency and voltage across the system. This research focuses on measuring frequency at each generator bus, calculating the Center of Inertia (COI) frequency across various operational scenarios. COI frequency curves for a 24% RE penetrated system under different scenarios and case studies are depicted in Figure 1.34(b).

For accurate dynamic voltage measurement across the entire system, both the average voltage and Voltage Control Zones (VCZ) methods have been employed in both RE penetrated systems. Figure 4.32 illustrates seven VCZs with their corresponding buses, linked active power loads, and pilot buses for measurement. Dynamic voltage profiles at these seven pilot buses following Scenario 1 in the 24% RE-penetrated system are displayed in Figure 1.35(a). Voltage changes over time vary among pilot buses in different VCZs, while voltage changes within a VCZ exhibit similarity, as shown in Figure 1.35(b). This effective implementation of VCZs ensures precise measurement of dynamic voltage system wide. Comparison between the estimated load and non-synchronous inertial responses produced by the proposed methodology and the corresponding plotted curves is conducted.

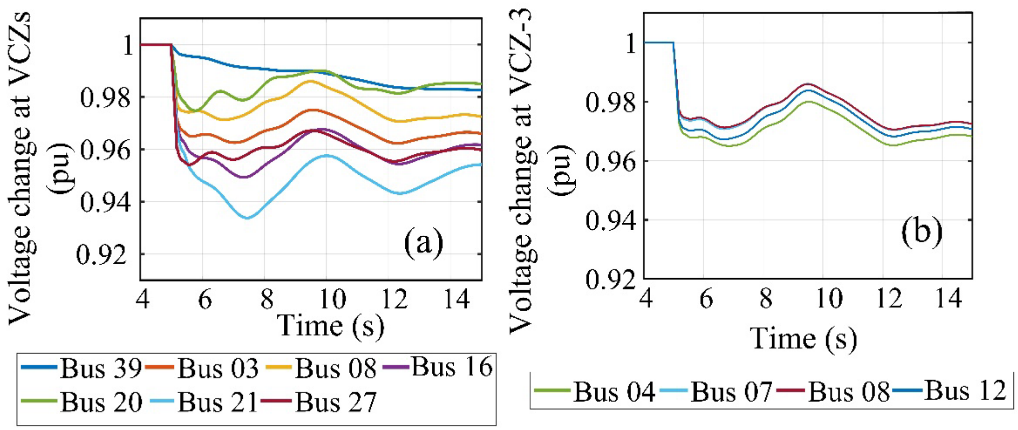

Figure 1.35: Voltage changes for Scenario 1 at (a) pilot buses of all VCZs and (b) all load buses at VCZ-3

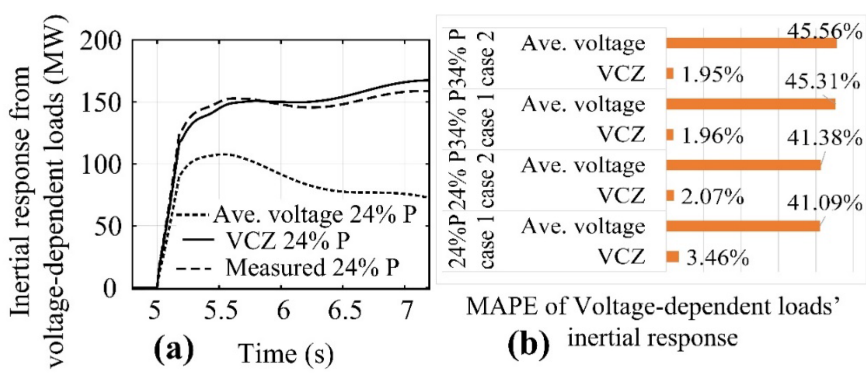

Figure 1.36: (a) Comparison of the estimated voltage-dependent load inertial response derived from voltage measurements using the average voltage method and the VCZ method (Scenario 1), and (b) Assessing the Mean Absolute Percentage Error (MAPE) of the voltage- dependent loads' inertial responses (Scenario 1). (P denotes the Renewable Energy (RE) penetration level.)

In Figure 1.36(a), a comparison is presented between the projected inertial response originating from voltage-dependent loads. This comparison involves the utilization of both the average voltage method and the VCZ method to measure voltage, juxtaposed with directly measured inertial contributions stemming from voltage-dependent loads. This analysis pertains specifically to Scenario 1 within the 24% RE-penetrated system.

Figure 1.36(b) showcases the Mean Absolute Percentage Error (MAPE) for the assessed voltage-dependent load inertia. This MAPE evaluation is conducted across various case studies and RE penetration levels, considering Scenario 1.

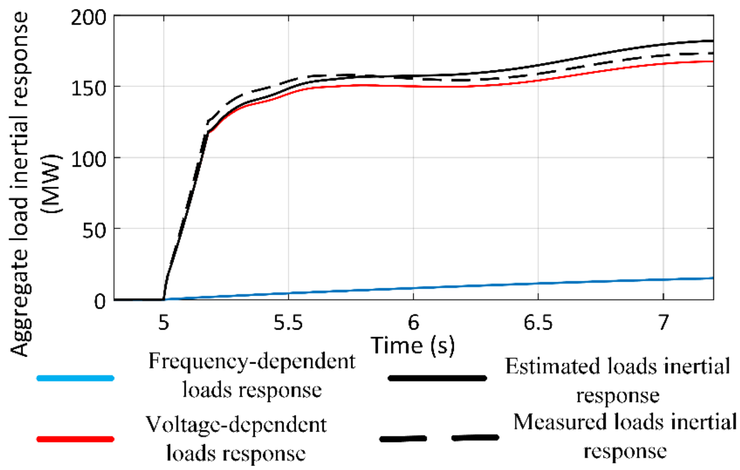

Figure 1.37: Load components of the inertial response (Scenario 1 & Case Study 1)

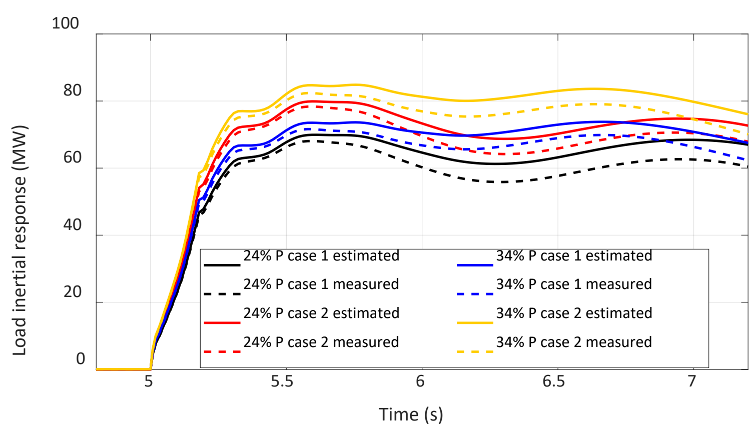

Figure 1.38: Comparison of estimated and measured inertial response of loads.

The study found that the average voltage method is not suitable for estimating inertial responses from voltage-dependent loads, as it results in high Mean Absolute Percentage Error (MAPE) values, exceeding 40%. Moreover, the MAPE increases with higher levels of Renewable Energy (RE) penetration. On the other hand, the VCZ method consistently maintains a MAPE of less than 5% across all operating conditions in Scenario 1. Therefore, the VCZ method is more effective at accurately measuring voltage dynamics throughout the power system and estimating load inertia under diverse conditions. In Figure 1.37, there is a comparison between the inertial responses derived from load components, including both frequency and voltage-dependent segments. This comparison is specifically focused on Scenario 1 and Case Study 1 within the 24% RE-penetrated system, as compared to directly measured load inertial responses.

Figure 1.38 and Figure 1.40(a) further contrast the estimated and directly measured load inertial responses for Scenario 2 and Scenario 3, respectively, highlighting the striking similarity between the estimated and measured responses. Similar estimations have been conducted for inertial responses from loads in other operational conditions.

The Mean Absolute Percentage Error (MAPE) values for the estimated inertial response remain within 4% for Scenario 1 and within 7% for Scenario 2, as outlined in Table 1.5. The load's inertial contributions (measured in MWs) for all operational conditions are detailed in Table 1.5.

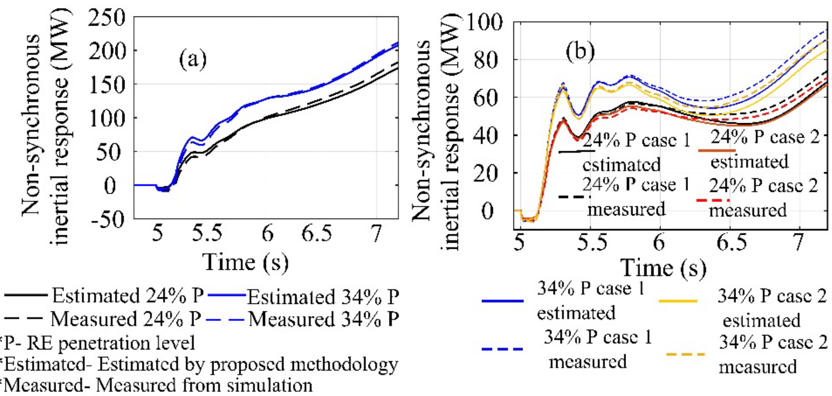

Figure 1.39: Estimated and measured non-synchronous inertial responses: (a) Scenario 1 & Case Study 1, (b) Scenario 2 & both the case studies.

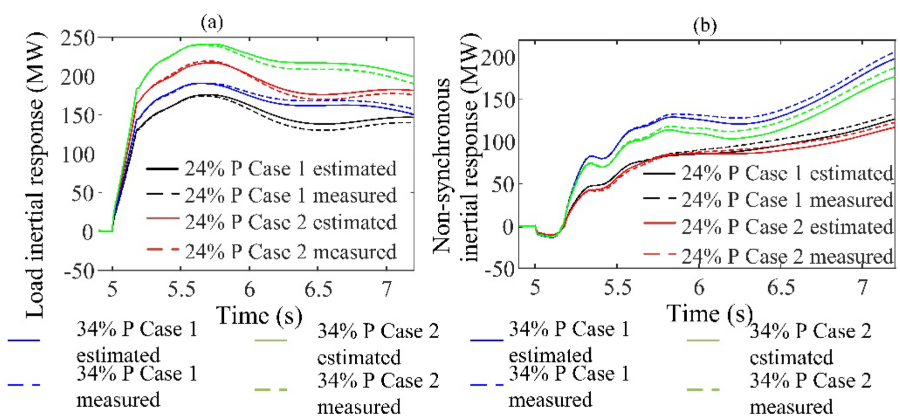

Figure 1.40: Scenario 3 results for both case studies and both the RE penetrations: (a) comparison of estimated and measured load inertial responses, (b) comparison of estimated and measured non-synchronous inertial responses.

Table 1.5: Estimation of load and non-synchronous inertial response

		24% P case 1	24% P case 2	34% P case 1	34% P case 2
Scenario 1	MAPE (Load Inertia)	3.27%	2.04%	1.92%	1.91%
	Load Inertia (MWs)	320.21	355.60	338.27	385.05
	MAPE (Non-SI)	8.57%	8.99%	4.58%	5.44%
	MAD (Non-SI) (MW)	5.16	3.53	3.16	3.58
	Estimated Non-SI (MWs)	206.68	202.47	260.86	247
	Measured Non-SI (MWs)	210.80	199.24	259.61	245.32
Scenario 2	MAPE (Load Inertia)	6.89%	4.84%	4.95%	5.07%
	Load Inertia (MWs)	130.18	146.13	141.2	161.39
	MAPE (Non-SI)	5.42%	8.50%	4.45%	5.19%
	MAD (Non-SI) (MW)	3	4.42	3.05	3.16
	Estimated Non-SI (MWs)	100.93	97.98	127.31	119.72
	Measured Non-SI (MWs)	105.78	104	133.39	126.44
Scenario 3	MAPE (Load Inertia)	4.12%	2.04%	2.43%	2.48%
	Load Inertia (MWs)	305.94	381.57	345.55	440.59
	MAPE (Non-SI)	5.21%	5.41%	3.40%	5.09%
	MAD (Non-SI) (MW)	4.34	4.53	4.75	6.22
	Estimated Non-SI (MWs)	171.03	162.61	254	223.88
	Measured Non-SI (MWs)	179.61	167.71	263.47	236.33

Estimation of Non-synchronous inertia: The study isolates the inertial responses arising from loads and synchronous generators caused by a known disturbance, allowing the determination of the non-synchronous inertial response. This response is then compared between the estimated and measured data in various scenarios and case studies, encompassing different levels of renewable energy (RE) penetration. Figure 1.39(b) and Figure 1.40(b) display these comparisons. Remarkably, all the estimated non-synchronous inertial responses closely match the corresponding measured responses.

1.3. Provision of Voltage Support from RE Generators in converter-interfaced power system

The growing adoption of RE generators (REGs) and their displacement of conventional generators pose significant challenges for the grid operators in ensuring safe, reliable, and stable grid operation. Synchronous generators have traditionally played a dominant role in providing dynamic voltage support to the grid. However, in recent years, the increasing presence of REGs has gradually displaced these generators without significantly compensating for their substantial voltage support capabilities. While devices like line or bus reactors and capacitors can partially assist with local voltage control, their installation is costly, and they lack the flexibility in providing reactive power support compared to conventional generators. Consequently, the reduction in reactive power reserves and diminished dynamic voltage support are inevitable if traditional voltage control methods are maintained.

A commonly employed strategy to address this challenge involves the installation of extra voltage support devices at crucial points within the grid, such as synchronous condensers, as well as flexible alternating current transmission system (FACTS) devices like static synchronous compensators (STATCOMs) and static VAR compensators (SVCs) [27]. However, implementing such solutions necessitates action from TSOs, either by installing these devices at their own cost or by procuring reactive power from the ancillary service market. Moreover, this approach is constrained by the need for multiple voltage control devices in a sizable grid, leading to substantial investments. In contrast, REGs incorporate power electronic interfaces and can flexibly adjust their active and reactive power output over a broad range with fewer constraints. Consequently, in larger power systems, TSOs are gradually devising grid codes that mandate substantial REGs, including Photovoltaic Power Plants (PVPPs), to provide ancillary services support, including dynamic reactive power and voltage support capabilities. Globally, many power networks operate PVPPs in compliance with stringent grid cods, and their provision of voltage support services is often remunerated through appropriate financial mechanisms [28].

PV inverters possess inherent architecture and operational features that enable them to provide reactive power support, both during daylight hours and at night. Typically, it is the large-scale plants connected to transmission voltage levels that are obligated to engage in voltage control, given the requirement of maintaining a suitable voltage profile. While recent research has expanded its focus to include the provision of reactive power support by PVPPs, there remains a lack of comprehensive attention on accurately estimating the reactive power support capability of these PVPPs. Numerous vital factors, particularly ambient weather conditions such as temperature, can significantly diminish the overall power conversion ability of inverters and, consequently, their reserve for reactive power. Additionally, most studies do not account for the individual contributions of PV inverters to overall voltage support or their collective role in meeting grid code requirements at the plant's connection point (POC).

A methodology for accurately calculating the reactive power capability of the PV inverters considering the ambient temperature, solar irradiance, and the terminal voltages of the inverter has been proposed in [29]. The suggested method was compared with the conventional approach currently in use, which neglects the influence of ambient temperature and inverter terminal voltages on the reactive power capacity of solar PV inverters. The outcomes from this study reveal that the ability to provide reactive power undergoes substantial fluctuations throughout the day. Failing to take these variations into account would result in an overestimation of the available reactive power reserve in numerous cases. Using the accurate estimation of the reactive power capacity, a self-adjusting voltage control strategy was introduced for each inverter to ensure the entire plant's effective contribution to voltage support services.

The current work serves as an extension of the study documented in [29]. The research progressed by introducing a centralized system for controlling reactive power in the PVPP. Instead of managing this at each individual inverter terminal, this centralized system calculates the total reactive power support capacity for the entire plant at the connection point to ensure compliance with grid code regulations. To achieve this, a proportional dispatch strategy has been adopted. This strategy assigns references to each individual inverter based on their available reactive power reserves, allowing them to collectively meet the required reactive power support at the connection point. Additionally, this approach takes into consideration losses of reactive power within the plant's internal systems, particularly in the high-voltage transformer that links the PVPP to the grid. Additionally, the strategy incorporates an adaptive voltage-reactive power droop control proposed in [29] allowing PVPPs to provide enhanced voltage support to the grid in critical scenarios. The effectiveness of this approach has been assessed under various conditions, including both stable and dynamic states of the connected grid, accounting for fluctuations in atmospheric conditions.

In typical large-scale power systems, voltage regulation has traditionally relied on the actions of large generators following schedules provided by system operators in advance. However, due to the increasing presence of variable and intermittently operating REGs, TSOs now require these generators to contribute to grid voltage support. In conventional power plants with synchronous generators, the injection and absorption of reactive power are usually characterized as dynamic. Consequently, they have the capability to continuously adjust their reactive power output within a limited power factor range. However, until recently, grid codes often did not clearly define the specific reactive power requirements for PVPPs.

Wind power initially gained prominence before widespread solar PV installations, and as a result, grid-scale wind power plants were typically designed to meet the power factor requirement of approximately ±0.95, aligning with the standards set for conventional generators. Conversely, PV inverters were initially configured to operate solely at unity power factor, mainly because solar PV technology was in its early stages of development. However, with the increasing adoption of PV systems, system operators have started imposing voltage support requirements on PV inverters, similar to those required of synchronous generators. To fulfill these voltage support demands, the inverters need to be oversized and have apparent power ratings that are sufficiently large to provide the necessary reactive power while operating at their rated active power.

Traditional synchronous generators have limitations on their reactive power capability, influenced by factors such as their maximum and minimum loading, thermal constraints due to rotor and stator-current carrying capacities, and transient stability constraints. Only certain generators, referred to as synchronous condensers, could provide reactive power at zero active power load. In contrast, the reactive power capability of a PV inverter is primarily restricted by its current limits based on its design. Having sufficient active power and apparent power ratings enables an inverter to operate at full current while delivering the required reactive power. In essence, PV inverters can offer reactive power support even at zero active power output, like a Static Synchronous Compensator (STATCOM). However, STATCOM functionality is not a standard requirement in grid codes as of now, and PV inverters are typically disconnected from the grid during periods of non-generation.

Several grid codes mandate that a PVPP must continuously produce or absorb reactive power equivalent to approximately 33% of the plant's actual real power output, thereby maintaining a power factor within the range of +/-0.95, as a minimum standard. Power plant controllers (PPCs) within PVPPs are programmed to regulate the reactive power generated by inverters to maintain the specified voltage or reactive power set point on the high-voltage side of the generator step-up transformer. Real-time assessment of the inverter's reactive power capacity is crucial for understanding the PVPP's ability to provide voltage support under varying operational conditions. The specific requirements for reactive power support can vary among different power systems, with some TSOs imposing stricter standards for minimum reactive power based on system strength and related characteristics. Similar to [29], this study has adopted Germany's minimum reactive power requirement as the mandatory criteria for the PVPPs.

1.3.1. Reactive Power Control Modes

PV inverters, similar to other inverter-based resources, can be controlled in one of three modes: reactive power, power factor, or voltage control modes within the limits of the mandated reactive power support [30]. Reactive power and power factor controls are prevalent in distribution networks. However, for facilities connected to transmission networks, such as wind power plants, the Q(V) control or voltage-based reactive power control is typically employed and has also been utilized in this study. The specific droop parameter for the Q(V) characteristic is determined by the system operator based on the system's characteristics to maintain voltage within a practical range. Considering that PV power generation typically reaches its peak in the afternoon, PV inverters are often underutilized for a significant portion of the day. This surplus generation capacity presents a valuable opportunity for PVPPs to actively participate in voltage control as an ancillary service, providing extended reactive power support well beyond the minimum requirements specified in exchange for appropriate financial compensation.

1.3.2. Calculation of Accurate Reactive Power Capability of an individual inverter

To accurately determine the available reactive power reserve within a PVPP, it is essential to precisely assess the reactive power capacity curves of each PV inverter. Achieving a realistic estimation of these capacities entails considering various critical factors that influence the reactive power capability of individual inverters. These key factors are outlined below [29].

- *Impact of solar irradiance and ambient temperature on solar PV array output*: The primary factor influencing the active power of PVPPs is the presence of solar irradiance and the air temperature. In theory, the calculation of active power can be accurately conducted by employing the single-diode model representation of the PV arrays [31]. An increase in irradiance levels typically results in higher power generation. However, this increase in irradiance is often accompanied by a rise in ambient temperature, which in turn elevates the cell temperature, causing a reduction in generated power. Due to these fluctuations, the reactive power reserve can be represented as:

$$Q\_res\ (G, T\_a\ ) = \sqrt{S_r^2 - P^2\ (G, T\_a)} \tag{1.18}$$

  where, S_r is the rated apparent power of the inverter, $P(G, T_a)$ is the active power produced by the PV array connected to the inverter as a function of temperature and irradiance.
- *Impact of air temperature on PV inverter performance:* The inverters' ability to carry current is influenced by the surrounding temperature, as it hampers the dissipation of heat from the power electronics switches to the external environment, resulting in an increase in temperature. To prevent such a scenario that could adversely affect the lifespan of the inverters, PV inverter manufacturers specify the maximum rated power that the inverters can deliver at a given temperature. Manufacturers employ a linear derating characteristic, leading to a complete shutdown of inverter operation beyond a certain threshold. The reduction in current-carrying

capacity is also linked to a substantial decrease in the reactive power capability. Consequently, the thermal derating aspect must be factored into the realistic calculation of the inverter's reactive power reserve, as outlined below:

$$Q\_res\ (G, T\_a\ ) = \sqrt{S_{rt}^2\ (T\_a) - P^2\ (G, T\_a)} \tag{1.19}$$

where, S_{rt} is the derated power of the inverter at a particular temperature.

- *Impact of terminal voltage on inverter reactive power capability:* The terminal voltages of an inverter can affect its reactive power capability by impacting the current magnitude through inverter switches for any value of apparent power. The inverter terminal voltage can be incorporated into the calculation for reactive power capability as follows:

$$Q\_res\ (G, T\_a\ ) = \sqrt{S_{rtv}^2\ (T\_av\ ) - P^2\ (G, T\_a\ )} \tag{1.20}$$

where, $S_{rtv} = V \times S_{rt}$, with V being the inverter terminal voltage, in per unit, typically in the range of 0.9-1.1 pu.

1.3.3. Adaptive Voltage Control Scheme

The conventional fixed droop characteristic for voltage-based reactive power control that complies with the mandatory reactive power requirements can be expressed by:

$$Q_{req} = k_{QV} \times \Delta V \tag{1.21}$$

where k_{QV} is the fixed droop defined by the system operator, and ΔV is the deviation in actual terminal voltage from the reference voltage. However, since solar irradiance is not always at its peak, the inverters could supply/absorb additional reactive power beyond the mandatory requirement. For tapping into this available reactive power reserve, a self-adaptive droop control scheme was proposed for PVPPs in [29], where the droop is adjusted continuously based on the varying reactive power capability of the inverter, as represented in Figure 1.41. Therefore, the availability of enhanced reactive power reserve will offer amplified voltage support, at the inverter terminals, as formulated in the below equation:

$$Q_{req} = k'_{QV} \times \Delta V \tag{1.22}$$

where $k'_{QV} = \frac{\mathrm{Q_{max}}(P, Ta, V)}{V_{max} - V_{db}}$ is the adaptive droop parameter. V_{db} is the voltage deadband maintained to avoid the unnecessary triggering of the control.

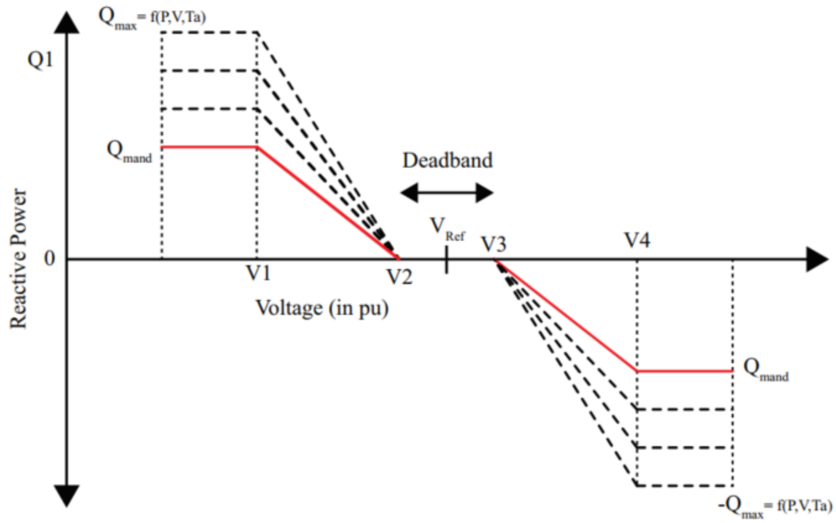

Figure 1.41: Representation of the conventional fixed QV droop and the discussed adaptive QV droop

1.3.4. Proposed Centralized Self-Adaptive Voltage Control Scheme for Voltage Support

The adaptive droop-based reactive power support proposed in [29] has been implemented at the individual inverter terminals. However, this approach overlooks the reactive power exchange within the collector system within the plant and the primary step-up transformer of the PVPP. To expand upon this method, the adaptive droop-based voltage control scheme has been extended to encompass the entire PVPP, as opposed to focusing solely on the individual inverters. Consequently, real-time calculations of the reactive power capability for all constituent inverters are combined to determine the collective reactive power reserve for the entire PVPP.

This approach offers a more comprehensive assessment of the actual voltage support capability of the PVPP at the POC. This is particularly pertinent because the criteria for voltage support are specifically mandated at the POC. The proposed enhancement considers the presence of a PPC, a common feature in most PVPPs today. The PPC communicates with all the inverters in the plant, gathering instantaneous reactive reserves and estimates the required reactive power support based on the measured voltage at the POC, which all the inverters collectively aim to meet while staying within their operational limits. Furthermore, the calculation incorporates the reactive power loss within the plant's step-up transformer and an estimated assessment of the reactive power losses in the AC collector system to ensure the necessary voltage support can be achieved at the POC.

$$Q_{ref,agg} = Q_{ref} + Q_{trafo} + Q_{col} \tag{1.23}$$

where, $Q_{ref,agg}$ is the aggregate reactive power reference for the PVPP, Q_{ref} is the calculated reactive power reference as per the adaptive droop scheme, $Q_{trafo}$is the calculated reactive power loss in the transformers, and Q_{col} is the estimated reactive power losses in the AC collector system.

To determine each inverter's role in providing collective reactive power support, a proportional loading approach has been employed. This method distributes the necessary reactive power reference proportionally among all inverters based on their individual reserves of reactive power to prevent excessive current loading in any of the inverters. After calculating the individual inverters' contributions to reactive power (Q-contribution), the Q-references are communicated back to each inverter's control system with minimal delay through fast communication channels. Each inverter receives both the Q-reference and the P-reference based on the available active power, which is controlled using the appropriate maximum power point tracking (MPPT) algorithm or as directed by the PPC. These references are then compared to the measured values, and any discrepancies are processed through proportional-integral controllers to generate the necessary d-axis and q-axis current set points. Subsequently, these d-q components govern the Pulse Width Modulation (PWM) pulses to regulate the inverter and achieve the desired outcome. The communication diagram for the entire PVPP with the PPC acting as the central controller is demonstrated in Figure 1.42.

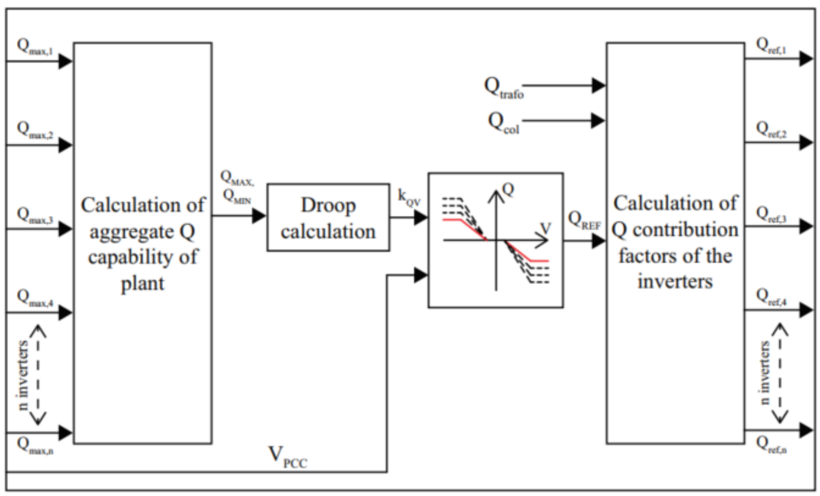

Figure 1.42: Block diagram for the PPC operating as the central Q-controller.

1.3.5. Results and Discussion

In the first stage, the performance of this method in the context of large-scale PVPPs was assessed under steady-state conditions. The evaluation was conducted using a typical irradiance and temperature profile from an actual location over the course of a day. This simulation also included scenarios simulating overcast conditions by incorporating occasional cloud passing events. In the second stage, the effectiveness of the proposed scheme was examined through time-domain simulations involving a large-scale PVPP subjected to grid disturbances. These simulations aimed to assess the transient stability of the control scheme. To validate these experiments, a comprehensive large-scale PVPP was modeled in DIgSILENT PowerFactory. This model included 130 PV arrays, following standard plant design procedures, which constituted the entire intra-plant collector network. Each inverter had a rating of 4.6 MVA and a rated power factor of 0.95. The cumulative apparent power rating of the entire plant amounted to 598 MVA. The voltage control strategy was evaluated within the context of the standard IEEE 39 bus system, where the PVPP was connected to Bus 38, displacing the conventional generator previously connected to it. From the standpoint of active power generation, two modes of operation have been considered in the PVPP, as follows:

- *Mode 1 - MPPT operation:* It is assumed that the PVPP operates in the MPPT mode during the day and extracts the maximum possible power from the arrays.
- *Mode 2 - Power reserve control (PRC):* It is assumed that the PVPP operates in PRC mode by maintaining 10% of its maximum available power as a reserve for potential frequency regulation.

Furthermore, it is assumed that the PVPP operates exclusively during daylight hours and does not participate in nighttime voltage support, which aligns with the common practice in most PVPPs at present.

It was observed that in MPPT mode, the plant could inject the maximum available power, whereas power injection was somewhat limited in Proportional Reactive Current (PRC) mode. Notably, when PRC mode was combined with adaptive voltage control, the PVPP could maintain a higher reserve of reactive power compared to the proposed scheme alone. Additionally, it was noticed that the brief passage of clouds, leading to a reduction in irradiance, promptly increased the reactive power reserve of the inverters and consequently, the PVPP. Therefore, it's crucial to account for the influences of these environmental variables to prevent overestimating the reactive power capabilities of the inverters and potential breaches of grid code regulations under varying conditions.

The PVPP generated more reactive power when employing adaptive voltage control in PRC mode, followed by MPPT mode, as opposed to using fixed Q(V) droop control. This was attributed to the additional utilization of previously untapped reactive power reserves in all inverters. This increased reactive power absorption contributed to improved POC voltages, as illustrated in Figure 1.43, compared to the fixed droop control.

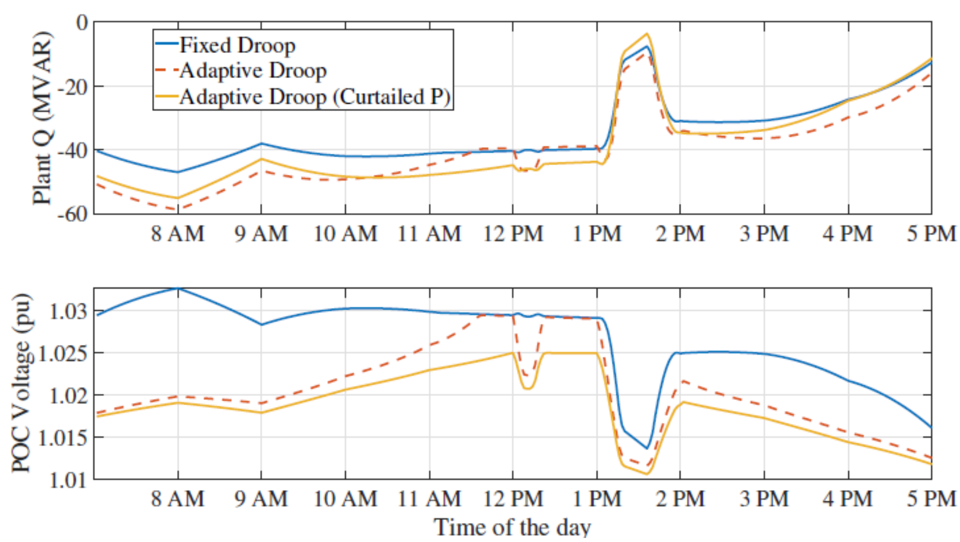

Figure 1.43: Reactive power (Q) response from the PVPP and the resulting PCC voltage under fixed droop and adaptive QV droop control.

1.3.6. Limitations in the Proposed Method

During the implementation of the proposed voltage control method in a typical PVPP, several limitations have been observed. One limitation pertains to the availability of reactive power reserve during midday hours when there is high irradiance, leading to increased active power generation. This situation can potentially result in low voltages at the POC. In such cases, having adequate reactive power support could be beneficial. However, most modern inverters are designed with an oversized apparent power rating and a minimum power factor of 0.90-0.95. As a result, the reactive power reserve for the plant reaches a minimum during these specific hours, leading to an adaptive droop parameter that is nearly equivalent to the fixed droop value. If maintaining a substantial reactive power reserve is crucial, reactive power compensation devices like STATCOMs or mechanically switched capacitors can be considered for installation. These devices can be used during brief periods when inverter-based voltage regulation is limited. Additionally, they can serve as a backup solution during communication link failures between the inverters and the PPC, providing temporary reactive power support. However, it's important to note that installing STATCOMs involves a significant monetary investment, as well as operation and maintenance costs. Therefore, conducting a thorough cost-benefit analysis is essential before opting for this approach. Lastly, the presence of a viable reactive power market is crucial for the successful implementation of this strategy that incentives the plant operator to offer reactive power support as a service.

1.4. Conclusion

This chapter presents an innovative approach for estimating non-synchronous inertia within a power system integrated with RE. This method is specifically designed to capture the distinctive characteristics of virtual inertia responses originating from sources influenced by supplementary controllers, which differ from synchronous inertia. Notable findings and highlights from the study include:

- In larger power systems, a significant portion of the inertial response is contributed by the load, which hinges on its voltage and frequency dependency. By accurately modeling the load, this contribution can be estimated.
- Precise estimation of load-based inertial contribution can be achieved through partial monitoring of the demand side. The Voltage Controlled Zone Virtual Controller Zero (VCZ) technique reduces the number of required voltage measurement Phasor Measurement Units (PMUs), leading to enhanced efficiency.
- Accurate estimation of non-synchronous inertial response post-disturbance, despite operational disparities and response times in comparison to synchronous inertia.
- Direct measurement of RE responses isn't imperative for estimating released non-synchronous inertia originating from Inverter-Based Resources (IBRs).
- Distinct separation of inertial contributions from both the demand side and RE sources following contingencies.
- Introduction of a well-justified time window for data measurement, enabling the estimation of various types of inertial responses.

Further, a methodology is proposed to precisely determine the reactive power capacity of an entire PVPP. This methodology builds upon a previously suggested approach, which leverages changes in solar irradiance, ambient temperature, and inverter terminal voltage to estimate the real-time power generation capability of the inverters. A self-adjusting Q(V) droop control mechanism is implemented aimed at maximizing the provision of reactive power by individual inverters for voltage support services. This control strategy was applied uniformly across a PVPP as a whole, ensuring that the plant can fulfill the required voltage support obligations at the PCC as per the grid code.

2. Distributed control schemes for smart integration of distributed energy resources

In recent times, there has been a notable increase in the adoption of electrification, primarily driven by the widespread installation of distributed energy resources (DERs) and the growing popularity of EVs and heat pumps (HP). The pivotal role of DERs in mitigating global temperature rise has motivated the implementation of policies that encourage their widespread adoption. One such policy is the *salderingsregeling* (net-metering) in the Netherlands, which has facilitated the installation of rooftop solar panels [32]. Under this scheme, households producing more solar energy than they consume can feed the excess electricity back to the grid. At the end of the year, these households receive financial compensation for the surplus solar energy supplied to the grid. This attractive financial incentive has led to a record increase in the deployment of residential solar capacity, with approximately 2 GW installed in 2022 alone [33]. The current geo-political landscape, particularly the Russia-Ukraine war, has also played a role in accelerating electrification efforts. In response to this situation, European Union (EU) nations have been compelled to diversify their energy sources and reduce dependence on Russian oil and gas. In line with the REPowerEU plan adopted by the EU in May 2022, EU member states have collectively achieved significant milestones, including a record high of 41-GW of installed solar energy capacity and a 16-GW increase in wind capacity, contributing to 39% of the EU's electricity generation from RE sources [34].

However, this collective move towards reduced reliance on fossil fuels, the growing adoption of electrification in households, and the rapid expansion of DER installations has led to its own share of negative consequences on the electric grid as well. In the Netherlands, cities like Amsterdam and provinces like Flevoland, Gelderland, and Noord-Holland are experiencing grid capacity limitations and congestion issues [35]. The current congestion of the electric grid in different provinces in the Netherlands can be viewed on the *capaciteitskaart* [36]. Liander, the Distribution System Operator (DSO) in these regions, has stated that they are unable to add new connections due to these constraints [37]. Expanding grid infrastructure seems like an obvious solution, but it poses significant logistical and financial challenges. Liander estimates that the required investments to upgrade the entire grid would amount to billions of euros, and even with such substantial funding, it may not fully resolve all capacity issues [38]. Therefore, DSOs are working on building various mechanisms or frameworks that utilize market-based flexibility to alleviate congestion and to operate the grid whilst providing security against overloading [39]. Market-based flexibility refers to flexibility that can be provided or used by all stakeholders of the electric grid, such as network operators, end users, balance responsible parties etc.

In general, there are two approaches towards flexibility-based congestion management that DSOs are investigating. The first is to develop and implement flexibility frameworks which quantify flexibility and trade flexibility by attributing a financial value to it (the transactive approach). The second is to incorporate congestion management into energy optimization approaches at the low-voltage grid to alleviate grid issues (the optimisation approach).

- In the following subsection of this chapter, we introduce the transactive approach consisting of flexibility frameworks that quantify flexibility into a quantity that can be traded. We also introduce an optimization approach that rely on using demand side management (DSM) techniques to optimize the order of activation of devices.

- In the second subsection, we discuss the promising concept of agent-based control in DSM and explain active and proactive control in the context of DSM with examples.
- In the third subsection, we discuss how various congestion management frameworks make use of both the transactive approach and the optimization approach to alleviate grid problems. Here we discuss existing literature as well as introduce the unique concept of energy modii.
- In the fourth and final subsection, we evaluate the concept of energy modii with a simulation of the Dutch demonstrator site.

2.1. Flexibility frameworks

The emergence of flexibility markets is a response to the increasing integration of RE sources and the need for more flexible and dynamic energy systems. Traditional electricity markets were primarily designed for centralized power generation from fossil fuels, which provided stable and predictable supply patterns. However, with the growing share of variable RE sources like wind and solar, the electricity supply has become more intermittent and less predictable. Flexibility markets aim to address the challenges posed by the variable RE sources by creating a mechanism to balance supply and demand in real-time or near real-time. The goal is to optimize the use of available resources, enable grid stability, and ensure a reliable energy supply even in the presence of fluctuations in RE generation.

Several factors have contributed to the emergence of flexibility markets in the energy sector. Firstly, the rapid expansion of RE installations, like wind farms and solar power plants, has led to an increase in variable energy supply, necessitating the balancing of intermittent generation with demand to ensure grid stability. Secondly, advancements in smart grid technologies, including smart meters, advanced metering, demand response systems, and real-time data analytics, have facilitated better monitoring and control of energy consumption and generation, forming the backbone to set up effective flexibility markets. Thirdly, flexibility markets are closely intertwined with demand response programs and energy storage solutions. Demand response empowers consumers to adjust their electricity consumption in response to price signals or grid conditions, while energy storage allows excess energy to be stored for use during peak demand or low generation periods. Moreover, supportive policies and incentives from governments and regulatory bodies have recognized the significance of flexibility markets in achieving energy transition goals, such as reducing greenhouse gas emissions and increasing RE adoption. Lastly, the integration of DERs, such as rooftop solar panels and small-scale wind turbines, has become more widespread. These resources contribute to flexibility by injecting surplus energy into the grid or providing support during peak demand periods. Altogether, these factors have driven the evolution of flexibility markets, creating opportunities for better grid management and optimization in the changing landscape of energy production and consumption.

The operation of flexibility markets involves pricing mechanisms that incentivize participants to adjust their energy consumption or generation patterns based on real-time grid conditions and energy prices. This allows the grid operator to manage electricity supply and demand in a more efficient and sustainable manner. Flexibility markets are still relatively new and are evolving rapidly. As technology and market mechanisms mature, they are expected to play a critical role in creating a more resilient, efficient, and sustainable energy system for the future. The following subsection presents various frameworks that allow for the exchange of and trade in flexibility by utilizing the advances in information and communication technologies.

2.1.1. FlexOffers

In order to facilitate the exchange of energy flexibility information among different entities within a cell, a standardized representation of flexible loads is necessary. The European project MIRABEL introduced a format called a "flex-offer" [40], [41] to encode this information. Figure 2.1 illustrates a visual representation of a simple flex-offer, where each bar represents a time slice of energy consumption. The lower part of the bar indicates the minimum energy that a flexible resource must provide for its service, while the upper part represents the range within which it can adjust its consumption while adhering to functional constraints like maintaining a specific comfort temperature. This flexibility in the energy amount is referred to as "energy amount flexibility." Additionally, Figure 2.1 demonstrates "time flexibility," where energy loads can be shifted within a defined time interval, indicated by an earliest start time and a latest end time. When a flex-offer is created, it is assigned a baseline schedule, reflecting the preferred consumption pattern of the associated flexible resource. To modify the consumption behaviour of the flexible resource and utilize its provided flexibility, updated schedules can be assigned to the flex-offers.

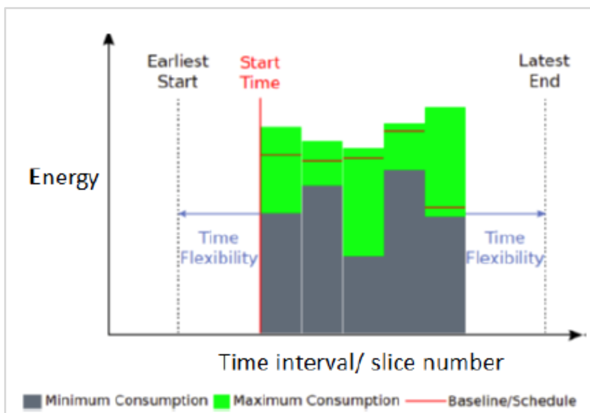

Figure 2.1: A visual representation of the simple Flex-Offer [42]

Flex-offer representation allows for practical exchange of flexibility information between different entities. However, individual flex-offers from specific flexible resources, such as heat pumps or EVs, often represent small loads, making them less impactful for electricity trading, peak shaving, and grid demand-supply balancing, which require higher balancing capacities. To address this, flex-offer aggregation [43] combines flexibilities from multiple appliances, presenting them in a more useful and effective aggregated form with larger energy amounts and flexibility margins. Aggregation is typically performed by BRPs, system operators, or entities known as Aggregators, who receive flex-offers from individual resources and aggregate them.

While the flexibility of aggregated flex-offers may be lower than that of their constituents, this reduction is necessary to simplify scheduling complexity and increase their value on the flexibility market. After aggregation, schedules are assigned to the aggregated flex-offers based on energy sold on the market while respecting inherent constraints. These schedules, specifying exact start times and energy amounts, are then disaggregated to individual flex-offer schedules, and forwarded to the corresponding flexible resources. This entire flex-offer aggregation, scheduling, and disaggregation process is illustrated in Figure 2.2.

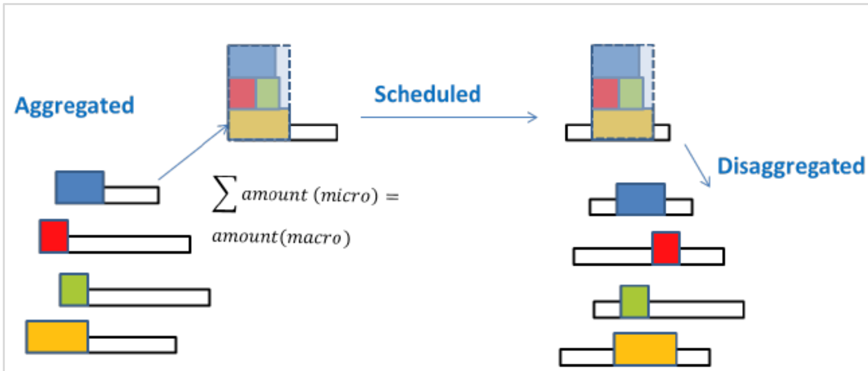

Figure 2.2: Flex-offer aggregation, scheduling and disaggregation process [42]

2.1.2. GOPACS

The growing energy transition and economic expansion are placing higher demands on the electricity grid, leading to increased instances of grid congestion. When the demand for electricity exceeds the grid's capacity, congestion is encountered, where the transport of electricity becomes challenging. Network operators are diligently working to upgrade and expand the electricity network to cope with this rising demand, but this process takes time. To address congestion effectively, GOPACS [44] serves as a valuable tool for grid operators to better match electricity supply and demand, reducing grid congestion.

During periods of congestion, network operators allocate the limited grid space to users. In congestion scenarios, network operators turn to large business customers via GOPACS, asking them to temporarily reduce their electricity consumption or generation for a fee. The freed-up capacity is then redistributed to other users of the grid, creating more space and compensating the customer for the unused capacity during that time, resulting in a beneficial win-win situation.

GOPACS facilitates both large and small market participants to capitalize on their available flexibility and contribute to resolving congestion issues. By fostering cooperation among network operators, congestion resolution in one part of the grid is achieved without causing problems in other areas operated by different network operators. This ensures more efficient and balanced electricity grid management.

There are two possibilities within GOPACS:

1. **Flexibility re-dispatch:** Market parties with a CSP accreditation and an electricity connection in the congested area can place a buy order on a connected energy trading platform (ETPA & EPEX SPOT). However, grid balance at the national level must be maintained. To achieve this, the reduction of electricity production within the congested area is balanced with a sell order from a market party outside the congestion area. Using GOPACS, the system quickly verifies if this order won't cause issues in other parts of the participating network operators' grids. If everything checks out, the network operators cover the price difference between the two orders, enabling them to match on the trading platform and resolve the congestion. Consequently, market parties gain additional income by providing capacity they didn't need at that time, while the network operators

successfully resolve the congestion in the Dutch electricity network, creating a favorable win-win situation for all involved parties.

2. **Capacity-limiting contract:** Market parties with a contract that restricts their capacity with a grid operator submit bids to disconnect the agreed-upon capacity. The specific amount of interrupted capacity and the compensation for doing so are defined in the contract with the network operator.

2.1.3. OpenADR

Next to aforementioned flexibility frameworks, there is also a need to exchange information and control commands to be able to implement such frameworks. Given the fact that a heterogeneous set of devices, from different vendors, needs to be controlled, it is important to also perform standardization of the protocols themselves. By clearly defining the communication protocols and required data, practical feasibility of such frameworks becomes viable.

One such standard is the OpenADR, which stands for "Open Automated Demand Response" [45]. It is an open and standardized communication protocol and framework that enables the automation of demand response (DR) programs in electricity systems. Demand response is a strategy used by utilities and grid operators to balance electricity supply and demand by adjusting or shifting electricity consumption in response to grid conditions or price signals. The OpenADR protocol was developed to facilitate the exchange of information and signals between utilities/grid operators and energy consumers (such as commercial and industrial facilities, residential buildings, and EV charging stations). By using OpenADR, utilities can send signals to participating energy consumers, instructing them to reduce or increase their electricity usage based on grid conditions, market prices, or system needs.

OpenADR offers a comprehensive set of advantages for demand response. Firstly, it provides a standardized format for demand response communications, ensuring seamless interoperability between various systems and devices. Secondly, the protocol enables automated communication and response, eliminating the need for manual intervention during demand response events. Thirdly, OpenADR's scalability allows it to be applied to a wide range of energy consumers, from individual buildings to large industrial facilities, making it adaptable to various demand response programs. Moreover, the protocol's flexibility supports different types of demand response events, such as price-based, emergency, and event-based, enabling utilities to customize their demand response strategies. Lastly, OpenADR's support for near-real-time communication facilitates swift responses to changing grid conditions and pricing signals, enhancing the effectiveness of demand response efforts. OpenADR is widely used in demand response programs around the world, helping to improve grid stability, manage peak demand, and integrate RE sources more effectively. It enables energy consumers to participate in demand response initiatives, contributing to a more reliable and efficient electricity grid.

2.1.4. OpenTherm

OpenTherm is a communication protocol specifically designed for heating systems in residential and commercial buildings [46]. Developed in the 1990s, it has gained widespread adoption in Europe, particularly in countries like the Netherlands and Belgium. The main goal of OpenTherm is to establish a standardized and open interface for bidirectional communication between heating appliances. This communication allows for continuous modulation, providing precise control over the heating system's output and enhancing energy efficiency while ensuring optimal indoor comfort for occupants. A significant aspect of OpenTherm is its adaptability to smart home technologies. It can integrate with modern home automation systems, set customized schedules and even employ data-driven strategies for optimal energy usage. The protocol's compatibility with smart devices ensures that heating systems can be part of a holistic and intelligent smart home ecosystem, providing enhanced convenience and efficiency to users. As a future-proof solution, OpenTherm continues to evolve and align with the latest energy efficiency standards and technological advancements, ensuring that heating systems remain up-to-date and efficient for years to come.

A framework such as FlexOffers offers a way to quantify the available flexibility into a transactive units and a framework such as GOPACS delivers a platform in using such flexibility units can be exchanged for financial renumeration to reduce peaks and grid congestion issues. In the next section, we discuss the energy optimisation algorithms that aim to use the available flexibility to locally alleviate grid issues.

2.2. Optimization frameworks

Flexibility frameworks quantify the available flexibility to be able to engage in trading the same to offset power peaks. In this section we discuss energy optimization frameworks that aim to determine the optimal device activation order that uses the available flexibility to locally achieve DSM objectives such as peak shaving. We discuss various optimization approaches by classifying them, first, on the basis of the type of approach used to achieve the desired objective, and second, on the basis of the control hierarchy used in the approach.

2.2.1. Classification based on optimization approach

Optimization problems in the field of smart grids can be approached using various optimization frameworks, each employing different techniques and algorithms. These frameworks can be classified based on the nature of the optimization algorithm employed and the nature of the control variables in the problem. Several common optimization frameworks, including mathematical solvers, heuristics, game theory approaches, and machine learning approaches, are considered the most used method for finding the management strategies for the problem.

Mathematical solvers are a well-established approach for solving optimization problems in smart grids [47]. One widely used type of mathematical solver is Mixed-Integer Linear Programming (MILP). MILP problems involve optimizing a linear objective function subject to linear constraints, where some or all the decision variables are required to be integers [48]. This framework is particularly useful for problems involving discrete decisions, such as power generation and distribution scheduling, energy storage management, or demand response [49]. MILP solvers employ algorithms that efficiently explore the solution space to find an optimal or near-optimal solution. These solvers utilize optimization techniques, including branch and bound, cutting planes, and primal-dual algorithms, to efficiently handle large-scale optimization problems [50].

Moreover, in several cases, optimization problems can be categorized as either deterministic or stochastic, depending on the variables involved in the problem [51]. Stochastic programming is particularly relevant for optimizing systems involving RE sources due to the inherent unpredictability and correlations associated with these sources [51]. The choice of optimization technique depends on the specific problem type. For example, an integer linear programming problem requires the application of an integer linear technique to derive the optimal solution. However, it's important to recognize that optimization does not guarantee the attainment of an optimal solution in all cases. Certain problems, such as NP-hard problems, may lack feasible solutions [52] or have excessively long computation times [53]. In such situations, traditional optimization approaches and deterministic methods are not applicable. Instead, heuristic approaches can be employed as they offer quick and near-optimal solutions when dealing with highly complex problem settings.

Heuristics do not guarantee an optimal solution, unlike mathematical solvers (deterministic method), but provide fast and near-optimal solutions, making them suitable for complex and computationally demanding problems [54]. Heuristics involve the use of rules of thumb, trial and error, or approximation algorithms to search for solutions iteratively. From the different types of heuristic methods, evolutionary algorithms, role base heuristics, metaheuristics, fuzzy logic, and swarm intelligence techniques are the most used method for energy management problems [55]. These approaches prioritize computational efficiency over optimality and are particularly useful when dealing with large-scale problems with numerous variables and constraints. Heuristic techniques, such as single and multi-objective versions of genetic algorithms [56], particle swarm optimization [57], and fuzzy logic approaches [58], have been successfully applied to various smart grid optimization problems, including power scheduling for different assets in the system, network optimization, and RE integration. Finally, some heuristic algorithms are crafted for a specific task and exploit domain specific knowledge of the problem at hand. One such heuristic algorithm is Profile Steering [59], which efficiently combines knowledge of tree structured power grids with laws of physics to efficiently find (near) optimal operation of low voltage grids.

Game theory approaches offer a unique perspective on optimization problems in smart grids, focusing on the interactions and decision-making of multiple entities within the grid. These approaches model smart grid systems as cooperative or non-cooperative games, where various stakeholders, such as power producers, consumers, and regulators, aim to optimize their own objectives while considering the actions of others [60]. Game theory provides a framework to analyse strategic interactions and derive equilibrium solutions that capture the interdependencies between different decision-makers in the grid. By considering the behaviour and incentives of participants, game theory approaches enable the study of market dynamics [61], pricing mechanisms [55], energy trading [62], and demand-side management [63] in smart grids.

Besides the heuristic and game theory approaches to be used in energy management systems, machine learning approaches have gained significant attention in recent years for their ability to optimize complex systems based on data-driven insights. Machine learning techniques can be employed to model and optimize various aspects, such as demand forecasting, load management, fault detection, and RE integration. These approaches leverage the power of artificial neural networks, reinforcement learning, and other learning algorithms to capture patterns, relationships, and nonlinearities within smart grid data [64]. By training models on historical data and real-time measurements, machine learning approaches can provide accurate predictions and optimize grid operations, leading to improved efficiency, reliability, and cost-effectiveness [65].

2.2.2. Classification based on decision-making hierarchy

In this sub-section, we classify optimization frameworks with respect to the decision-making hierarchy employed in the framework. The three types of control hierarchies are visualized in Figure 2.3.

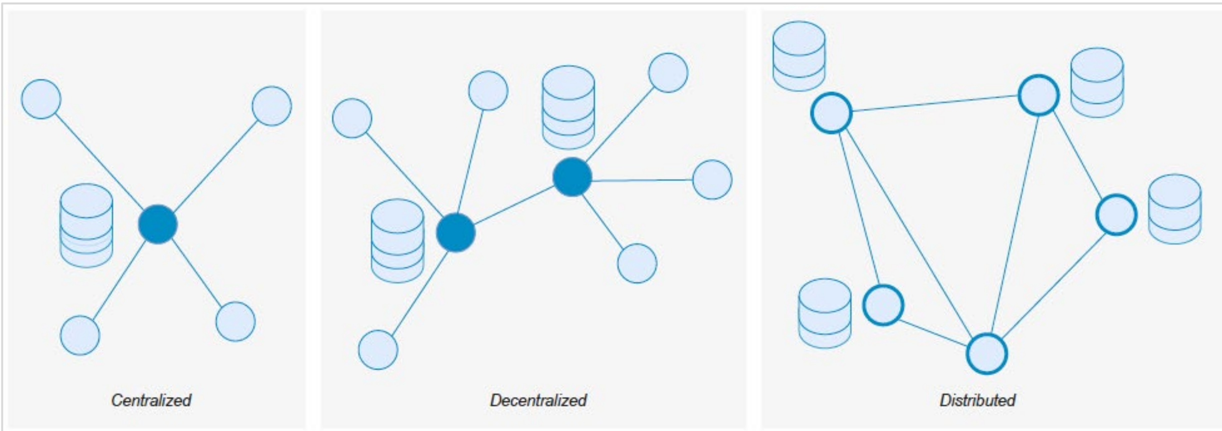

Figure 2.3: Configuration of the 3 network types: Centralized, decentralized and distributed [66]

In a centralized control strategy framework, the decision-making authority and control mechanisms are concentrated at a central entity within the smart grid infrastructure. This central entity is typically equipped with advanced computational capabilities and an optimization algorithm (methods in the previous section). Centralized frameworks provide a comprehensive perspective of the entire smart grid, facilitating optimizing energy management for different assets and prompt responses to unexpected changes or disruptions [67].

The centralized management capacity to apply advanced algorithms and optimization techniques that solve the proposed grid problems is the main advantage of the method [68]. However, centralized control also presents certain challenges. The reliance on a single decision-making entity could lead to potential vulnerabilities and single points of failure [53]. Additionally, the method needs heavy computational resources to manage the large system. It is difficult to employ a centralized controller to control such a large-scale system for many reasons, such as limited communication capability among the subsystems as well as limited computation ability in one single controller [69].

In contrast to centralized frameworks, decentralized control strategy frameworks distribute decision-making authority across multiple localized entities within the smart grid [59]. Each localized entity, such as a microgrid or a smart building, possesses its control system, allowing it to make decisions autonomously based on local data and grid conditions. These decentralized units are interconnected and can collaborate through communication networks to achieve overall grid optimization.

Decentralized control offers several advantages, particularly in terms of scalability, flexibility, and resilience. As each localized entity (child node in decentralized communications) operates independently and all child nodes talk to a coordinator node one level up [70]. Using decentralized and distributed control strategies leads to less susceptibility to single points of failure, making it more robust and adaptable to changing conditions. Moreover, unlike the centralized method in which one of the optimization methods can be used to optimize the management strategy, here, each child can use a different optimization method based on the nature of the problem in that node [53].

Nevertheless, the coordination of decision-making among localized entities can prove complex, necessitating efficient communication protocols and control mechanisms to maintain grid-wide stability [71]. Additionally, the absence of a comprehensive view and shared goals for grid operations in local nodes may result in suboptimal energy management, posing difficulties in implementing global optimization algorithms and resulting in unstable operation of the smart grids [72].

Recognizing the strengths and limitations of both centralized and decentralized approaches, researchers and grid operators have been exploring hybrid control strategy frameworks. These frameworks combine the benefits of centralized and decentralized control to create a more robust and efficient energy management system [73]. In a hybrid approach, certain critical decisions and control actions are still managed centrally, ensuring global grid stability and optimization [73]. At the same time, decentralized entities maintain a level of autonomy, allowing them to respond to local variations and contribute to overall grid flexibility. The hybrid strategy strikes a balance between efficiency and adaptability, making it an attractive option for large-scale smart grid deployments [74].

A step further than decentralization is the concept of distributed systems. In distributed systems no coordinating node is present, meaning that node failure cannot lead to a disruption of the system. Instead, all control nodes organize themselves autonomously and through coordination. This can be done in two different ways: through competition or joint cooperation. For the former, often game theoretical approaches are used to ensure that the actions of individual nodes, even with peer-to-peer communication, lead to stable and desired system behaviour by crafting proper incentives. In cooperative systems, a set of rules is agreed upon by all nodes. As long as all nodes behave accordingly, the system is stable.

An example of a cooperative distributed system is blockchain. Here, nodes collectively find a stable and common view of the system (in this case transactions) through a set of rules. It have been shown that these methods can also be applied to energy management [66]. More specifically, by defining the rules of the system, the decentralized Profile Steering algorithm can be performed in a fully distributed manner by removing the coordinator role and making all nodes jointly responsible for replacing this role. These distributed concepts are explored further in the next section.

2.2.3. Comparing control topologies

Based on the presented literature, the advantages and disadvantages of the different control topologies are summarized in Table 2.1.

Table 2.1: Comparison of advantages and disadvantages of the three network control types

Topology type	Advantages	Disadvantages
Centralized	• Easy to set up and manage. • Clear control and oversight, making it efficient for specific tasks. • Easier to implement security measures.	• Single point of failure; if the central node goes down, the entire network may become inaccessible. • Bottleneck in data transfer and processing, leading to potential performance issues.

		• Scalability limitations as the network grows in size.
Decentralized	• Increased fault tolerance as there is no single point of failure. • Improved scalability since additional nodes can be added easily. • Better resistance to byzantine behaviour or control by a single entity.	• Coordination and consensus challenges when multiple nodes have to agree on decisions. • Potential for data inconsistency and conflicts between nodes. • Initial setup and configuration may be more complex.
Distributed	• High fault tolerance and robustness due to the absence of a single point of failure. • Efficient use of resources as processing and storage are distributed across nodes. • Superior performance and scalability as the network grow.	• Complexity in managing and coordinating a large number of nodes. • Synchronization challenges maintaining consistent data across all nodes. • Higher infrastructure and maintenance costs.

In summary, frameworks such as GOPACS implement the transactive approach to solving grid problems by quantifying flexibility into a transactive quantity for solving grid problems. Energy optimization approaches aim to use the available flexibility to solve grid problems, for e.g., using a heuristic approach to calculate a power profile that is within grid limits. However, the growing proliferation of smart devices in the low-voltage grid has led to an increase in the network size and data traffic. Optimization approaches cannot directly be applied in such a vast and distributed landscape. There is a need for a robust light-weight control system approach that can execute DSM approaches regardless of network issues such as losses, Byzantine behaviours, and device crashes, to name a few problems. In the next chapter, we introduce the concept of agent-based control as a means of implementing energy optimization approaches over a distributed network.

2.3. Distributed control systems

For smaller networks, data traffic and computational demands can be managed with a few controllable nodes. However, with the increasing number of smart devices, network sizes are increasing and the optimization requirements in terms of communication overhead will escalate rapidly. There has been a recent shift towards investigating more scalable approaches to DSM from conventional centralized approaches. In this section, we describe the concept of agent-based control and how it lends to scalable DSM. Thereafter we introduce another approach to DSM classification based on the optimization period of the DSM approach. Note that optimization techniques, as presented before, may be embedded within these agents, but that the exchange of information between agents allows for problem partition to make the overall system scalable.

2.3.1. Agent Based Control

In the realm of control theory, agent-based control is a well-established concept. Since control systems can become quite extensive, especially in the context of smart grids, it is crucial to introduce a structured and modular approach that allows for the development of standalone subsystems that can seamlessly integrate into the larger system. An agent in this context refers to a control algorithm responsible for optimizing the behavior of a group of actuators. This optimization is based on external inputs, which could be information received through ICT systems or even preferences expressed by the end user. Using this input, along with the current state of the system, the agent regulates the actuator(s) accordingly. One of the key benefits of this concept is that models are created and processed locally, enhancing efficiency, and reducing the need for external communication.

In a local setting where there is no interaction with external systems, the system operates autonomously and solely within its local context. A typical example of this is a house thermostat system, where the thermostat controls the heating system and sometimes the domestic hot tap water generation based on preset setpoints provided by the end user. However, for electricity-to-heat integration, these systems need to evolve into agent-based systems that consider external *stimuli*, such as electricity market prices. Consequently, the systems must strike a balance between providing comfort for the end user and ensuring overall system efficiency.

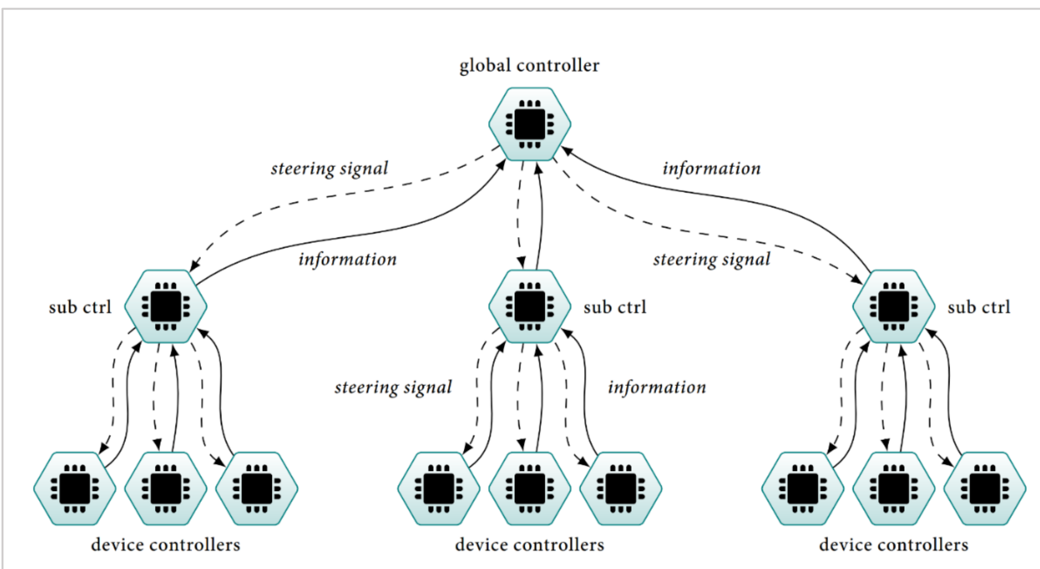

Figure 2.4: A multi-level agent-based system with bi-directional communication [75]

In this context, the external stimuli or steering signals can be viewed as originating from a higher-level steering agent, as illustrated in Figure 2.4. This higher-level agent indirectly controls the system by influencing lower-level decisions. As a result, there is no direct control over actuators; instead, device-agnostic signals are utilized to modify the behavior of lower-level agents. This abstraction level with generic information flows allows the system to be scalable and facilitates the smooth integration of new technologies. Note that this exchange of information can also be provided through the flexibility frameworks and their standardized interfaces, such as OpenADR, as previously discussed. Additionally, the information and models of the actual assets can remain within the low-level agents, limiting complexity since higher-level agents do not need to know and process this detailed information.

Apart from merely sending out steering signals, a higher-level agent may also coordinate its subordinate agents. Similarly, while lower-level agents read sensors and provide information, the higher-level agent can make informed decisions or perform coordinating tasks based on this feedback. An example of this is *transactive energy* [76], a known concept where bidirectional communication ensures that lower-level agents' responses are known when specific stimuli are applied. This can be achieved through mechanisms like auction models and ensures coordination among agents to prevent overreactions and system instability. This concept is applicable to both reactive observation-based control as model-predictive and optimization-based methods. Crucially, in both cases, it is essential to clearly define the information to be exchanged, requiring an interface definition. Furthermore, it is worth noting that these agents do not necessarily have to execute on a specific location or computer system. Instead, they may also be centralized in separate processes, yet they establish a structure that is easy to extend and build upon.

Therefore, a critical aspect of transactive energy management algorithms is the ability of agents to negotiate with other agents on behalf of their respective actuators or devices. One example of transactive algorithm is the PowerMatcher [77].

2.3.2. Classification based on optimization period

Besides the optimization approach and decision-making hierarchy, another classification based on the optimization period is introduced in [78], [79]. The first type, called *active* control, optimizes energy flows only for the next time interval, relying on the last observed system state. The second type, known as *proactive* control, considers multiple future time intervals to optimize energy profiles over a longer span. In [78], refers to these as real-time control and planning-based control, respectively.

Reactive Control - PowerMatcher

One example of a reactive DSM approach is the PowerMatcher [80]. The PowerMatcher is a scalable multi-agent distributed software system designed for near-real-time coordination that targets the increasing number of distributed generators, energy storage systems and demand response units. The PowerMatcher mechanism consists of 4 types of control agents organized in a decentralized hierarchy as visualized in Figure 2.5 [81]. The role of each control agent is as follows:

1. **Device agents:** Devices (washing machines, battery etc.) are represented by a device control agent. Device agents send bids and receive prices. The device agent can change device setpoints based on market prices and create new bids. Essentially, a device agent *transacts* on behalf of the device it represents.
2. **Concentrator agents:** Concentrator agents aggregate bids from device agents below it and sends the aggregated big upwards in the hierarchy. In the other direction, the concentrator agent passes price updates to the device agents in its cluster. The presence of concentrator agents allows for the scalability of the mechanism.
3. **Auctioneer agent:** The auctioneer agent is placed at the top of the decentralized hierarchy and aggregates all the bids to find the equilibrium price. The auctioneer communicates this price downwards to its concentrator agents who in turn, communicate it to their device agents.

4. **Objective agent:** The objective agent interfaces to the business logic of the entire cluster and gives a clear optimization purpose to the cluster. For example, the objective of the cluster can be to minimize CO2 emissions in the aggregate profile or to optimize for a flat aggregate profile. The objective agent steers the cluster towards the pre-decided upon objective.

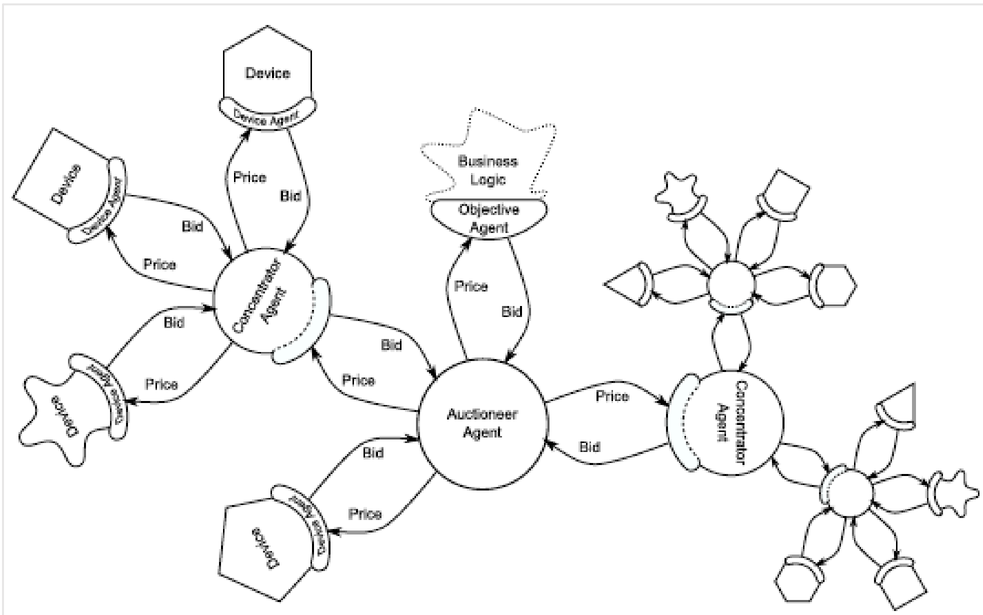

Figure 2.5: PowerMatcher agents arranged in a decentralized hierarchy [77]

The individual actions of local agents, driven by their self-interest, lead to a shift in electricity consumption towards periods with low electricity prices and electricity production towards periods with high prices. Consequently, this creates a situation where the supply and demand start to align on a broader scale within the entire system. The combined bids of all local control agents in the cluster, managed by the auctioneer agent, can be seen as a dynamic merit-order list of all DERs participating in the cluster. Using this list, the most efficient units are selected to respond to specific events. This coordinated approach optimizes the cluster's (near-)real-time coordination activities as a cohesive unit.

Proactive Control - Profile Steering

Profile Steering (PS) [59] is a hierarchical heuristic for scheduling the power profiles of a certain number of child nodes, all of which are linked to a coordinator node. The child nodes can be for example, household appliances such as a washing machine or dishwasher. The coordinator node can be some embedded system added to the smart meter. The PS coordinator agent at the smart meter steers the profiles of the appliances and aggregates them. These aggregated profiles at the household level act as the child profiles at the EC level. The PS agent at the smart meter acts as the child nodes whose profile is steered by the PS agent at the EC level. The hierarchical nature of PS is visualized in Figure 2.7.

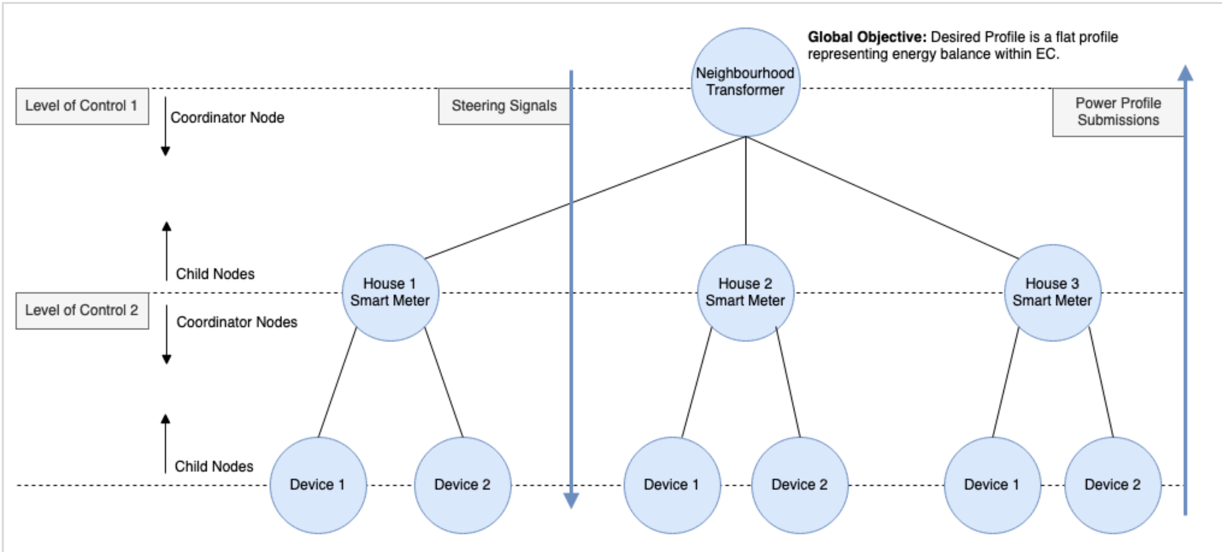

Figure 2.6: Network structure of PS visualized in the form of a low voltage grid example

PS is an approach used for day-ahead planning. The coordinator node at the highest level formulates a global objective for the planning period in the form of a desired profile. This desired profile is sent to its child nodes. As an example, the neighborhood transformer can require a flat profile (e.g., zero profile) at the EC level and send this desired profile as a steering signal to the smart meters of each house. The smart meters act as coordinator nodes for their respective household devices. The smart meter sends the desired profile to the devices, which in turn send their power profiles for the planning period to the smart meter. These power profiles are called candidate profiles or submissions. Profile Steering is an iterative heuristic. In the first iteration, the candidate profiles are aggregated to form an actual neighborhood profile. The goal of the successive iterations is to steer the child nodes to submit new candidate profiles that can lead to an aggregate that is closer to the desired profile. In each iteration, the difference between the desired and aggregated profile is calculated. If the new candidate submission reduces the difference between the actual and the desired profile (leads to an improvement from the previous iteration), then the candidate profile is accepted as the new child profile. The submission of that child node in the aggregated profile is replaced with the new submission. If the aggregate is not improved, then the candidate profile is dropped.

The proactive approach of PS is adaptable across all levels of the grid hierarchy, commencing from the highest level. The benefit of this strategy lies in its initial focus on achieving a locally flat planning approach. For instance, it aims to minimize power consumption fluctuations within each individual house. Only when this local approach proves insufficient and peaks arise at the neighbourhood level, does the neighbourhood planner intervene by requesting houses in that area to contribute towards resolving the issue. The universal applicability of PS is illustrated in the work by Pappu et al. who show that decentralized DSM approaches such as PS can also be implemented over a distributed network [66]. They implement a 3-step approach to achieve the same. Firstly, all algorithmic roles are available for all nodes. Each node can perform the role of local optimization (child node role) and the role of profile selection and aggregation (coordinator role). Secondly, the concept of operational redundancy is applied. During PS iterations, each node executes the role of a child node while also receiving the candidate submissions from all the other nodes. Each node executes the 'coordinator node task' of selecting the candidate profile with the highest improvement in each iteration and merges that candidate into the total aggregate. Lastly, nodes engage in a consensus round to determine which single node's solution is accepted as the truth and stored in each node. The storage itself takes the form of a distributed ledger with the final profiles of each planning period hash-connected to those of the former period for security. The authors showcase the use of different consensus mechanisms from blockchain, such as Proof of Work (PoW) and Proof of Stake (PoS) for achieving the consensus.

2.4. Congestion Management and Energy Modii

2.4.1. Congestion Management Frameworks

In this section, we briefly explain the working of three congestions management frameworks currently being developed and tested in Europe.

PaVn - Germany

The 'Das Proaktive Verteilnetz' (PaVn) is a congestion management mechanism based on the 'Smart Grid Traffic Light Concept' framework published by the German Association of Energy and Water Industries [82]. In this project, localized network congestion is managed using distributed flexibility via an associated communication process between the market and the grid. Figure 2.7 illustrates the traffic light model of PaVn, with the introduction of the yellow regime in the German energy market being the novel contribution.

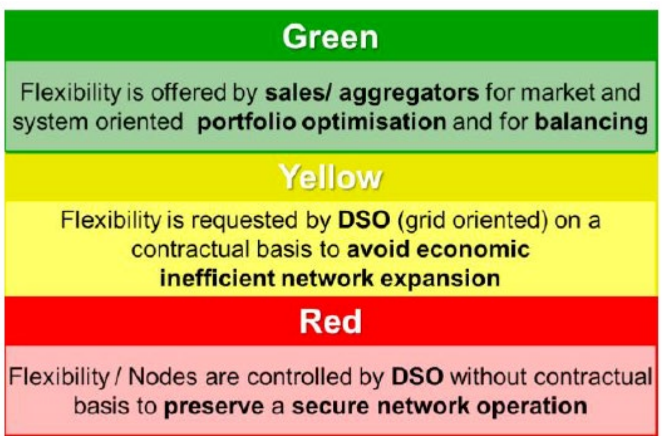

Figure 2.7: PaVn's traffic light scheme for congestion management [82]

Using forecasts, metering data and baseline profiles, the DSO predicts overload and voltage violations for relevant grid sections up to three days in advance. If the DSO discovers an area where congestion is expected, then it publishes a flexibility request to known sources of flexibility. This request is labelled as a *flexibility call* and is announced via a communication and service platform that aims to select flexibility options in a non-discriminatory way. Aggregators then step in to determine whether they can service this flexibility call while maintaining their respective contractual obligations to their customers.

Additionally, to optimize the process further, the DSO gives the aggregator a list of all required flexibility, its types, and technical requirements. This is because flexibility's impact on congestion can vary depending on the grid location, topology, and predicted power flow. To optimize the process of selecting the appropriate flexibility asset for a specific congestion point, aggregators assign a congestion-specific sensitivity to each flexibility type in their portfolio. Marking flexibility assets with a sensitivity value allows the aggregator individually value elements within its portfolio and optimize their assets.

Grid Control – Germany

The aim of the research project 'grid-control – Advanced Decentral Grid Control' was, partly, to develop an integrated process between the market and the DSO for generating load flow forecasts [39]. Extending the traffic light concept Figure 2.8, this research project has developed a non-discriminatory quota-based approach for congestion management with specific solutions for each stakeholder role in the electric grid. Each phase in the traffic light concept has associated rules that guide the interaction between the DSO and the market and flexibility usage, as shown in Figure 2.8. The non-discriminatory quota model is implemented in the yellow phase.

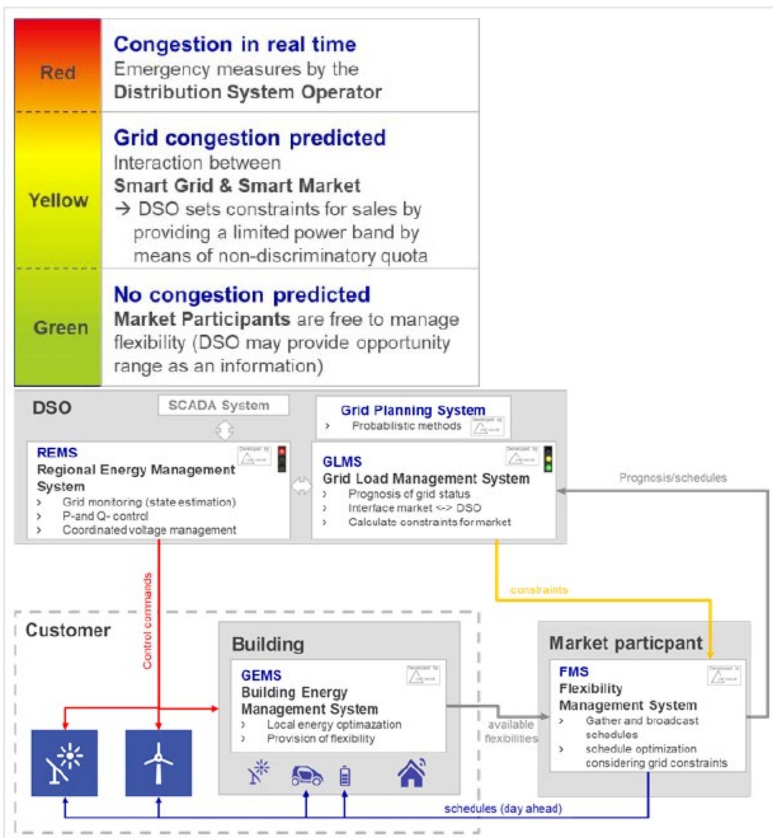

Figure 2.8: Rules for interaction between DSO and market in each phase [39]

The DSO does not participate in the market itself but calculates and provides the constraints for the market action by using the non-discriminatory quota (in yellow phase) or opportunity range (in green phase). The DSO calculates the grid constraints by using the schedules of the market participants and forecasts for inflexible loads/generation units on a quarter-hourly, day-ahead time scale. These constraints are provided to market participants as quotas. When a congestion point is predicted, the market participants use the constraints as part of their regular optimization and either send their final profiles to the HEMS (Home Energy Management Systems) at the prosumer side or directly control the flexibility assets. The DSO identifies multiple grid clusters within the relevant section of the grid to calculate grid constraints (quotas). The cluster levels are based on the network structure and natural congestion areas. Quotas represent the flexibility share that each grid cluster can activate at a certain point in time without causing congestion. Market parties can trade quotas in a secondary market as long as they stay within the DSO's restrictions. Lastly, the DSO directly controls the flexibilities in the red phase.

Universal Smart Energy Framework - Netherlands

The Universal Smart Energy Framework (USEF) was developed to create an inclusive smart energy market that involves all participants, including Distribution System Operators (DSOs) and residential prosumers. This framework introduces a market structure, rules, and tools necessary for integrating flexibility and can be applied alongside various energy market models, extending their capabilities to accommodate both new and existing energy markets. USEF's primary goal is to establish a comprehensive flex market model that incorporates all stakeholders within the energy system. The trading of flexible requirements and offers takes place in this market, with the aggregator role at its centre. Both the Balancing Responsible Party (BRP) and DSO roles have direct access to this market. The aggregated flexibility offered through the market allows for portfolio optimization, Transmission System Operator (TSO) balancing, and TSO/DSO congestion management. The TSO accesses the market through the BRP. The framework's goal is to foster sustainability by ensuring equitable market access and benefits for all active stakeholders. USEF proposes a traffic light concept consisting of four operating regimes as shown in Figure 2.9.

Figure 2.9: USEF's traffic light model with different operating regimes [39]

USEF proposes four operating regimes going from Green to Red in order of decreasing magnitude of free market participation and order of increasingly autonomous participation of the DSO. Optimal use of flexibility is possible for the BRPs (Green and Yellow regimes) and for the DSO (Yellow regime). In the

Orange regime, the DSO plays can make decisions to curtail loads in order to avoid an outage in case the Green and Yellow market-based flexibility trading is unable to avoid a congestion point.

2.4.2. Energy Modii

The increasing intermittency of the electric grid and the congestion and scarcity issues being faced by the electric grid showcase the importance of incorporating information about such undesirable situations in the planning itself. Having information about undesirable scenarios as part of the planning signal can help the EMS of a household and a community to appropriately activate flexibility and better prepare for an undesirable event. Such a planning signal can be sent from higher-level fleet controllers to child controllers for the children to incorporate into their planning. Thus, the concept of energy modii can be implemented within a decentralized control hierarchy to protect the EC grid from foreseen and unforeseen problems.

There are 4 different energy modii defined in terms of mathematical formulations. They are (i) connected, (ii) congested, (iii) scarcity and (iv) islanded. Of these four, the connected mode is the only desired mode and the other three are undesired modes.

2.4.3. Definitions of the four modes

A mode refers to a specific state that the grid arrives in at a given time. The grid can be classified into four distinct modes, as elucidated below, depending on the overall energy demand or power values it experiences.

Connected Mode

The Connected Mode is the only desired mode. It is characterized by two key conditions. Firstly, the power flowing through the transformer is within its limit (the power condition). Secondly, the energy demand of the community must be met with its own DERs and/or the energy supply from the external grid (energy balance condition).

Congested Mode

An EC is said to be in Congested Mode when the aggregated power level in a certain time period is higher than the power rating of the transformer in that time period.

Scarcity Mode

An EC is said to be in Scarcity Mode during a certain time period, when the energy demand of the community exceeds the available energy supply in that time period.

Disconnected Mode

An EC is said to be in Disconnected Mode during a certain time period, when the physical connection with the external grid is not available during that time period.

2.4.4. Theoretical definitions for energy modii

$\vec{p}$ is the day-ahead aggregated power profile of the neighbourhood. If we assume N total intervals in 1 day ahead planning, then $\vec{p}$ can be defined as a vector of N samples, going from 0 to N-1.

$$\vec{p} = [p_0,\, p_1, \ldots,\, p_{N-1}] \tag{2.1}$$

A positive power value represents power production, and a negative power value represents power consumption.

$\vec{j}$ is the day-ahead aggregated energy profile of the neighbourhood. The energy profile is defined as a vector of N samples, each sample representing the energy consumed or produced in that interval. A positive value represents energy consumption, and a negative value represents energy production.

$$\vec{j} = [j_0,\, j_1, \ldots,\, j_{N-1}] \tag{2.2}$$

Furthermore, we distinguish between the aggregated energy profile of the neighborhood and the energy profile (availability) from the main grid or the external grid.

$\vec{j}_{grid}$ is the energy supply from the main grid for N intervals.

$\vec{j}_{ec}$ is the energy demand of the EC for N intervals.

The day-ahead planning is done for N time intervals. It consists of N-1 samples. A contiguous set of time intervals defines a time period. An energy mode is defined as a state the grid is in during a certain time period. Thus, an energy mode can apply for 1 or more contiguous intervals of time. This is visualized in Figure 2.10. It is important to note that the energy mode time period $\{0,1, \ldots M-1\}$ is always part of the the day-ahead time period $\{0,1, \ldots N-1\}$.

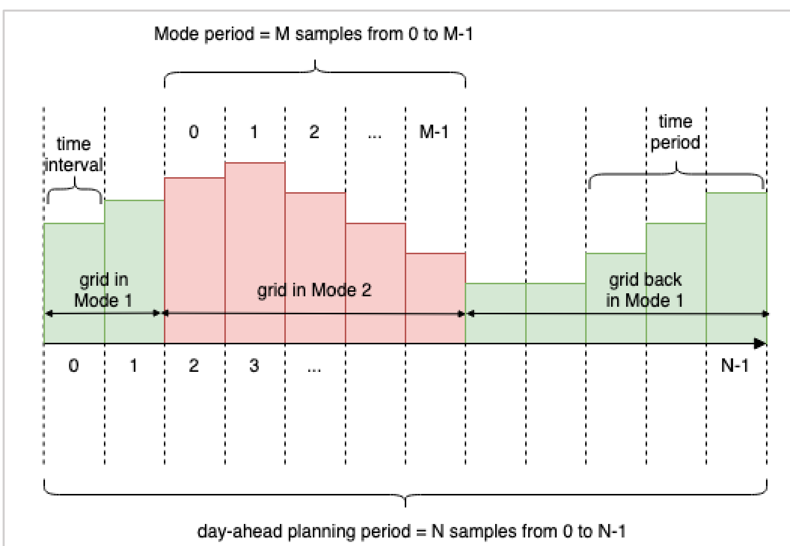

Figure 2.10: A day-ahead planning of N intervals consists of one or more energy modii. Each modii stretches over one or more time intervals (M intervals).

Using these variables, Table 2.2 puts forward the theoretical definitions of each energy modii.

Table 2.2: The four physical EC grid energy modii and their theoretical definitions

Grid mode	Nature	Domain	Explanation	Theoretical description
Connected	Desired	Power	Power via transformer is within limits.	$\vec{p}_k < \vec{p}_{upper}$ $\vec{p}_k > \vec{p}_{lower}$
		Energy	Energy consumption of EC is fulfilled.	$\vec{J}_{ec_k} < \vec{J}_{grid_k}$
Congested	Undesired	Power	Power via transformer is exceeding cable power limit.	$\vec{p}_k > \vec{p}_{upper}$ and / or $\vec{p}_k < \vec{p}_{lower}$
Scarcity	Undesired	Energy	Energy consumption of EC cannot be fulfilled by external main grid.	$\vec{J}_{ec_k} > \vec{J}_{grid_k}$
Disconnected	Undesired	Energy	Connection with the external grid is broken. This mode can be a result of the Congested Mode.	$\vec{p}_{upper} = \vec{p}_{lower} = 0$ $\vec{p}_k = 0$

2.4.5. Modii mitigation strategies

The connected mode is the desired energy state of the EC, enabling periodic forecasting for undesired modes. It serves as preparation for the remaining three undesired modes and includes both regular PS planning and backup plans for grid congestion or energy scarcity. These backups are activated promptly during predictable intervals when undesired modes may occur.

To manage congestion intervals, understanding their nature is crucial. For example, excess PV production from the community can lead to congestion if the production exceeds the transformer power rating. Increasing the community's energy sink potential can be achieved by charging batteries or raising the end state of charge for EVs, since they act as buffer devices. On the other hand, congestion can also be triggered by excess demand from the community leading to power peaks. A DSM algorithm such as PS can shift flexible devices in time to reduce the power peak below the rated value. If necessary, demand curtailment strategies, like reducing EV end state of charge, can be implemented. These mitigation strategies aim to resolve undesirable scenarios at minimum compromise to user comfort.

The Scarcity Mode can be triggered if the EC's energy demand is higher than the available energy supply. In such a scenario, demand curtailment strategies are activated. Flexible devices are utilized to bring the net community demand within the available energy capacity. Optimization algorithms can simulate various demand reduction options, considering their mitigation potential and impact on user comfort. The choice of which demand reduction options can be left to the end user.

In disconnected mode, the EC grid is physically isolated from the external main grid, possibly due to unsuccessful congestion mode mitigation strategies. Demand curtailment strategies become more extreme in this mode, with critical devices receiving priority energy allocation while moderate and least important devices may get minimal or no energy. Energy rationing measures are collectively implemented by the HEMS of all houses in the EC, highlighting the need for clear target-specific user feedback. Investing in energy storage and optimizing its size is crucial in this mode, such as setting a non-usable lower threshold for emergency energy that is reserved for energy rationing in Disconnected Mode. The energy modii with their respective mitigation strategies are visualized in Figure 2.11.

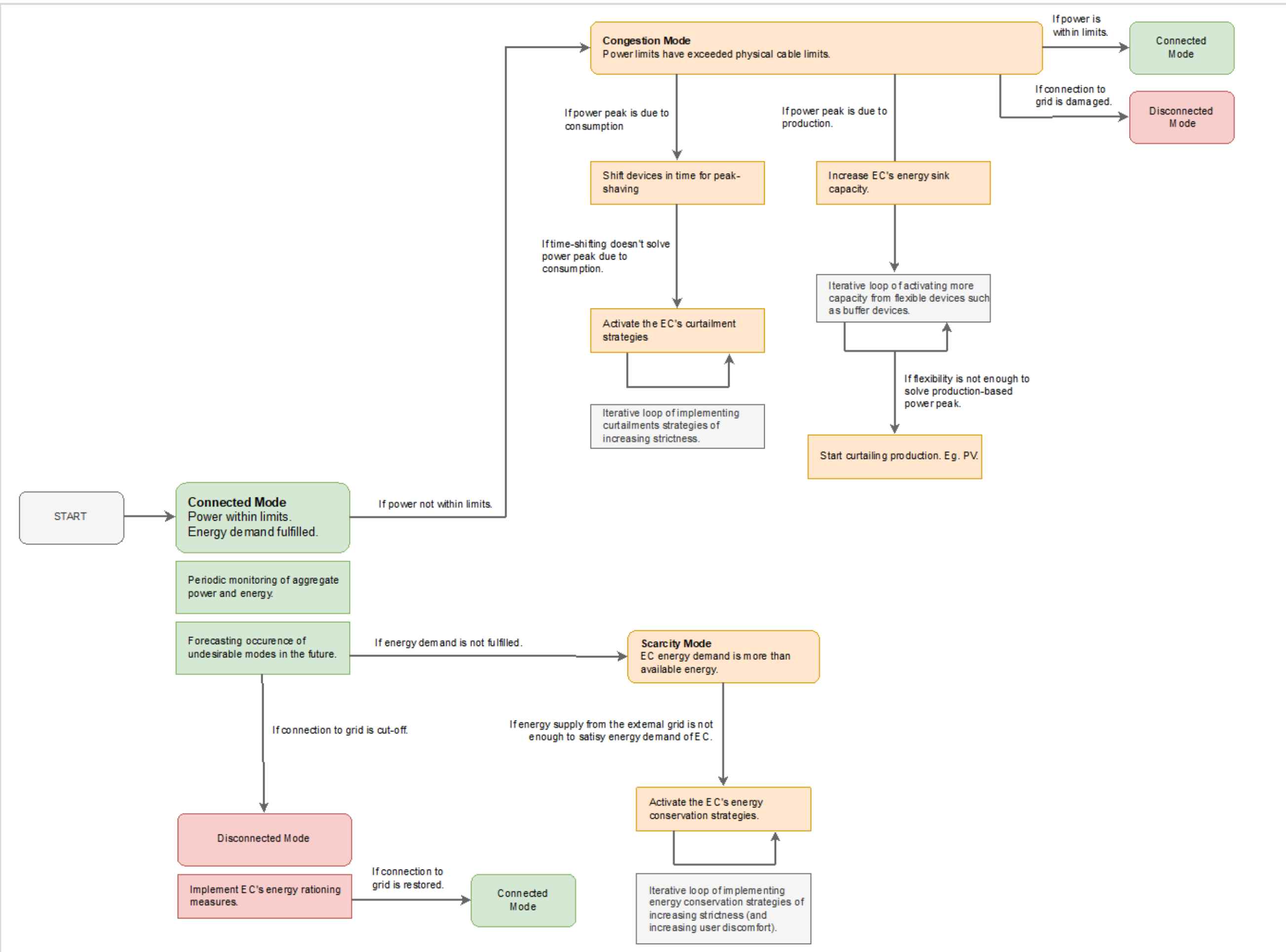

Figure 2.11: The four energy modii with their respective mitigation strategies

2.5. Evaluation

2.5.1. Dutch Demonstrator – Vriendenerf

Vriendenerf is an energy community located in the municipality of Olst-Wijhe. The Vriendenerf community consists of 12 houses for the elderly and one central common building where the community gathers. The 12 houses are built with a focus on sustainability in mind. The following sustainability measures have been taken:

- The installed PV panels produce 6400 kWh/year for a single corner house and 5600 kWh/year for a single in-between house on average.
- Of this annual PV yield, it is estimated that annually 3500 kWh is used for heating, cooling, ventilation, and domestic hot water production.
- The houses are built according to the “Zero-on-the-Meter" (ZOM) or “Zero Energy Building” (ZEB) principle; each house produces as much energy as it consumes yearly. This energy balance is calculated for which an average thermostat setting of 20 °C is taken, as well as 150 litres of hot water is stored and consumed every 24 hours.
- The houses in Vriendenerf are designed to minimize energy consumption for space heating. This has been achieved by three design decisions:
    a. High insulation factors
    b. Heat recovery ventilation system
    c. Heat pumps with a ground heat exchanger networks.

The main demonstrator specifications are as follows:

- 12 houses divided into groups of 3 as shown in Figure 2.12.
- 69 PV panels for each group of 3 houses.
- Each house is equipped with a heat pump, domestic hot water storage and ground source.
- Houses are fully insulated.
- Equipped with active air ventilation system.
- 5 EV charging stations.

Figure 2.12: 4 groups of 3 houses and 1 common house

2.5.2. DEMKit

DEMKit [75] is an open-source toolkit for simulating and conducting real-world experiments on smart grids and energy flexibility. Designed with as a cyber-physical systems approach, it includes diverse algorithms to optimize and coordinate power profiles among different devices. It serves as a versatile tool for modelling the energy grid, its flexible entities, and implementing energy optimization and planning algorithms. In DEMKit, the energy grid can be modelled modularly and hierarchically. Each device, such as a battery, has its own controller agent, making the model scalable and adaptable to changes in components. This allows for the modelling of various physical device structures within a microgrid. In addition to the physical part, DEMKit includes modeling components for the digital system, using an agent-based approach. This hierarchical structure enables bidirectional communication between devices and their respective agents with higher-level controllers. For instance, household devices and controllers communicate with a group controller at the household level, which, in turn, communicates with a group controller at the neighbourhood level. Each controller serves as both a child to a higher-level coordinator controller and a coordinator controller to lower-level child controllers. The control methods encompass optimization algorithms like Profile Steering (proactive control) [59] and double-sided auctions such as in PowerMatcher (reactive control) [80]. The modular design allows experts to test various algorithms and control strategies on the same physical model. Refer to Figure 2.13 for an illustration of such a model.

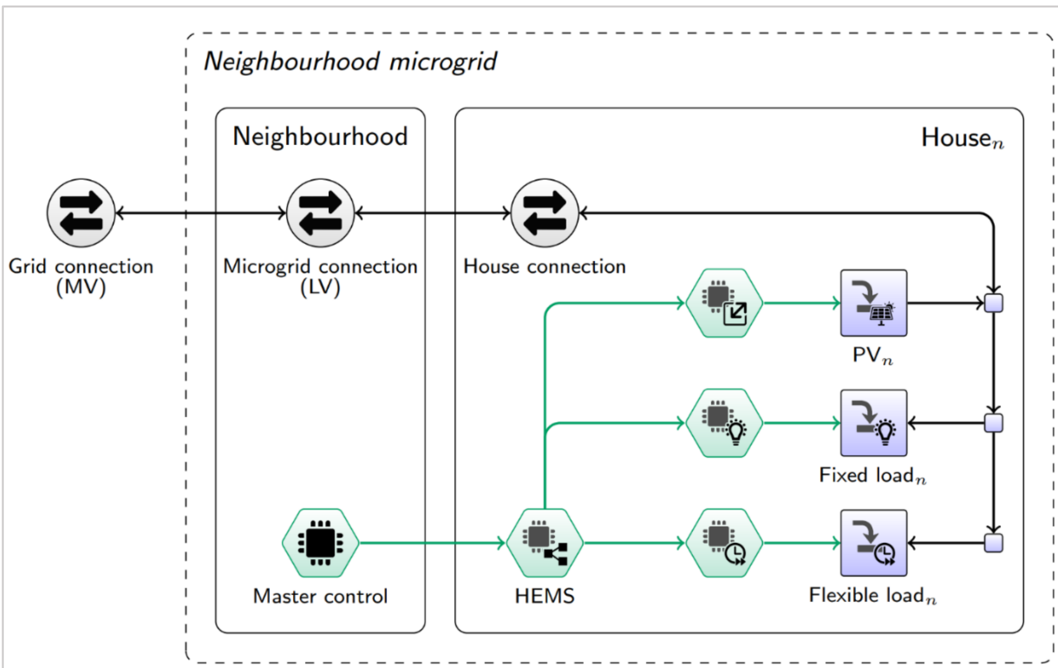

Figure 2.13: Generic DEMKit model for a household. Blue rectangles indicate physical device models, green hexagons indicate optimization algorithms and controllers controlling the devices [83]

2.5.3. Vriendenerf DEMKit model

A DEMKit model was created for the 13 houses in the Vriendenerf EC. Each of the 12 residential dwellings were allotted an EV with 42 kWh capacity and 7kW charging power. The 13th dwelling is a common house (non-residential) and was not allotted an EV. All 13 dwellings were allotted a battery with 10kWh capacity and 10kW charging rate (1C) and a 150 L buffer tank. Lastly each of the 12 dwellings were assigned 23 PV panels and the common house was assigned 14 panels mirroring on-site information. These are the base parameters of our simulation and are illustrated in Table 2.3.

Table 2.3: Model parameters for Vriendenerf baseline model simulation

EV	12 houses have EV EV with 42 kWh capacity, 7 kW charging power for each house. Common house (13th dwelling) not assigned an EV
Battery	All 13 dwellings have a battery Battery capacity 10kWh per house 1C Rate – charging power 10kW
Heat pump	150 L buffer tank per house
PV	23 panels per house, 260 Wp each = 5.98 kWp total for each of the 12 houses 14 panels for common house, 260 Wp each = 3.64 kWp 0.975 inverter efficiency.

2.5.4. Simulating energy modii - Connected Mode and setting congestion limit

We begin by simulating the first 7 days of January with 50% of the dwelling battery capacity allotted to the PS algorithm (Figure 2.14). This means 50% of the 10kWh battery capacity per dwelling is controlled by the PS algorithm. The minimum power value (production) in Figure 2.14 (production) is -5.4 kW. It is important to note that normally an operator (e.g., aggregator) might only use 50% of the battery to ensure that on unpredictable days it has enough flexibility to make up for the forecast errors (imbalance penalties). However, in this case, we consider the avoidance of comfort loss due to the announced modii as more urgent, allowing for the larger capacity to be allotted to PS in planning when an undesirable modii is detected. This is demonstrated in the successive steps of the simulation.

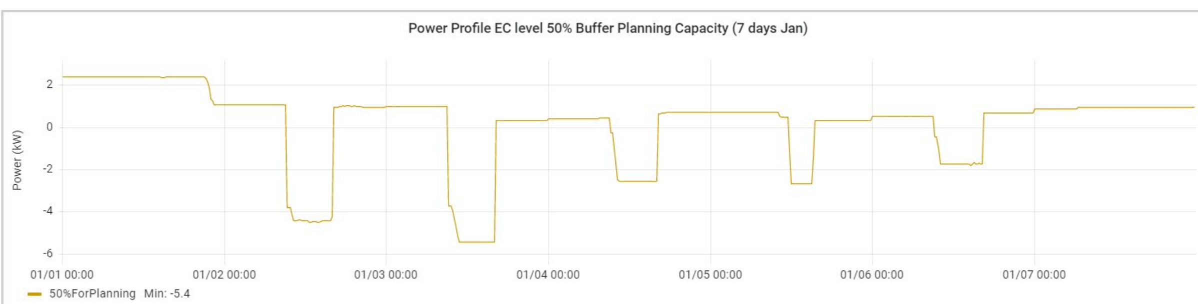

Figure 2.14: First 7 days of the Vriendenerf demonstrator DEMKit simulation

Using this simulation, we set a congestion limit of -4.4 kW, as illustrated in Figure 2.15. This leads to 2 instances where the planning crosses the negative congestion limit triggering the undesirable Congestion Mode. These 2 instances are marked in Figure 2.15. Therefore, a congestion mitigation strategy needs to be activated to (re-)plan a power profile within the congestion limits.

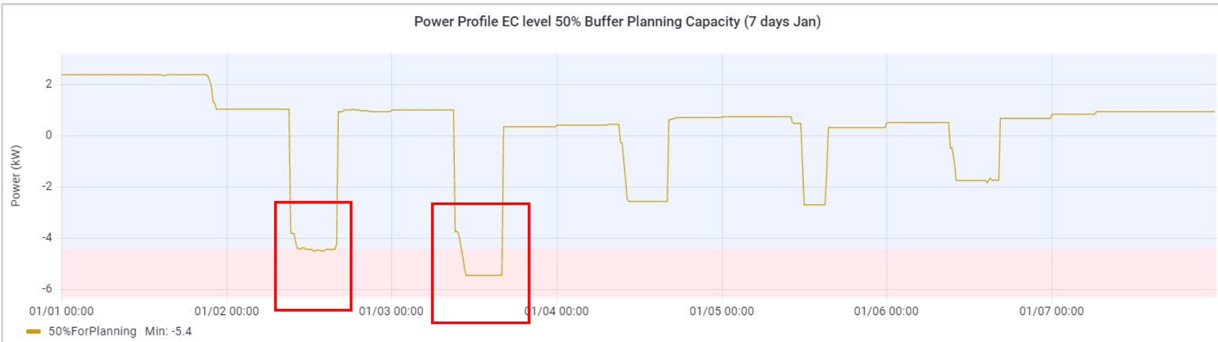

Figure 2.15: Congestion limit set to -4.4 kW. Red marks the undesirable Congestion Mode

2.5.5. Investigating energy modii – Congestion Mode

The buffer storage is used to activate congestion mitigation measures in the Vriendenerf EC. Figure 2.16 illustrates simulations for the 7-day period but with 75% buffer capacity allotted to the PS algorithm. Allotting 75% buffer planning capacity to the PS algorithm mitigates the first congestion point bringing the power profile within the -4.4-kW limit. However, 75% buffer planning capacity reduces the second congestion point but is not enough to bring it within the -4.4-kW limit. Figure 2.17 shows the effect of increasing the buffer planning capacity to 90%. This allocates more planning capacity to the PS algorithm and mitigates the second congestion limit as well.

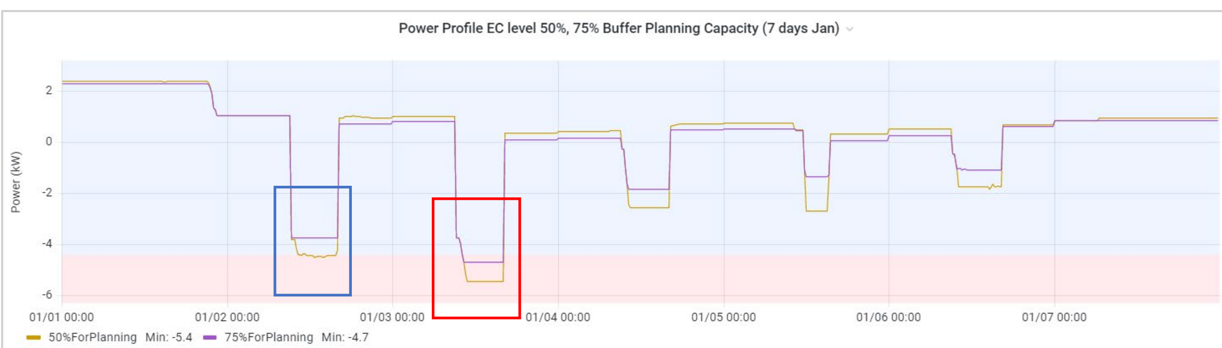

Figure 2.16: Changing 50% buffer planning capacity to 75% helps mitigate the first congestion point in the planning

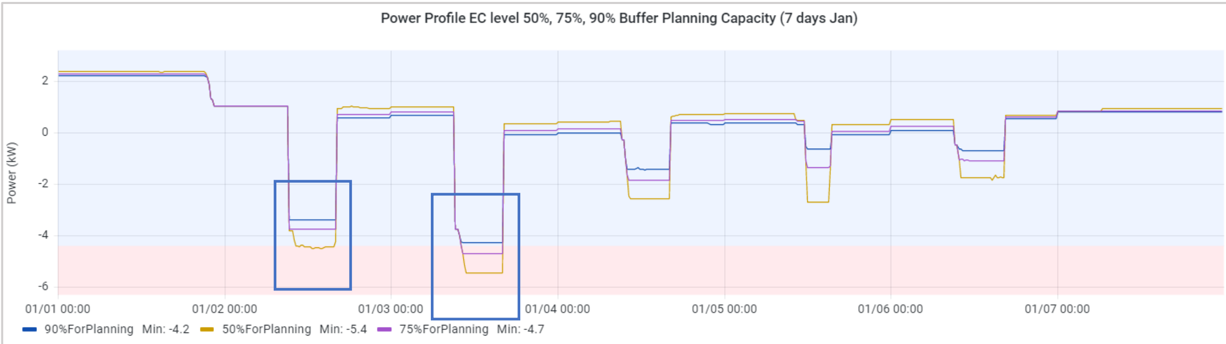

Figure 2.17: Increasing buffer capacity allotted to PS planning to 90% to mitigate second congestion point

Increasing buffer capacity for the planning algorithm is a congestion mitigation strategy aligned with the USEF "traffic-light" model described in the section on Congestion Management Frameworks. Mitigation strategies execute a base planning and then use the planning to discover upcoming congestion points (Green Mode> Yellow Mode). The EC group controller then activates increasingly strict measures, reflected by greater buffer capacity allotted to it. The controller assesses the effectiveness of each measure in mitigating congestion while minimizing user discomfort (Yellow Mode > Green Mode). If congestion persists, load shedding options (Orange Mode) may be employed as a last resort. However, energy modii offers the flexibility to explore various options to mitigate undesirable modes before resorting to extreme measures like forced curtailment.

2.6. Real-Time Reduced Model of Active Distribution Networks for Grid Support[2]

In an effort to minimize the computational effort associated with modelling complex active distribution networks (ADNs), this subsection proposes a novel practical approach for creating a reduced real-time steady-state model of an ADN using synchrophasor measurements. Such models prove advantageous for conducting co-simulations involving the bulk power system (BPS) and multiple ADNs, specifically for grid support applications. With the emergence of distribution-level phasor measurement units (D-PMUs), these synchrophasor measurements are harnessed to promptly determine the reduced model parameters and monitor the dynamic operating condition of the ADN. The proposed method formulates a comprehensive three-phase four-wire reduced model capable of substituting any given feeder configuration within the confines of D-PMUs. By explicitly modelling the neutral wire for various neutral-grounding scenarios, this approach ensures a precise depiction of unbalanced and intricate distribution feeder segments, encompassing, distributed generators, transformers, n-phase laterals and loads. Furthermore, the reduced model is adapted to accommodate embedded distributed generation, enhancing the accuracy of estimating grid support capabilities at the interface between transmission and distribution. Rigorous validation of the proposed reduced model is carried out on the highly unbalanced IEEE-13 bus feeder system across multiple test scenarios, including scenarios involving a high penetration of autonomous photovoltaic (PV) inverters. The model accuracy is demonstrated using DIgSILENT PowerFactory MATLAB co-simulation as the execution platform.

2.6.1. Introduction

The adoption of DERs within distribution networks has undergone substantial growth in the last two decades. This evolution has resulted in an active role for ADNs in grid operations. Consequently, there is a pivotal need for more precise representations of distribution networks in both planning and operational studies. Despite their electrical interconnection, transmission and distribution systems are conventionally studied separately. This is primarily due to the intricate modelling needs and increased computational load. For instance, in many distribution network analyses, the transmission network is simplified to a substation with a fixed voltage, while in TN simulations, the distribution network is approximated as aggregated load at the substation. These simplifications are not suitable for modern power systems, where distribution networks, enriched with DERs, actively impact the grid unlike traditional passive distribution networks. Notably, the significant penetration of DERs in DNs affects the steady-state and dynamic BPS operations. The increasing deployment of Distributed Energy Resources (DERs) has introduced new complexities in the planning and operations of both distribution system operators (DSOs) and transmission system operators (TSOs) due to their impact on the existing transmission and distribution infrastructure. Fortunately, DERs equipped with power electronic interfaces and controllable loads offer newfound flexibility for Advanced Distribution Networks (ADNs). In addition to ensuring a reliable power supply, ADNs can offer various grid support services to the Bulk Power System (BPS). Consequently, close collaboration between TSOs and DSOs becomes crucial for effectively managing DERs and other

[2] Contents from this chapter are a part of the following article published under the SUSTENANCE project: M. Prasad, Z. H. Rather, R. Razzaghi and S. Doolla, "Real-Time Reduced Model of Active Distribution Networks for Grid Support Applications," in *IEEE Transactions on Power Delivery*, doi: 10.1109/TPWRD.2023.3293791.

controllable assets within ADNs, with the goal of maintaining power system stability and reliability. Therefore, the co-simulation of transmission and distribution systems becomes a vital requirement for developing and validating innovative control strategies for the integrated operation of the BPS and multiple ADNs.

The inherent complexities of ADNs, including unbalanced phases, DER-equipped laterals, and bidirectional power flows, necessitate modelling numerous components for analysis. As a result, modelling of ADNs requires a comprehensive knowledge of various parameters within the distribution networks, in addition to the computational demands involved. Further, modelling modern BPS with a detailed depiction of multiple ADNs can substantially escalate both the dimensions and intricacy of the comprehensive system model. This increase often surpasses practical thresholds concerning factors such as computational time, data accessibility, and operational feasibility. Consequently, model simplification with high accuracy becomes necessary for BPS-multiple ADNs co-simulation.

Reduced equivalent network models are useful in various applications, including simulation of large-scale power systems, estimating network operating states, computing control asset setpoints, and performing dynamic security analyses. An effectively reduced network model can accurately reproduce the behaviour of the system at the retained nodes, eliminating the need for detailed modelling of the remaining network components.

Because of the inherent stochastic nature of DERs and the dynamic nature of load compositions, it is of utmost importance to create a real-time reduced model of ADNs that can adapt to changes in operational point variations. Given the challenges of limited distribution network data and lack of complete system observability, a measurement-based approach presents a promising solution to develop the reduced model of an ADN. From this perspective, the emergence of synchrophasor technology provides high-resolution, high-accuracy, and time-synchronized voltage and current phasor measurements in real-time. Notably, the synchrophasor technology has been modified to align with the unique features of DNs, resulting in the devising of distribution-level phasor measurement units (D-PMUs). A D-PMU provides phasor measurement data with phase angle accuracy of 0.01° and transmit measurements within sub-second intervals. Thus, the synchrophasor measurements can be harnessed to develop a simplified steady-state model of an ADN, which can be updated in real-time with the ADN operating point variations.

This subsection proposes a new practical approach aimed at creating a real-time reduced steady-state ADN model [84]. The key contributions of this approach are outlined below:

1. Development of a Real-Time Reduced Model:
    - A reduced model is formulated with three-phase four-wire configurations, and its parameters are updated in real-time.
    - The reduced model effectively tracks the dynamic shifts in the ADN's operational state, demonstrating its adaptability.
2. Enhanced Model Accuracy through Explicit Neutral-Wire Modelling:
    - The model incorporates an explicit representation of the neutral wire, enhancing accuracy particularly for highly unbalanced feeder segments.

- Furthermore, the model reduction approach accommodates different neutral grounding conditions of the D-PMU nodes.

3. Incorporation of Estimated PV Power for Operating Point Prediction:
    - The reduced model is modified to include estimated photovoltaic (PV) power, enabling anticipation of the steady-state operation-point of distributed PVs.
    - This adaptation aids in estimating the potential support within the ADN for the TN at the transmission and distribution interface.
4. Comprehensive Model Validation:
    - Thorough validation of the reduced model is conducted across various realistic scenarios, such as feeder sections with unbalanced feeders, multiple D-PMU nodes, and high penetration of locally controlled distributed PV inverters.

2.6.2. Proposed Real-time Reduced Steady State Model

In the proposed approach, the electric network segment enclosed by two D-PMU nodes can be simplified into a reduced equivalent model, as shown in Figure 2.18.

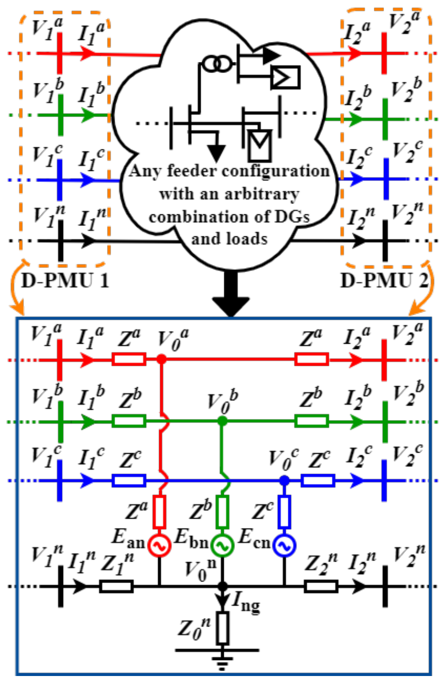

Figure 2.18: Reduced equivalent model of three-phase four-wire electric segment using synchrophasor measurements from two boundary D-PMUs [84]

The process involves extracting the fundamental components from time-synchronized voltage and current phasors. Subsequently, KVL equations are applied to compute the real-time parameters of the reduced model. Utilizing the voltage and current phasor data obtained from the respective D-PMUs for each wire, these KVL equations are used to determine complex variables, which are phasor values of impedances and the voltage source for each T-configured wire. As depicted in Figure 2.18, the two Distribution-level Phasor Measurement Units (D-PMUs) furnish the synchrophasor voltages and line currents pertaining to the three phase-wires as well as the neutral-wire. These measurements are essential for the real-time synthesis of the reduced model.

2.6.3. Model reduction with multiple D-PMUs

Based on the positioning of D-PMUs and their corresponding current measurement configurations, the enclosed network can be simplified in either a star-polygon configuration or a radial configuration, as illustrated in Figure 2.19.

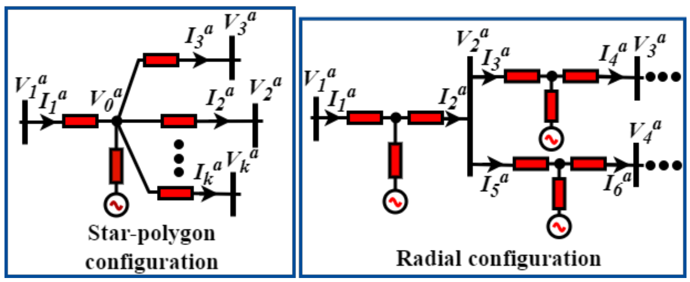

Figure 2.19: Phase-reduced model configuration with multiple D-PMUs

In the radial configuration, every electric network between adjacent D-PMUs is substituted with the reduced model depicted in Figure 2.18. In the star-polygon configuration, the process involves two steps: First, the feeder segment linking two selected D-PMU nodes undergoes simplification, as shown in Figure 2.18. Subsequently, each D-PMU node, apart from the two chosen D-PMU nodes, is linked to the reduced model's T-junction node via a series impedance. The value of this impedance is computed in real-time, utilizing the voltages and currents phasor data of the T-junction node and the respective D-PMU node.

2.6.4. Modelling of PV Generation in the Reduced Network Model

The shunt branch of the reduced model is modified to include the aggregated PV generation for each phase. This modified reduced model is depicted in Figure 2.20.

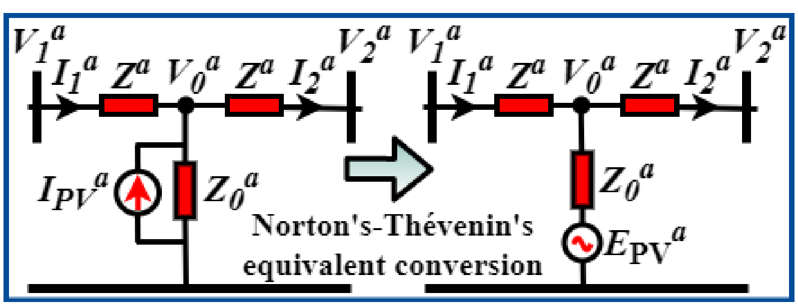

Figure 2.20: Modification of Phase for PV-power estimation

The aggregated current from the PV inverter, consolidated at the T-junction for each phase, is determined by employing the estimated PV power and the voltage at the T-junction. The representation of the PV generation, combined for each phase and treated as a current source at the T-junction, is subsequently transformed back into the original reduced topology illustrated in Figure 2.18. This transformation is achieved by utilizing Norton's equivalent to Thévenin's equivalent conversion.’

2.6.5. Accuracy of the reduced model

The reduced model’s accuracy is established by an extensive analysis of various possible test cases in the highly unbalanced IEEE-13 bus feeder system with distributed PVs. These test cases include different neutral grounding of the D-PMU node, different nominal voltages of the D-PMU nodes, multiple D-PMUs, the electric network segment with single-phase and two-phase laterals, and the high penetration of distributed PVs. Figure 2.21 presents a case-study in which IEEE-13 bus system with 70% penetration of distributed PVs is reduced at the HV-MV substation (node RG60). Here, a quasi-dynamic simulation is executed for the detailed model and the reduced model during the sunshine hours from 6 AM to 5 PM, and the substation current phasor values are determined at every 15 min.

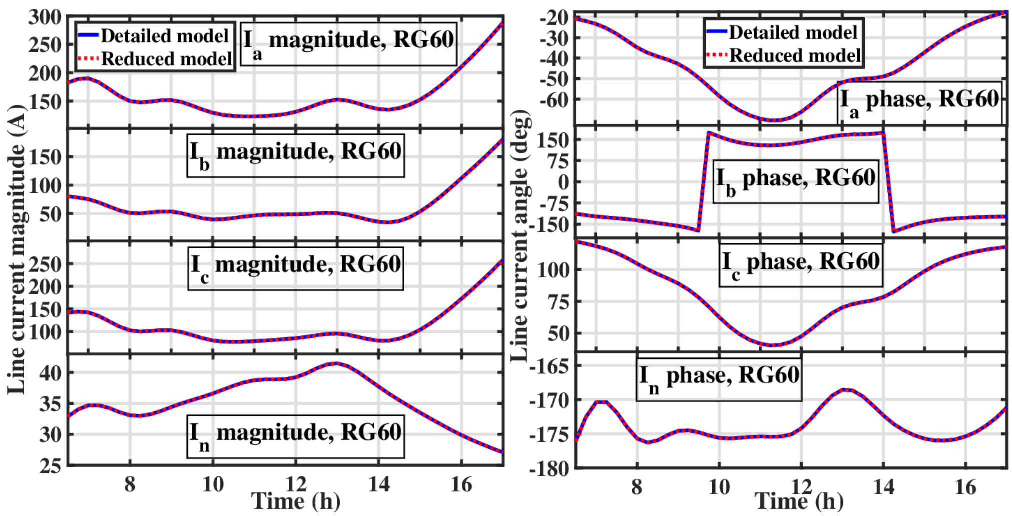

Figure 2.21: Current phasor in each wire at the substation of the detailed model and the reduced model

It is evident that the reduced model accurately tracks the changing operating point of the ADN. During the quasi-dynamic simulation, conducted between 6:30 AM and 5 PM, on PC equipped with an Intel® Core™ i7-6700 CPU operating at 3.40 GHz with 8.0 GB RAM, and utilizing the DIgSILENT-MATLAB execution platform, the detailed model concluded the quasi-dynamic simulation in 7.407 seconds. In contrast, the reduced model accomplished the identical task in a mere 0.586 seconds. This translates to a substantial reduction of approximately 92% in computational time when utilizing the reduced model in this case.

2.7. Conclusion

In this chapter, a distributed control system is implemented for integrating renewable energy sources (RE sources) with energy storage, which has been simulated on the PowerFactory platform. The purpose of this study is to explore the demand response and control mechanisms for local integrated energy systems, aiming to improve energy management, enhance the hosting capacity of renewable energy sources, and make local electric grids smarter. Additionally, a smart controller for EV charging is developed, offering various charging options such as droop control, scheduled charging, and participation in grid power regulation. If the user does not select any of these options during charging, the EV is charged at its rated power until it is fully charged or disconnected. Users have the flexibility to choose from these charging options and combine them as needed. This diverse range of charging options and combinations within the simulation environment allows the investigation of issues related to grid loading and voltage stability in existing residential electricity distribution networks.

Furthermore, this chapter introduces a novel practical approach for creating a simplified steady-state model for Active Distribution Networks (ADNs). This model is continuously updated in real-time using synchrophasor measurement data. By employing nodes equipped with D-PMUs (Digital Phasor Measurement Units), any electrical segment enclosed by D-PMUs can be reduced into a simpler configuration, significantly reducing the complexity when co-simulating Bulk Power Systems (BPS) with multiple ADNs. The real-time synchrophasor measurements, well known for their high accuracy, fine resolution, and time-synchronized voltage and current phasor data, play a pivotal role in deriving real-time reduced model parameters and effectively tracking the dynamic ADN operational state. A comprehensive validation, employing a joint DIgSILENT PowerFactory-MATLAB framework, is conducted on IEEE 13 bus feeder system characterized by substantial phase unbalances and heavy loads. The study yields the following noteworthy conclusions:

- The reduced model is obtained directly from real-time synchrophasor measurements, circumventing the need for an intricate offline model of the detailed original system.
- The incorporation of neutral-wire modelling enhances the reduced model's accuracy, particularly for unbalanced feeders with varying neutral grounding conditions of the D-PMU node.
- Inclusive of phase-wire, neutral-wire modelling provides the retention of each D-PMU node in its totality, and the model accuracy is demonstrated for different neutral-grounding statuses.
- D-PMUs positioned at nodes sharing the same nominal voltage deliver higher accuracy in the reduced model of the enclosed electrical segment, encompassing transformers, multi-phase laterals, and a substantial penetration of distributed PVs.
- A reduced model based on multiple D-PMUs can be structured either in a star-polygon or radial topology, depending on D-PMU placement and configuration.
- Small-scale distributed PV systems connected to non-D-PMU nodes are assimilated within the reduced model. The adaptation of the reduced model to include estimated PV power facilitates pre-emptive insight into the steady-state performance of distributed PVs, allowing estimation of the available grid support at the transmission-distribution points.

3. Integration of electric vehicles for sustainable transport in energy communities[3]

Uncontrolled charging of electric vehicles (EVs) can cause various technical issues in the local distribution network, such as voltage instability, phase imbalance, increased peak load, overloading, power loss, and power quality issues, as shown in Figure 3.1. The high resistance-to-reactance ratios (R/X) in distribution networks can often lead to voltage sags due to considerable power drawn, that can breach the stable voltage limits if precautionary measures are not taken. The growth of EV usage exacerbates this vulnerability due to the corresponding rising power demand, potentially leading to increased voltage stability issues in low-voltage grids [85]. Concurrently, EV charging often coincides with evening peak demand, which could further worsen the voltage stability. It can also cause overloading of the transmission lines and the distribution network assets such as transformers and cables. This sudden surge in load could prompt higher electricity generation and electricity prices and intensify the stress on the overall ramping limits of the system. Moreover, this progression towards sustainable transportation may lead to overloads in the distribution network elements, shortening equipment lifespan and diminishing energy transmission efficiency. Additionally, the influx of EV charging current elevates the power losses, undermining the overall power supply efficiency. Imbalanced loading further compounds losses across phases. EV chargers constitute power electronic converters that introduce non-linear loads, inducing voltage and current harmonics proportional to the number of active chargers [85]. In this context, the integration of EVs through smart charging strategies is a potential solution to overcome the issues related to uncontrolled charging.

[3] Contents of this chapter are derived from the work conducted under SUSTENANCE under the below-mentioned articles:

- P. V. Dahiwale and Z. H. Rather, "Centralized Multi-objective Framework for Smart EV Charging in Distribution System," *2023 IEEE PES Conference on Innovative Smart Grid Technologies - Middle East (ISGT Middle East)*, Abu Dhabi, United Arab Emirates, 2023, pp. 1-5, doi: 10.1109/ISGTMiddleEast56437.2023.10078604.
- P. V. Dahiwale and Z. H. Rather, 'Congestion Management in High Solar PV Penetrated Distribution System using Smart Charging of Electric Vehicles', *ISES Solar World Congress 2023* (Accepted for publication).
- A. P. Nath and Z. H. Rather, 'Design of Adaptive Control Scheme for Provision of Frequency Regulation Service from Electric Vehicle Fleet', *IEEE ISGT Europe 2023*, Grenoble, France (Accepted for publication).
- P. Nath and Z. H. Rather, 'Application of Electric Vehicle Charging Station for Power Factor Correction of Industrial Load', 7th E-Mobility Power System Integration Symposium, Copenhagen, Denmark, 2023. (Accepted for publication)

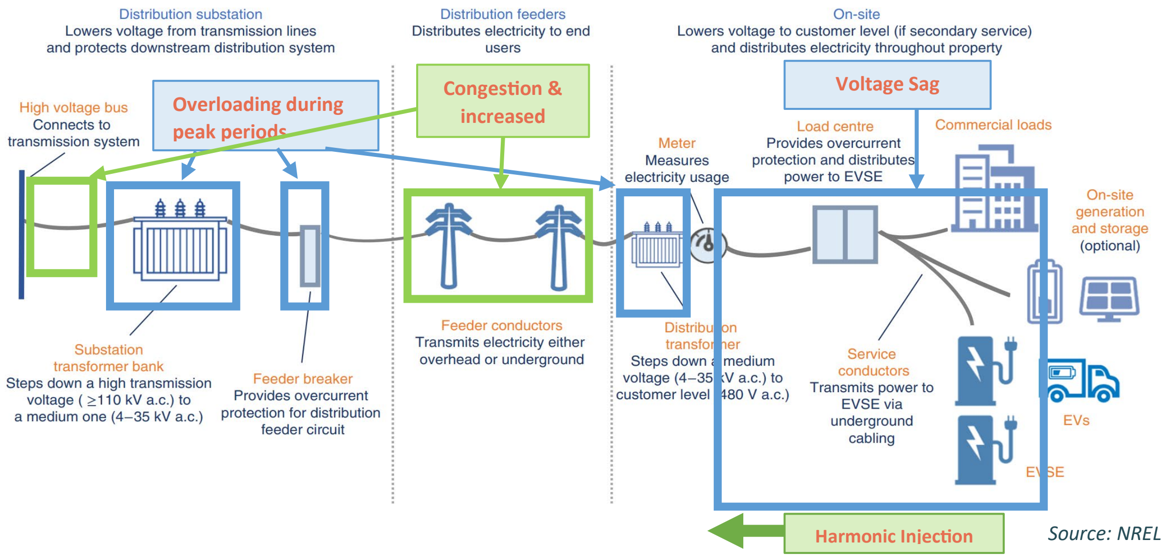

Figure 3.1: Impacts of uncontrolled EV charging in distribution system [86]

Smart charging control for EV charging is dependent on the EVs demand and network conditions, such that the EV charging load does not lead to network instability issues in terms of voltage, thermal loading, etc. For determining the charging schedule, the strategies for smart charging consider some of the temporal and spatial characteristics of the loads, travel pattern, and the charging behaviour of the EVs [87]. Spatial distribution of public EV charging stations, residential or private EV charging stations significantly impacts the electrical network in the locality. The temporal distribution of the EVs on top of the spatial distribution layer enhances the impacts of uncontrolled EV charging on the local grid especially in terms of increased peak load and overloading of the network components.

Smart charging of EVs can be performed to achieve various technical objectives such as congestion management, increasing the self-utilization of renewable energy (RE) generators, load leveling and valley filling to name a few [88]. It also contributes to ancillary support services such as voltage and frequency support services. The faster response time of power electronic converters that interface the EV batteries with the grid allows the aggregated EVs to participate and provide grid support services.

The preferences of the EV user play a vital role in EV charging, as it can influence the experience of EV charging and adoption of EVs on a larger note. The preferences and the interest of the EV user include the choice on the rate of charging, type of charging, and the charging power [89]. Depending on the available charging duration for an EV, the priority of charging can improve the charging experience and the potential of achieving the desired state-of-charge (SoC). In addition to the connection duration of EV, the preference for the charging type set by the EV users, namely, AC or DC charging, also needs to be taken into consideration. Additionally, the charging power determined by the EV users can indirectly enhance the control of the EV user on the charging process and degradation of the battery, since the latter is accelerated typically at fast charging or with a higher charging power.

3.1. Developed Control Strategies

3.1.1. Centralized smart charging for charging cost minimization and load leveling

To mitigate the increased peak loading due to uncontrolled EV charging, a centralized charging strategy is developed for the objectives of DSO and EV user. The objectives of minimization of charging cost for the EV user, as well as load levelling and minimization of peak-to-average ratio for the system operator have been implemented in this study. It aims to counteract the adverse effects of unregulated EV charging on distribution networks and encourage smart EV charging engagement. Investigating controlled charging methods, this study employs electricity price signals and a centralized control strategy [90]. The analysis covers the impacts of uncontrolled EV charging and implementation of proposed smart charging framework, utilizing the IEEE 33-bus radial distribution network as a test case.

In literature, coordinated charging control based on distinct control objectives, architectures, pricing mechanisms, and algorithms have been explored [91]. The centralized strategy predominantly targets system-level goals due to the adaptable control potential of EV charging at the operator level [92]. Meantime, the strategy for decentralized charging adaptively modifies the signal for electricity pricing to impact the charging patterns, taking into account the system load [93]. Within the literature [94], [95], [96], objectives such as flattening load curves, reducing peak-to-average ratios, filling load valleys, and minimizing charging costs are primary objectives at the distribution system level. Some articles significantly focus on EV owner's charging preferences, catering to both their convenience and the coordination of EV charging [97]. Charging mechanisms proposed by charging stations are designed to enhance station profits and user benefits [98]. Employing a multi-objective optimization approach that combines user convenience and charging cost through electricity price-based mechanisms and smart and transactive energy management frameworks help integrate EVs, EV aggregators (EA), and distribution system operators (DSO) to collaboratively manage control and grid functions [99]. To cater to customer preferences, the study in [89] determines maximum charging power based on user selections, allowing users to choose appropriate charging options in terms of rate and anticipated charging duration. Investigating direct load control and pricing mechanisms for optimal charging, the study in [100] aims to minimize maximum transformer loads.

In this study, the proposed method is implemented on the conventional 33-bus radial distribution network, which has a peak load capacity of 4 MW. The study considers 170 EVs with a maximum charger rating of 6.6 kW. The arrival, departure, and arrival SoC are taken as per normal distribution. The impact of uncontrolled charging for different penetration levels of EV loads are demonstrated in Figure 3.2 [90].

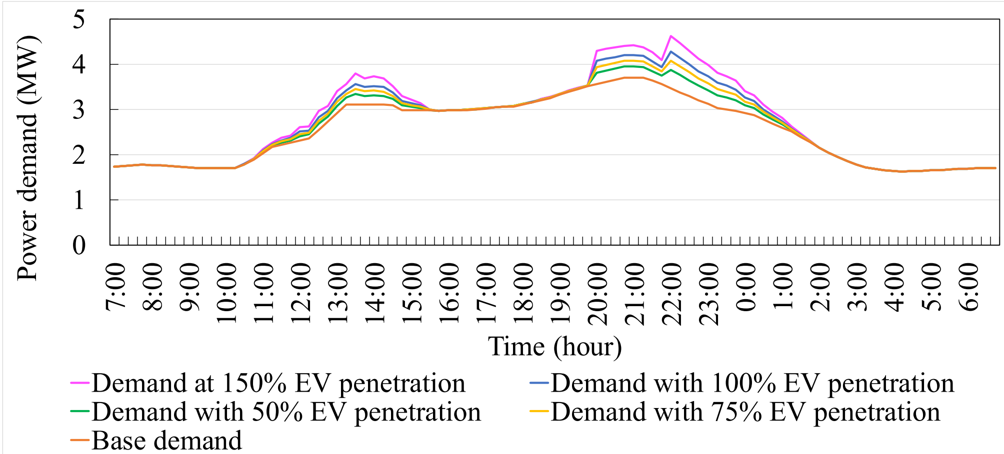

Figure 3.2: Impact of uncontrolled charging on total power demand [90]

It shows that the increasing penetration of EVs directly increases the peak loading on the system whereas the peak-to -valley ratio is also increasing. The impact of various penetration levels of EVs on power loss is also depicted in Figure 3.3. The voltage profile is also deteriorating with increasing uncontrolled EV penetration as given in Figure 3.4 [90]. The rise in the voltage at node 19 is because node 19 is directly connected to node 2 and similarly node 26 is connected to node 6.

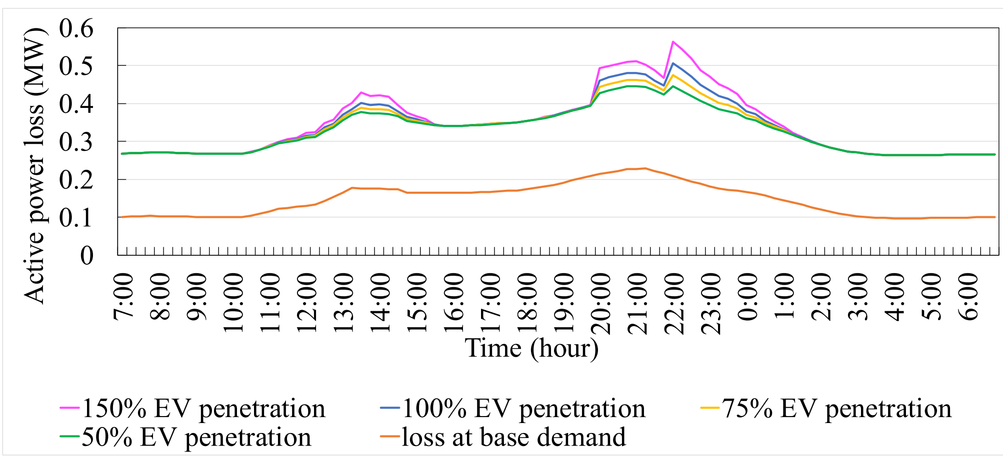

Figure 3.3: Impact of uncontrolled charging on total active power loss [90]

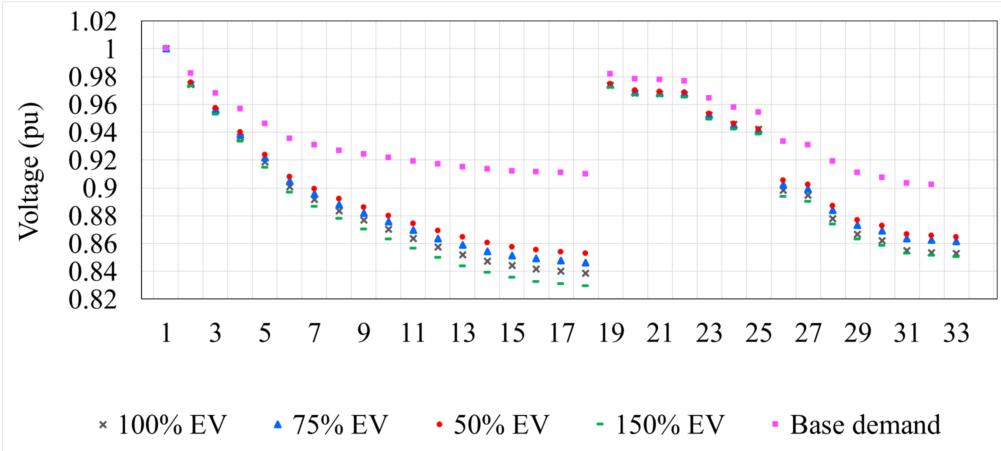

Figure 3.4: Minimum and average bus voltages under EV penetration [90]

The time-of-use (ToU) charging method based on the ToU price curve shown in **Error! Reference source not found.**5 is implemented for indirectly influencing the EV charging to an off-peak period [90]. The comparative EV demand profiles of EV with uncontrolled, immediate peak time, and off-peak time shows that off-peak ToU method majorly shifts the EV demand in off-peak time. Whereas the immediate ToU price method shifts the EV load from peak time but create another peak at immediate ToU time as shown in Figure 3.5.

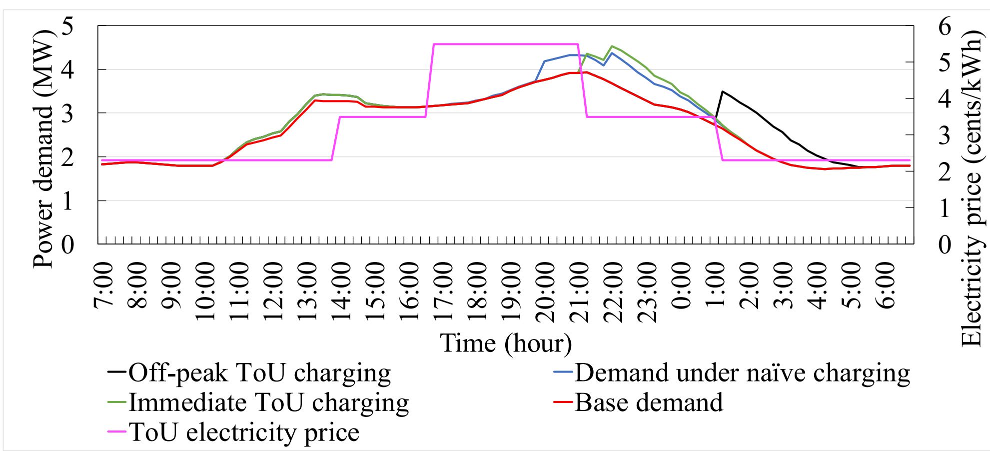

Figure 3.5: ToU-based EV charging [90]

In this study, the implemented centralized charging framework considers EV aggregators and DSO to achieve the formulated objectives. Here the EV aggregator receives the inputs from EV users that includes the information of arrival and departure time, arrival, and departure SoC, and EV specifications. The developed method also includes the EV user's preference of maximum charging power. The collective information from all the subscribed EVs to that aggregator then further undergoes EV charging optimization. EV aggregator performs the optimization of charging cost minimization. The aggregated power requirement of the EVs is then communicated to the DSO. DSO aggregates the power requirement from all the aggregators and then performs load leveling and peak-to-average ratio minimization. The result of smart charging widely spread the EV charging across the connection time as compared to uncontrolled and time-of-use EV charging method as shown in Figure 3.6 [90].

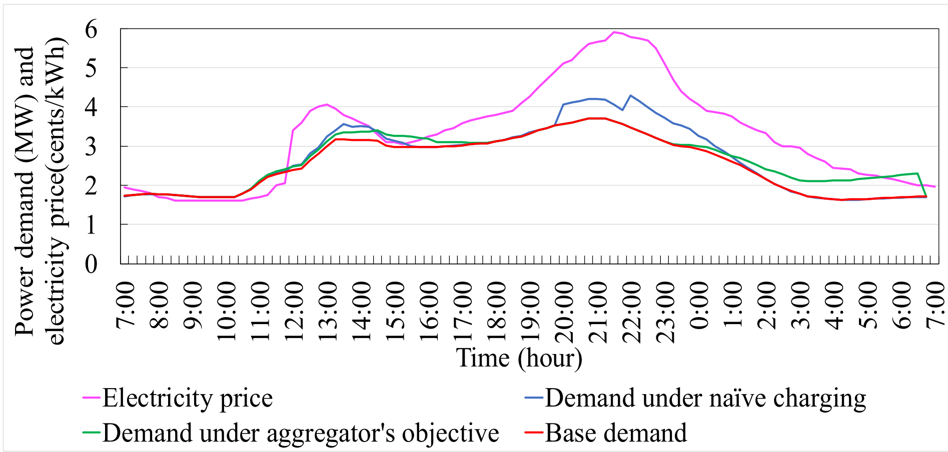

Figure 3.6: EV aggregator level smart charging for charging cost minimization [90]

The results depict that the implemented centralized smart charging algorithm limits the increased peak demand due to uncontrolled EV charging. It shifts the EV charging demand from peak time into off-peak time whereas the DSO objectives shift the demand curve of EV towards the average value of load.

3.1.2. Congestion management using smart charging of EVs with high solar PV penetration

A substantial integration of solar PV power within the distribution system can result in amplified power losses, reverse power flow, voltage elevation, network congestion, voltage disparities, variable reactive power, compromised power quality, and challenges in protective measures [101]. Moreover, when the distribution system encounters network limit breaches, it experiences congestion, impeding further capacity for power transmission through the lines [102], [103]. To reduce this rising instance of network congestion in terms of bus voltages in the presence of higher solar PV penetration, the smart charging of EVs (V1G) is studied [104]. The central congestion management algorithm is implemented to reduce network losses and adhere to different requirements like active and reactive power flow and voltage limits. This algorithm is executed one day ahead of the scheduled EV charging load for a 15-minute timeframe [23]. While performing the congestion management of the network the charging requirements of the EVs are also taken into consideration by deploying the desired SoC constraint of EVs.

The 33 bus system with 4 solar PV generators are considered and analyzed at different PV penetration [105]. The voltage profile in Figure 3.7 at different percentage penetration of PV shows that the voltage at the terminal buses of the solar PV generators is rising with the increasing PV penetration. The rise in the voltage at node 19 is because node 19 is directly connected to node 2 and similarly node 26 is connected to node 6.

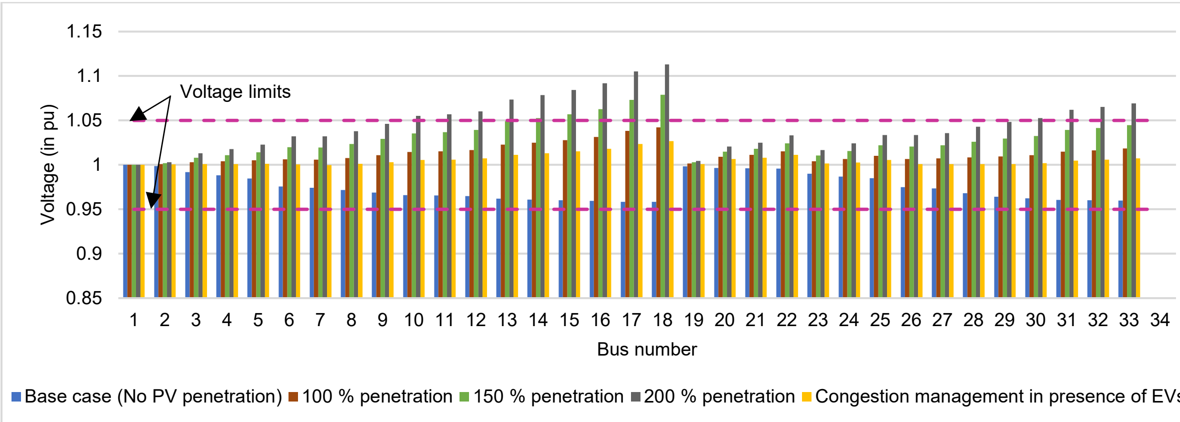

Figure 3.7: Voltage profile of IEEE 33 bus distribution system with different solar PV penetration [104]

At higher PV penetration, the voltages exceed the upper voltage limit which leads to congestion in the network. The implementation of developed congestion management algorithm shows that the EV charging is aligned with the PV power availability such that the bus voltages will be in the tolerance band. It also ensures that the EVs in the system reach the desired SoC value at the end of the connection period.

3.1.3. Frequency Regulation using V2G Technology

The purpose of frequency regulation services is to maintain the system frequency within the predetermined limits during regular operation. This service is among the ancillary offerings acquired by system operators, usually through energy markets. Frequency regulation service involves the addition or reduction of active power from resources, in direct response to control signals dispatched by the system operator, which are influenced by the actual grid frequency at that moment. Frequency regulation services from EVs have been demonstrated to be technically feasible in different studies around the world.

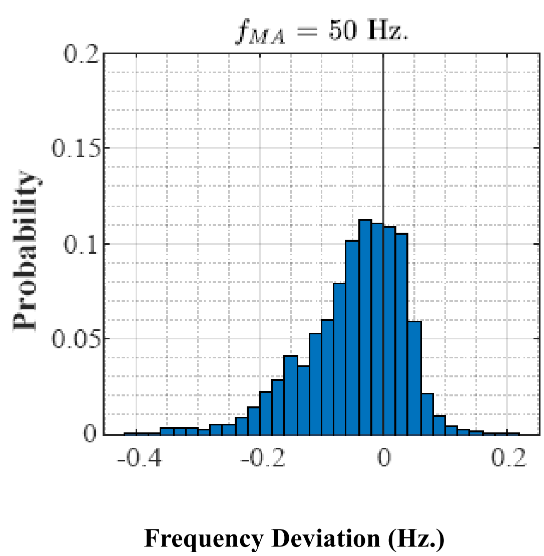

Figure 3.8: Deviation of frequency from the nominal frequency of 50 Hz [106]

The significance of the frequency pattern is particularly pronounced for assets with constrained energy reserves, like EVs and battery storage systems engaged in frequency regulation services. In many grids, the frequency tends to conform to a Gaussian distribution centered around the nominal frequency. In India, the frequency profile for the duration under consideration was non-Gaussian as shown in Figure 3.8. Hence, frequency regulation services in India would involve non-zero energy requirements, rendering it unsuitable for resources characterized by limited energy capacity, such as battery storage systems and EVs [106].

A novel methodology has thus been proposed for the provision of frequency regulation service from EVs in power systems with non-Gaussian distribution of frequency. In the proposed methodology, the EVs provide regulation service based on the deviation of frequency from a moving average of the measured frequency over a window of 15 minutes. The difference in the SoC profile of EVs participating in frequency regulation using the proposed reference frequency and the nominal reference frequency has been shown in Figure 3.9.

For participating in the frequency regulation services, the EV users can potentially earn significant amount of revenue. Based on our study, it was observed that an EV user can annually earn around \$283.71±64.93 by participating in frequency regulation service. The revenue earned is dependent on the number of times the individual EV user participated in the service, which is again correlated with the number of charge requirements of the EV user. However, there exists a balance between the income generated by the EV user and their SoC status. Opting for greater earnings through participation in regulation services might result in more pronounced SoC fluctuations for the EV user, potentially affecting their travel pattern.

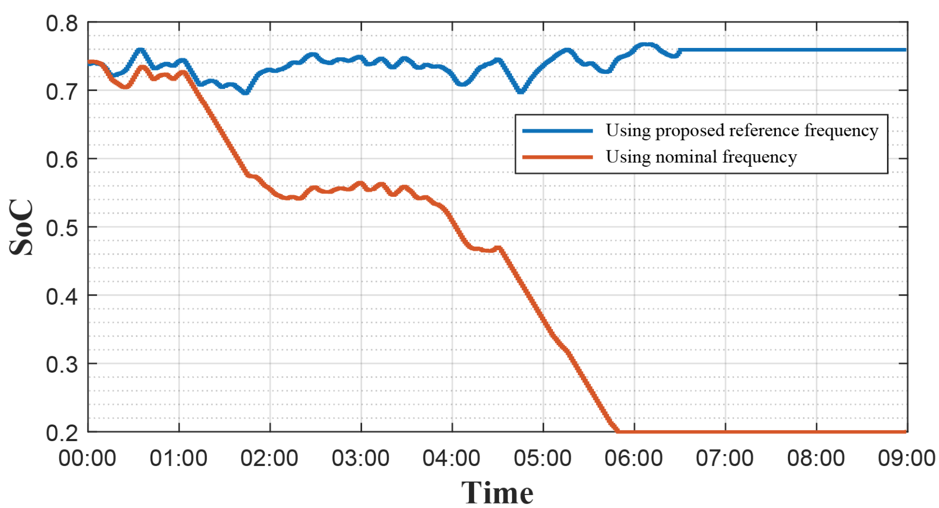

Figure 3.9: Comparison of SoC profile for EV providing frequency regulation services using proposed reference frequency and the nominal reference frequency [106]

3.1.4. Reactive power support from DC fast EV chargers

Ensuring the well-being of the system relies on having a sufficient reserve of reactive power. Typically, this reactive power is preferred to be generated within the local distribution network. Network operators frequently invest significantly in acquiring and setting up devices like capacitor banks and synchronous condensers to compensate for reactive power. Nevertheless, DC EV chargers offer an alternative solution by being adaptable to operate in all four quadrants, thereby aiding in reactive power compensation for the network. The versatility of four-quadrant operation in DC chargers allows them to furnish reactive support, regardless of whether the charger is engaged in EV charging.

To showcase the advantages that an EV charging station can offer to an industry, a practical scenario involving a food processing facility in Delhi has been examined. Food processing plants generally exhibit a low power factor, indicating a substantial consumption of reactive power. The specific food processing plant in Delhi is linked to the grid through the 11 kV connection point [107].

The voltage controller has been designed to achieve a power factor of at least 0.98 lagging at the PCC point of the industry. Depending on the existing power factor, the controller dispatches the required reactive power from the available margin in the charging station. The reactive power required is distributed among the EV chargers based on the availability margin.

The incorporation of reactive power support from the charging station decreased the apparent power drawn from the grid. This leads to a decrease in both the demand charge and the energy charge for the industrial establishment. By leveraging the reactive power support offered by the charging station, the facility can lower its monthly demand charges from INR 3,28,687 (EUR 3,882) to INR 3,07,596 (EUR 3,633), resulting in a monthly savings of INR 21,090 (EUR 250) or an annual savings of INR 2,53,087 (EUR 2,990). In terms of energy cost reduction, the charging station has the potential to bring down the daily energy expenditure from INR 1,24,725 (EUR 1,473) to INR 1,01,789 (EUR 1,202), translating to daily savings of INR 22,936 (EUR 271) or a yearly savings of INR 71,79,234 (EUR 84,810).

3.2. Battery Storage

Battery storage (BS) is used for charging the batteries with PV (photovoltaic) or grid when the price is low. The BS is further used for charging the EV or supplying other loads behind the meter when the energy price is high.

Figure 3.10 shows the schematic of the system configuration model, to implement distributed control scheme for RES integration with energy storages, developed in the DIgSILENT PowerFactory simulation tool. The simulation is carried out to investigate the demand response and control scheme of local integrated energy system operation for energy management while increasing the hosting capacity of RES and smartening local electric grids.

Based on the configuration shown in Figure 3.10, the PV system is feeding loads behind the meter such as EV, HP, other household loads, and charging the battery energy storage system based on the battery management system. The balance in load and generation is satisfied by the flexible operation of energy devices such as EV, HP, and battery storage system. In need of excess energy to satisfy the load demand, energy is imported from the grid. On the other hand, excess generation of PV is exported to the grid. When a grid outage occurs, excess power cannot be exported. In this case, excess energy produced is either stored or curtailed.

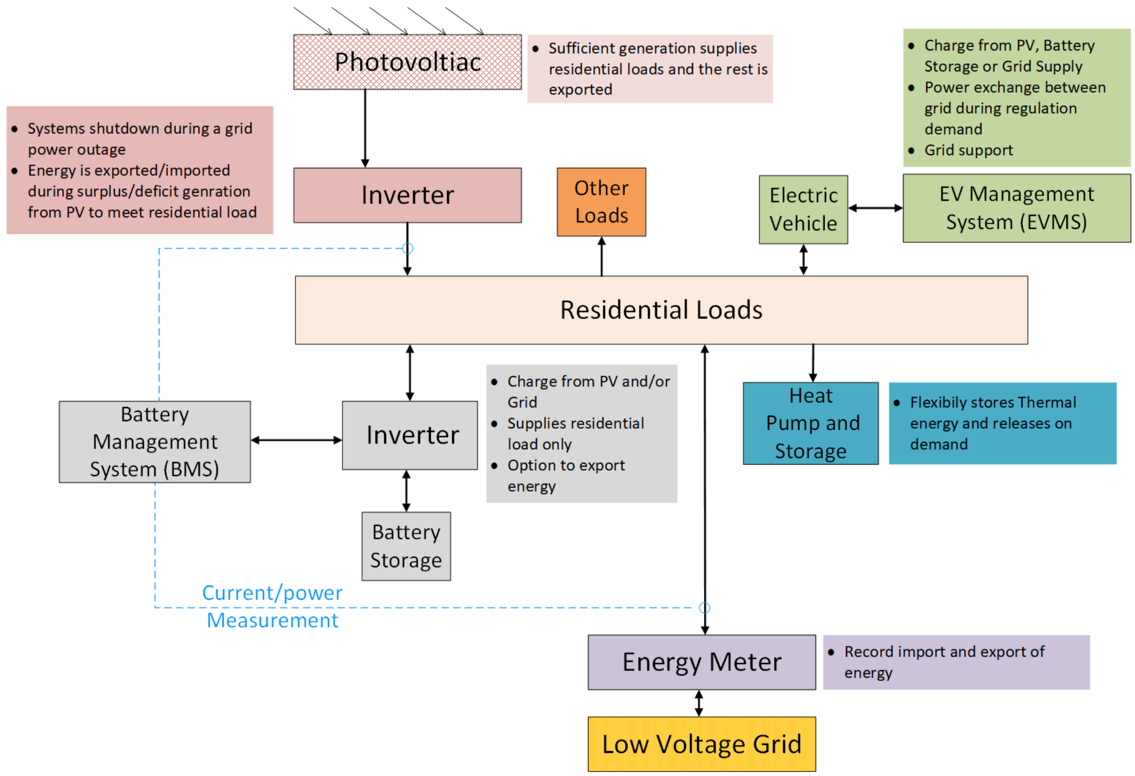

Figure 3.10: System configuration for distributed control scheme for RES integration with energy storage

3.3. Operation of Flexible Loads:

Electric loads such as HP with thermal energy storage, EV and battery storage offer flexibility in the electric distribution grid. Flexibility from these various loads is discussed below.

- *Heat pump (HP) with thermal energy storage:* This unit provides flexibility by storing electric energy in the form of thermal energy used for space heating and domestic hot water. The detailed model and content are presented in deliverable D2.2.
- *Electric Vehicles:* This unit provides flexibility by charging based on the EV management system. The charging is from PV, grid, or battery storage to minimise the energy price and support electric grid voltage. EV also participates in grid regulation (by charging or discharging EV) to support grid voltage and frequency.
- *Battery Storage (BS):* The BS system can provide flexibility in terms of load as well as generation. During excess generation from PV or lower electricity price, energy is stored in the battery and later used when the energy price is higher. The battery management system governs the battery status and determines the charging and discharging power of the battery as an optimal solution to energy price and demand forecast. It can also sell power to the grid based on grid regulations and users' choices.

3.4. Battery Management System:

Terms and definitions

$SOC(t)$	State of charge of the battery at any given instant of time (t) [%]
SOC_{min}	Minimum SOC level of the battery. The battery is not able to discharge beyond this level of SOC. Discharge is further suspended until the $SOC(t)$ is greater than $SOC_{min} + 20\%$
SOC_{max}	Maximum SOC level of battery to indicate the fully charged condition (100%). Charging of battery is stopped once battery is attained to this level and further charging is suspended until the $SOC(t)$ is less than $SOC_{max} - 10\%$
Note: 10% and 20% of a dead zone are selected for charging and discharging of the battery as the boundary condition (SOC_{max} and SOC_{min}) is attained, to avoid the haunting effect of switching battery charging and discharging respectively.	

3.4.1. Charging and discharging conditions:

The battery management system determines the charging and discharging power of the battery storage as an optimal solution for energy price and demand forecast. The simulation scenario is set up to charge the battery storage from PV and use it to charge EV only to analyse the demonstration case. The following conditions are evaluated to ensure charging and discharging within the defined boundary condition of the state of charge of the battery. The battery storage is capable of charging and discharging under the following conditions.

Charging condition 1 [$\mathbf{CC_1(t)}$] (Fully charged condition): When the SOC of the battery is attaining 100%, further charging is disabled until the battery is discharged to level ($\mathrm{SOC_{max}} - 10\%$) as seen from (3.1)

$$\mathrm{CC_1(t)} = \begin{cases} 0 & \mathrm{SOC(t)} \geq \mathrm{SOC_{max}} \\ \mathrm{CC_1(t-1)} & (\mathrm{SOC_{max}} - 10\%) \leq \mathrm{SOC(t)} \leq \mathrm{SOC_{max}} \\ 1 & \mathrm{SOC(t)} < (\mathrm{SOC_{max}} - 10\%) \end{cases} \tag{3.1}$$

Charging condition 2 [$\mathbf{CC_2(t)}$] (Peak saving mode [PS]): When PS mode is selected by the user [$\mathrm{PS} = 1$], charging of battery storage is disabled during the peak hour period between 17:00-20:00 hrs (3.2).

$$CC_2(t) = \begin{cases} 1 & PS = 0 \\ 1 & PS = 1 \; and \; 20 < t < 17 \\ 0 & PS = 1 \; and \; 17 \leq t \leq 20 \end{cases} \tag{3.2}$$

Thus, the battery storage charging condition [$CC(t)$] is satisfied when charging condition 1 and 2 is fulfilled (3.3).

$$CC(t) = \begin{cases} 1 & CC_1(t) = 1 \; AND \; CC_2(t) = 1 \\ 0 & CC_1(t) = 0 \; OR \; CC_2(t) = 0 \end{cases} \tag{3.3}$$

Discharging condition 1 [$\mathbf{DC_1(t)}$] (Fully discharged condition): battery storage is considered fully discharge when the SOC is 20% or below. This SOC level is considered as $\mathrm{SOC_{min}}$ (Minimum SOC level of the battery). The battery is not able to discharge beyond this level of SOC (3.4). Discharge is further suspended until the $\mathrm{SOC(t)}$ is greater than $\mathrm{SOC_{min}} + 20\%$.

$$DC_1(t) = \begin{cases} 0 & SOC(t) \leq SOC_{min} \\ DC_1(t-1) & SOC_{min} \leq SOC(t) \leq SOC_{min} + 20\% \\ 1 & SOC(t) > SOC_{min} + 20\% \end{cases} \tag{3.4}$$

Discharging condition 2 [$\mathbf{DC_2(t)}$] (Power export mode [$\mathbf{PE}$]): Power export mode is selected by the user to [$\mathrm{PE} = 1$] to allow selling of power to the grid. When disabled [$\mathrm{PE} = 0$], BMS limit power discharge from the battery and prevent power selling to the grid from battery storage. In this mode of operation, the BMS (battery management system is constantly monitoring the power at the main meter and power generation from the PV [$PV_{gen}(t)$] (3.5). When the power exported to the grid [$P_{export}(t)$] is greater than power generated from the PV, the battery storage reduces the discharged power. This allows users to sell power generation from PV to the grid during high price and use battery storge to fulfil residential load.

$$DC_2(t) = \begin{cases} 1 & PE = 1 \\ 1 & PE = 0 \; and \; P_{export}(t) < PV_{gen}(t) \\ 0 & PE = 0 \; and \; P_{export}(t) > PV_{gen}(t) \end{cases} \tag{3.5}$$

3.4.2. Charging Power:

The charging power of the battery storage [$P_{char}(t)$] at any time (t) is determined by the BMS as [$PB_{char}(t)$] and is limited to P_{max} as the maximum rated charging power of the inverter (3.6).

$$\begin{gathered} P_{char}(t) = [PB_{char}(t)] \times CC(t) \; [W] \\ 0 \leq P_{char}(t) \leq P_{max} \end{gathered} \tag{3.6}$$

3.4.3. Discharging Power:

The discharging power of the battery storage [$P_{dis}(t)$] at any time (t) is given by (3.7) and is limited to P_{max} as the maximum rated charging power of the inverter. The BMS determines the discharging power [$PB_{dis}(t)$].

$$\begin{gathered} P_{dis}(t) = \begin{cases} PB_{dis}(t) & DC_1(t) = 1 \\ 0 & DC_1(t) = 0 \\ PB_{dis}(t) - [PV_{gen}(t) - P_{grid}(t)] & DC_1(t) = 1 \; AND \; DC_2(t) = 0 \end{cases} \\ 0 \leq P_{dis}(t) \leq P_{max} \end{gathered} \tag{3.7}$$

The simulation model of battery storage system is modelled and verified in DigSILENT PowerFactory for further simulation work with integration of EV, HP-PCM Storage, PV, and other household loads.

3.5. Grid Integration of EV and Smart controller for charging of EV

Smart controller for EV charging is in developed in DigSILENT Power factory with different charging options based on:

- droop control
- scheduled charging
- participation grid power regulation

If none of these options are selected by user during charging, the EV will charge with rated power of charger until fully charged or disconnected. Users can select any of the above-mentioned charging options and its combinations. The variety of charging options and its combinations within the simulation environment allows researchers to investigate grid loading and voltage issues of existing electricity distribution networks of residential areas.

The charging conditions and power level of charging EV based on inputs from user is further described hereafter.

3.5.1. Feasibility of charging EV based on availability and SOC status of EV during charging:

The state of charge (SOC) of EV battery [$SOC(t)$], at time (t), is monitored while the EV is conned to the charger. Favorable conditions for charging EV are determined based on $SOC(t)$, as seen from (3.2) and Table 3.1. Information of $SOC(t)$ and estimated time of departure also helps the responsible party to assess how much energy is available for trading in electricity market and grid balancing and voltage/frequency regulation at interval, based on user preferences.

The signal for availability of EV [($X(t) = 1$] is set high only if EV is physically connected for charging at the charging station. The signal [$S(t)$] determines if the EV is favorable for charging based on $SOC(t)$ as in (*3.8*) and in Table 3.1. When the vehicle is conned to the charger and the battery is not in fully charged state, i.e., EV is ready for charging. The charging power of EV [$P_{char}(t)$] depends upon the flexibility option selected by user such as priorities, participation in flexible charging (with schedule and droop control preference), and participation in grid regulation as V2G.

$$S(t) = \begin{cases} 1 & SOC(t) < 100\% \; and \; X(t) = 1 \\ 0 & SOC(t) = 100\% \; or \; X(t) = 0 \end{cases} \quad (3.8)$$

Table 3.1: Summary of charging condition of EV based on X(t) and SOC(t)

Conditions		Output
$\boldsymbol{X(t)}$	$\boldsymbol{SOC(t) \geq 100\%}$	$\boldsymbol{S(t)}$
0	x	0
0	x	0
1	0	1
1	1	0

It can be summarized that EVs can only be charged when connected to charger while SOC is below 100%.

3.5.2. Minimum SOC level

The minimum required SOC [SOC_{min}] at the time of estimated departure is set by the user while EV is plugged in for charging. This helps the responsible party to determine how much energy is available for trading in the electricity market at intervals as well as for grid balancing and voltage/frequency regulation. EV can be charged to 100% based on favorable conditions such as voltage condition and available power. Logic signal $S_{min}(t)$ determines if the minimum charging requirement of EV is fulfilled or not (3.9).

$$S_{min}(t) = \begin{cases} 1 & SOC(t) < SOC_{min}\ and\ X(t) = 1 \\ 0 & SOC(t) \geq SOC_{min}\ or\ X(t) = 0 \end{cases} \tag{3.9}$$

Summary: The controller prioritizes the charging process to meet the minimum SOC level by the estimated time of departure.

3.5.3. Droop Control

Voltage regulation in a long radial feeder of electric distribution grid is often challenging with increment of load or generation (PV, V2G) in the existing infrastructure. On the other hand, grid congestion on transmission cables due to increment of loads is also possible.

Flexible operation of the load with the help of appropriate demand response and demand response management can solve the problem of voltage regulation and grid congestion to some extent. However, implementation of offline controller for limiting and sharing system load during low voltage at the point of coupling [$V_{POC}(t)$] of EV or line loading [$I_{line}(t)$], increases the security of grid limit locally. This flexibility in limiting power of connected load can be achieved by implementing droop control based on $V_{POC}(t)$ and $I_{line}(t)$ of the selected cable in the grid network.

The EV user can choose option to participate in grid flexibility based on droop control [C_{droop}]. Voltage and loading are measured on a per unit basis. The droop coefficients based on $V_{POC}(t)$ and $I_{line}(t)$ is calculated based on (3.11) and (3.12) respectively.

Droop coefficient [$k_v(t)$] is implement based on $V_{POC}(t)$ to vary charging and discharging power of EV (3.11) in order to regulate the $V_{POC}(t)$ as seen from Figure 3.11(a). On the other hand, the droop coefficient for $I_{line}(t)$ [$k_l(t)$] is selected for line loading between critical limit (i_{crit}) and 100% loading of the selected cable [Figure 3.11(b)]. To limit the number of measurement instruments, only selected lines based on state estimation or high loading can be taken into consideration.

Finally, the droop control coefficient [$k(t)$] is selected as the minimum value between $k_v(t)$ and $k_l(t)$, as in (3.13). The summary of selection of droop coefficient [$k(t)$] is presented in (3.13) based on Table 3.2.

$$\mathrm{k(t)} = \begin{cases} 1 & \mathrm{C_{droop}} = 0 \\ \mathrm{k_v(t)} & \mathrm{C_{droop}} = 1 \text{ and } \mathrm{k_v(t)} \leq \mathrm{k_l(t)} \\ \mathrm{k_l(t)} & \mathrm{C_{droop}} = 1 \text{ and } \mathrm{k_l(t)} < \mathrm{k_v(t)} \end{cases} \quad 0 \leq k_v(t) \leq 1 \tag{3.10}$$

If the user does not opt to participate in droop control, the droop coefficient is selected as constant 1.

$$\mathrm{k_v}(t) = \begin{cases} \left(1 - \dfrac{V_{POC}(t) - 0.98}{0.98 - 0.92}\right) & P_{reg}(t) \leq 0 \\ \left(1 - \dfrac{V_{POC}(t) - 1}{1.1 - 1}\right) & P_{reg}(t) > 0 \end{cases} \quad (3.11)$$
$$0 \leq k_v(t) \leq 1$$

$$k_l(t) = \left(1 + \frac{i_{crit} - I_{line}(t)}{1 - i_{crit}}\right) \quad (3.12)$$
$$0 \leq k_l(t) \leq 1$$

$$k(t) = \begin{cases} 1 & C_{droop} = 0 \\ k_v(t) & C_{droop} = 1 \; and \; k_v(t) \leq k_l(t) \\ k_l(t) & C_{droop} = 1 \; and \; k_l(t) < k_v(t) \end{cases} \quad (3.13)$$

Table 3.2: Selection of droop coefficient [k(t)]

Conditions		Selection
$[\boldsymbol{C_{droop}}]$.	$\boldsymbol{k_v(t) \leq k_l(t)}$	$\boldsymbol{k(t)}$
0	x	1
1	1	$k_v(t)$
1	0	$k_l(t)$

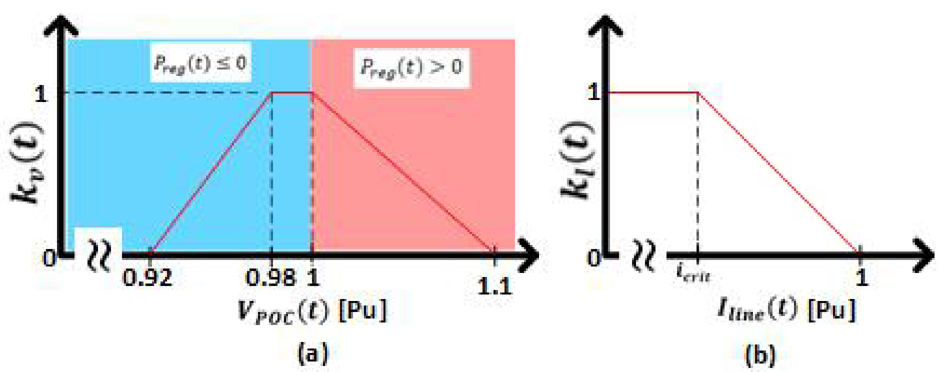

Figure 3.11: Droop coefficient for (a) voltage and (b) loading

Summary: Active power for charging or discharging EV is controlled based on droop coefficient to regulate $V_{POC}(t)$ as per users' preference.

3.5.4. Flexibility offers with schedule charging and droop control preference

Users are allowed to select an option (C_{sch}) to participate in scheduled EV charging. Scheduled power [$P_{sch}(t)$] is either generated by cloud computing based on an optimal solution for power regulation in the grid (online) or app based optimal solution defined by user and stored in the controller(offline). There is a separate section to discuss on the optimal charging of EV. In case the user does not want to charge based on scheduled power, the EV will start charging immediately with rated power of the charger [$P_{rated}(t)$]. Thus, the flexible power [$P_{flex}(t)$] and its associated control signal [$C_{flex}(t)$] is selected based on user preference to participate in schedule charging as in (3.14) based on Table 3.3.

Table 3.3: Selection of flexible power [P_flex (t)]

Condition	**Output**	
C_{sch}	$C_{flex}(t)$]	$P_{flex}(t)$
0	0	$k(t) \times P_{rated} \times S(t)$
1	1	$k(t) \times P_{sch}(t) \times S(t)$

$$P_{flex}(t) = \begin{cases} k(t) \times P_{rated} \times S(t) & C_{flex} = 0 \\ k(t) \times P_{sch}(t) \times S(t) & C_{flex} = 1 \end{cases} \tag{3.14}$$

Summary: Flexible charging (in terms of time and power level) of EV is possible with selection of schedule charging. By selection of droop control, charging time and power level can be varied despite of schedule to regulate $V_{POC}(t)$ and line loading of selected cable.

3.5.5. Participation in up-down power regulation as vehicle to grid V2G:

The ability to provide additional generation in response to the power system operator is considered as up-regulation. The down regulation is the capability to reduce generation or store energy on regulated signal. Users can select C_{reg} option to participate in grid regulated power exchange between vehicle and grid [$P_{v2g}(t)$]. To participate in V2G power exchange, $SOC(t)$ must be between 20-100%. This limit ensures that EV battery is not drained below 20% when EV is supplying regulated power to grid, and EV is not accepting any power consumption when $SOC(t) = 100\%$. The EV can be connected to a charger despite being fully charged (idle state) to participate in V2G operation. Conditions to participate in V2G [S_{reg}] based on $SOC(t)$ and regulated power requirement [$P_{reg}(t)$] is presented in Table 3.4 and (3.15)-(3.17).

Table 3.4: Conditions to participate in V2G based on SOC of EV

Conditions				**Output**
$\boldsymbol{X(t)}$	$\boldsymbol{P_{reg}(t)}$	$\boldsymbol{SOC(t) > 20\%}$ [$\boldsymbol{S_{up}(t)}$]	$\boldsymbol{SOC(t) < 100\%}$ [$\boldsymbol{S_{dn}(t)}$]	$\boldsymbol{S_{reg}(t)}$
0	x	x	x	0
1	0	x	x	0
1	+ve (> 0)	0	x	0
1	+ve (> 0)	1	x	1
1	-ve (< 0)	x	0	0
1	-ve (< 0)	x	1	1

$$S_{up}(t) = \begin{cases} 0 & SOC(t) < 20\% \\ 1 & SOC(t) \geq 100\ \% \end{cases} \tag{3.15}$$

$$S_{dn}(t) = \begin{cases} 0 & SOC(t) = 100\% \\ 1 & SOC(t) < 100\ \% \end{cases} \tag{3.16}$$

$$S_{reg}(t) = \begin{cases} 0 & X(t) = 0\ or\ P_{reg}(t) = 0 \\ S_{up}(t) & X(t) = 1\ and\ P_{reg}(t) > 0 \\ S_{dn}(t) & X(t) = 1\ and\ P_{reg}(t) < 0 \end{cases} \tag{3.17}$$

Table 3.5 shows the various conditions to determine activation of V2G signal [$C_{v2g}(t)$] and power transferred [$P_{v2g}(t)$]. The regulated power requirement [$P_{reg}(t)$] is then sent from the cloud by the responsible parties. $P_{reg}(t)$ is +ve for discharging EV (i.e., increase generation to power system) and -ve for charging. EV (store energy). Thus $P_{v2g}(t)$ is -ve when $P_{reg}(t)$ is +ve and vice versa. Based on Table 3.5, (3.18) and (3.19) is derived.

Table 3.5: Conditions of V2G power regulation [P_v2g (t)] and activation signal [C_v2g (t)]

Conditions			Outputs	
C_{reg}	$P_{reg}(t)$	$S_{reg}(t)$	$C_{v2g}(t)$	$P_{v2g}(t)$
0	x	x	0	0
1	=0	x	0	0
1	≠0	0	1	0
1	≠0	1	1	$-P_{reg}(t) \times k(t)$

$$C_{v2g}(t) = \begin{cases} 0 & C_{reg} = 0\ \ or\ P_{reg}(t) = 0 \\ 1 & C_{reg} = 1\ and\ P_{reg}(t) \neq 0) \end{cases} \tag{3.18}$$

$$P_{v2g}(t) = \begin{cases} 0 & C_{v2g}(t) = 0 \\ 0 & C_{v2g}(t) = 1\ and\ S_{reg}(t) = 0 \\ -P_{reg}(t) \times k(t) & C_{v2g}(t) = 1\ and\ S_{reg}(t) = 1 \end{cases} \tag{3.19}$$

The EV will participate in power regulation if the user has chosen the option to participate in it. Equation (3.18) determines activation of power regulation [$C_{v2g}(t)$] based on user preference [C_{reg}] and power regulation requirement [$P_{reg}(t)$]. When the power regulation signal is active, power transfer [$P_{v2g}(t)$] is commenced based on (3.19). When the EV is fully charged during down power regulation or discharged up to 20% during up power regulation, then there is no power transfer between EV and grid while power regulation signal [$C_{v2g}(t)$] is activated to stop charging of EV during power up regulation.

Summary: EV can participate in grid power regulation based on SOC level of EV and user preference. When selected for participation in power regulation, no power is exchanged between EV and grid during up and down regulation, while $SOC(t) < 20\%$ and $SOC(t) = 100\%$ respectively.

3.5.6. Priority Signal:

Priority signal [$C_{priority}(t)$] is generated by the controller based on battery $SOC(t)$ information and minimum SOC required at the time of estimated departure, as defined by the user.

There may arise the condition where EV is not charged to its minimum defined level before estimated departure, due to following reasons.

- Error in schedule signal or failure of data transmission network.
- Charging with lower power than scheduled due to droop or power regulation.

The total time required for minimum SOC charge and remaining time for departure is calculated in (3.20) and (3.6) respectively. Then the priority signal [$C_{priority}(t)$] is generated as in (3.22) and charging power in (3.23).

$$t_{socmin} = \frac{[SOC_{min} - SOC(t)] \times C_{battery} \times 3600}{P_{rated} \times 100}\ [s] \tag{3.20}$$

$$t_{remain} = t_{departure} - t\ [s] \tag{3.21}$$

$$C_{priority}(t) = \begin{cases} 0 & T_{remain} > T_{socmin}\ or\ S(t) = 0 \\ 1 & T_{remain} \leq T_{socmin}\ and\ S(t) = 1 \end{cases} \tag{3.22}$$

$$P_{priority}(t) = \begin{cases} 0 & C_{priority}(t) = 1 \\ P_{rated} & C_{priority}(t) = 1\ and\ SOC(t) < SOC_{min} \\ k(t) \times P_{rated} & C_{priority}(t) = 1\ and\ SOC_{min} \leq SOC(t) \leq 100\% \end{cases} \tag{3.23}$$

When priority signal is activated [$C_{priority}(t)$] EV charges with rated power of charger (until $SOC(t) < SOC_{min}$) without participating in any other activities of flexible power transfer or power regulation. Then when $SOC(t) \geq SOC_{min}$ it continues to charge with $k(t) \times P_{rated} \times S(t)$ so as not to stress the grid. However, it will not participate in grid regulation or scheduled charging as users may depart any time here onward.

Thus, the priority signal ensures that the EV is at least charged to minimum defined SOC level at the time of departure. EV charges with nominal rated power despite low volage and schedule. Under favorable conditions, EVs can be charged to more than minimum SOC level with rate power and droop control if selected.

Table 3.6: Conditions of priority signal [C_priority (t)] activation and power [P_priority (t)]

Conditions			**Outputs**	
$S(t)$	$T_{remain} > T_{socmin}$	$S_{min}(t)$	$C_{priority}(t)$	$P_{priority}(t)$
0	x	X	0	0
1	0	0	0	0
1	1	1	1	P_{rated}
1	1	0	1	$k(t) \times P_{rated}$

Summary**:** Priority signal is activated by controller, when charging time of EV to minimum SOC level is less than 15 minutes prior to estimated departure time. Once the priority signal is activated, EV is charged up to minimum SOC level with rated power and then with droop control until fully charged or disconnected. Further, EV is not allowed to participate in grid regulation as EV needs to be ready for departure.

3.5.7. Charging Power of EV [P_char (t)]

The charging power of EV is based on the various options selected by the user to participate in grid flexibility, droop control and V2G. The charging power based on activation signals such as Priority [$C_{priority}(t)$] and grid power regulation [$C_{v2g}(t)$] is presented in (3.24) and summarized in Table 3.7.

$$P_{char}(t) = \begin{cases} P_{priority}(t) & C_{priority}(t) = 1 \\ P_{v2g}(t) & C_{priority}(t) = 0 \; and \; C_{v2g}(t) = 1 \\ P_{flex}(t) & C_{priority}(t) = 0 \; and \; C_{v2g}(t) = 0 \end{cases} \quad (3.24)$$

Table 3.7: Selection of charging power of EV [P_char (t)]

Conditions		Output
Priority [$C_{priority}(t)$]	Grid Regulation [$C_{v2g}(t)$]	Charging power (kW) [$P_{char}(t)$]
0	0	$P_{flex}(t)$
0	1	$P_{v2g}(t)$

The variation in charging power [$P_{char}(t)$] is limited by 1%/s as power output from commercial charger increases or decreases slowly.

3.5.8. Simulation Results

The simulation is carried out in DigSILENT PowerFactory with eight households in a radial feeder as shown in Figure 3.12. Each house is equipped with a heat pump and EV along with its other regular loads. The flexible operation of HP is demonstrated in D2.2. Here, the flexible operation of EV based on (23) is demonstrated with the help of three case studies in Table 3.8. The simulated results are presented in Figure 3.13, Figure 3.14, and Figure 3.15 for each case study respectively. The final SOC required and time of departure of each EV is presented in Table 3.9.

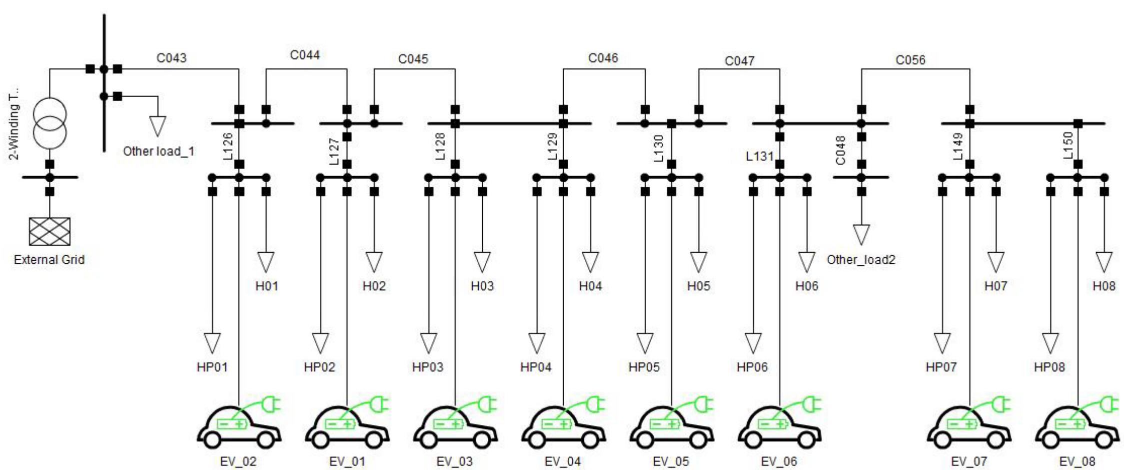

Figure 3.12: Test Grid

Table 3.8: Case Studies

Case Study	Droop control	Scheduled charging	Participation in grid power regulation
Base case (all EV)	No	No	Yes
Case I (all EV)	Yes	No	Yes
Case II (all EV)	Yes	Yes	Yes

Table 3.9: EV charging requirements

EV	Departure (hour)	$\mathbf{SOC_{min}}$(%)
EV1	8	80
EV2	10	80
EV3	8	70
EV4	5	80
EV5	5	80
EV6	5	80
EV7	5	80
EV8	5	80

Table 3.10: Other Parameters for controller and charger

Parameters	Unit
$C_{battery}$	42 kWh
P_{rated}	7.2 kW
i_{crit}	80% (0.8)

Figure 3.13, Figure 3.14 and Figure 3.15 shows the simulation result for base case, case I and case II respectively.

- Sub figure (a): droop coefficient [$k(t)$]
- Sub figure (b): terminal voltage at POC [$V_{POC}(t)$]
- Sub figure (c): charging power (kW) [$P_{char}(t)$]
- Sub figure (d): SOC of EV [$SOC(t)$]

When user does not want scheduled charging and droop control, the EV starts to charge immediately when plugged in. $V_{POC}(t)$ increases and decrease rapidly during and after up power regulation of grid respectively as seen in red circle from Figure 3.13(b).

With the selection of droop control, the $V_{POC}(t)$ improves compared to base case seen in red circle from Figure 3.14(b), however the charging and regulation power Figure 3.14(c)) decreases based on droop coefficient.

The $V_{POC}(t)$ further improves with Case III when flexible charging is preferred along with droop control Figure 3.15(b). It is worth noting that when all the EVs are subject to charging (Figure 3.15(c)), e.g., during lower electricity prices, the EV at the far end of the feeder with lower voltage is charged with lower power based on droop coefficient. Thus, in weak or long radial feeder grids, the EVs at the far end are not able to take full benefit of lower spot electricity price. However, the grid parameters such as voltage and line loading are maintained within the limit. Provision of appropriate compensation for such users is recommended.

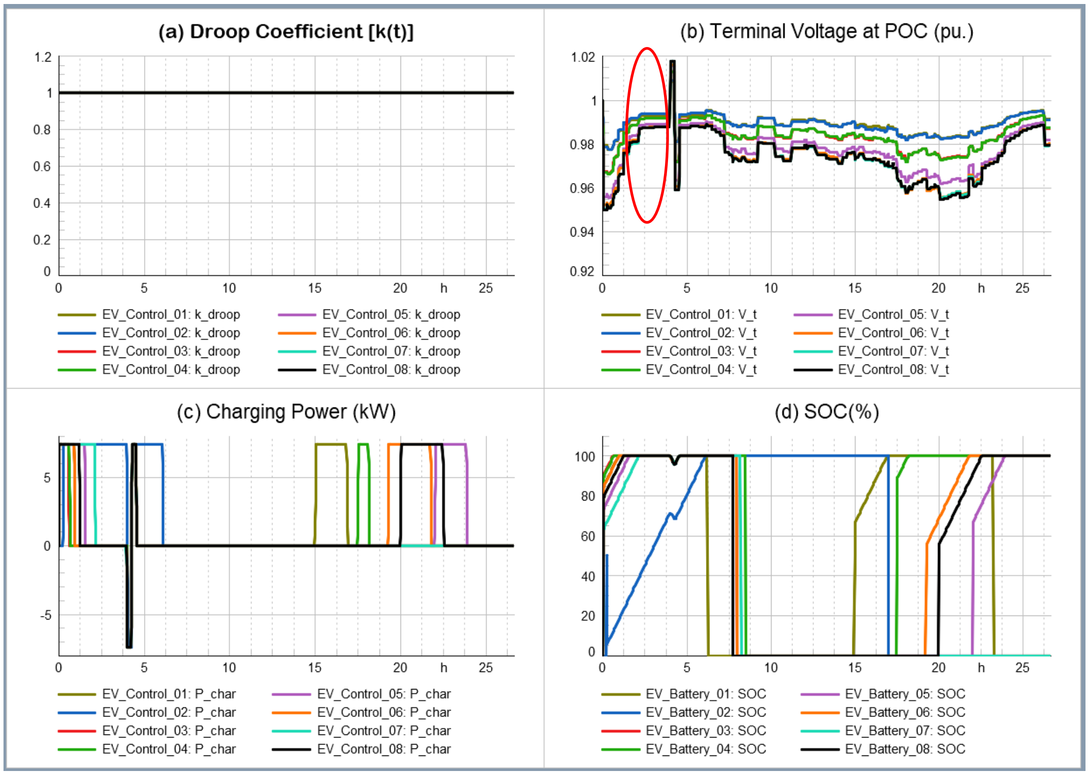

Figure 3.13: Base case

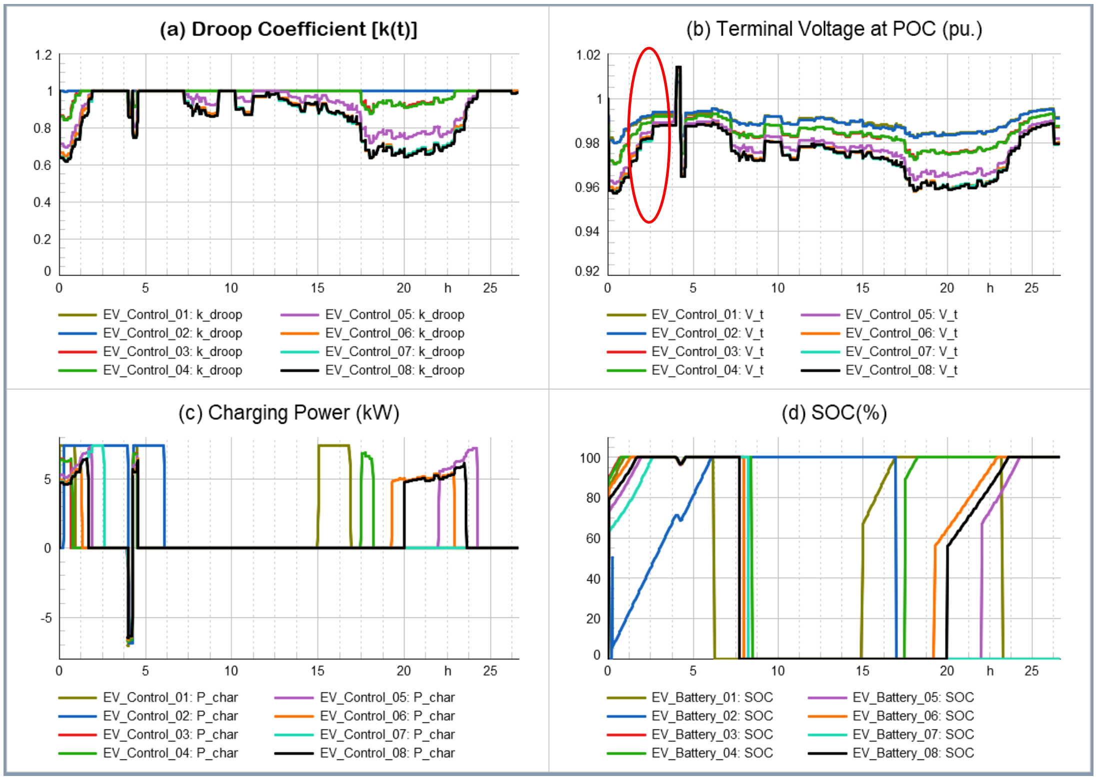

Figure 3.14: Case I

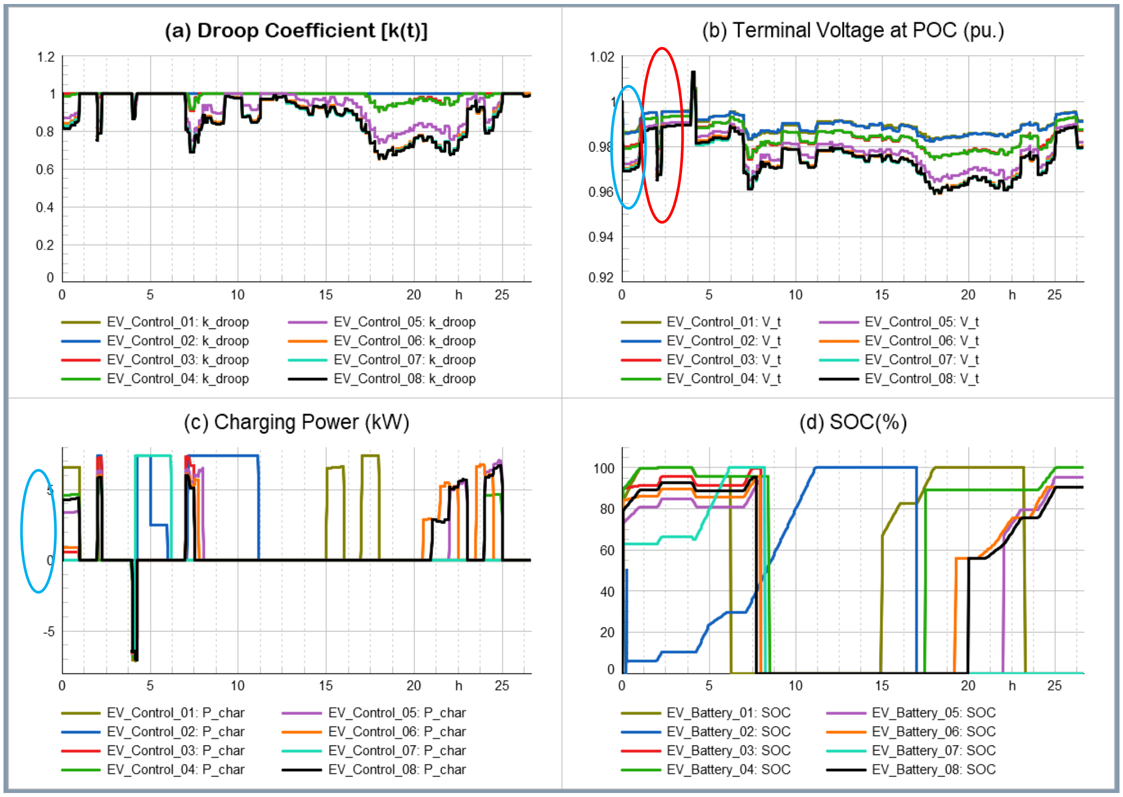

Figure 3.15: Case II

3.6. Conclusion

Unregulated EV charging can lead to various technical problems within distribution networks. These issues encompass voltage instability, phase imbalance, increased peak loads, overloading, power loss, and power quality concerns. Distribution grids, which have high resistance-to-inductance ratios, are particularly vulnerable to voltage drops when experiencing high power consumption, resulting in voltage deviations from normal levels. The growth in EV usage worsens this susceptibility due to the significant power demand of EV charging. Additionally, EV charging often coincides with the evening's peak electricity demand, exacerbating the challenges related to voltage stability. One potential solution to address these issues is the integration of EVs through smart charging control. Smart charging control for EVs is responsive to both EV demand and network conditions. This approach ensures that the charging process does not impact network stability and maintains the voltages in nominal levels while considering thermal loading of distribution lines. In this context, a centralized charging strategy has been developed to tackle multiple challenges associated with unregulated EV charging. This strategy aims to minimize charging costs for EV users, distribute the grid load more evenly, and reduce peak-to-average ratios for system operators.

4. Modelling and integration of sustainable and smart water pumping, waste management systems[4]

Water is fundamental to human survival, health, ecosystems, and economic progress [108]. Yet, millions, particularly in rural areas, lack access to clean water [109]. Globally, 2.2 billion people lack safe drinking water facilities [110]. Distance from modern water systems and low socioeconomic status often underlie this crisis [111]. Solving this challenge is vital for sustainable development. Water is typically transported from sources to storage using mechanical systems powered by electricity generated from sources like coal, petroleum, or RE [112]. Reliable energy is crucial for efficient water pumping [113], [114], especially in remote areas lacking power infrastructure [115]. RE like solar photovoltaics (PV) offer a sustainable solution [116], [117]. Solar PV water pumping systems (SPVWPS) harness sunlight for water delivery, reducing costs and emissions [118]. Precise sizing and design are critical [119]. Site selection and dimensioning calculations ensure efficient operation [120], [121]. Site choice involves complex multi-criteria decision-making (MCDM) [122]–[124]. After selection, components like PV modules and pumps must be correctly sized [125], [126]. Oversizing incurs extra costs, while undersizing compromises performance [127], [128]. Our study addresses these challenges through comprehensive analysis and proposes an integrated solution.

An MCDM-based software tool was formulated that aids SPVWPS deployment. Unlike existing tools, it considers criteria importance, incorporates triangular fuzzy numbers (TFN), and provides holistic site evaluation [129], [130]. It optimizes component sizing using empirical relations. The tool offers pre-feasibility technical estimates, suggesting PV module quantities, pumping equipment, and tank size for minimal investment. It bridges the gap between site selection and sizing, serving as a complete SPVWPS deployment package. The tool was corroborated through a case study focused on small, remote, economically challenged communities with complex terrains. The lack of an all-inclusive SPVWPS tool was addressed, offering both sizing and site selection [131]. Our proposed solution fills this gap by combining algorithms for both aspects. The primary goal of the tool is to provide users with limited insight on SPVWPS with the know-how to obtain a pre-feasibility technical and economic estimation for their project. By offering a holistic approach to SPVWPS implementation, we aim to contribute to addressing water access challenges and promoting sustainable solutions.

4.1. A software tool for finding the optimal location for installing the solar photovoltaic water pumping system

Selecting the right location for a project or plant installation has a significant influence on how efficiently resources are utilized, highlighting the importance of making a suitable choice for the site. Determining the best location for a solar PV plant is a complex task falling into the category of Multiple Criteria Decision

[4] Contents from this chapter are a part of the following articles published/to be published under the SUSTENANCE project:
N. S. Rengma, M. Yadav, and N. Kishor, 'Solar photovoltaic water pumping system: A software tool development-based optimal configuration investigation for system installation location, sizing and deployment', *Renewable Energy Focus*, vol. 46, pp. 236–255, Sep. 2023, doi: 10.1016/j.ref.2023.07.001.

Making (MCDM) problems. It involves the consideration of a range of criteria encompassing social, technical, environmental, economic, and political facets [123]. Each of these criteria is further broken down into various sub-criteria, as depicted in Figure 4.1, and these sub-criteria are jointly utilized to pinpoint the deployment site for solar energy generation. Consequently, the solar energy site selection process is an intricate process. Therefore, when implementing a solar PV project, it is crucial to consider a diverse set of criteria and sub-criteria to identify the best location. This approach leads to an energy-efficient, cost-effective solution that minimizes environmental impact for consumers.

The selection of the evaluation criteria often depends on factors like the study's objectives, the complexity of the study area, the availability of geospatial data, and existing literature. The choice of criteria is tailored to the specific context and application of renewable energy. In the context of deploying solar power projects, crucial criteria for assessing feasibility and sustainability include solar irradiance, land availability, and terrain characteristics. Additionally, factors such as land use, proximity to roads and settlements are also effective criteria to take into consideration.

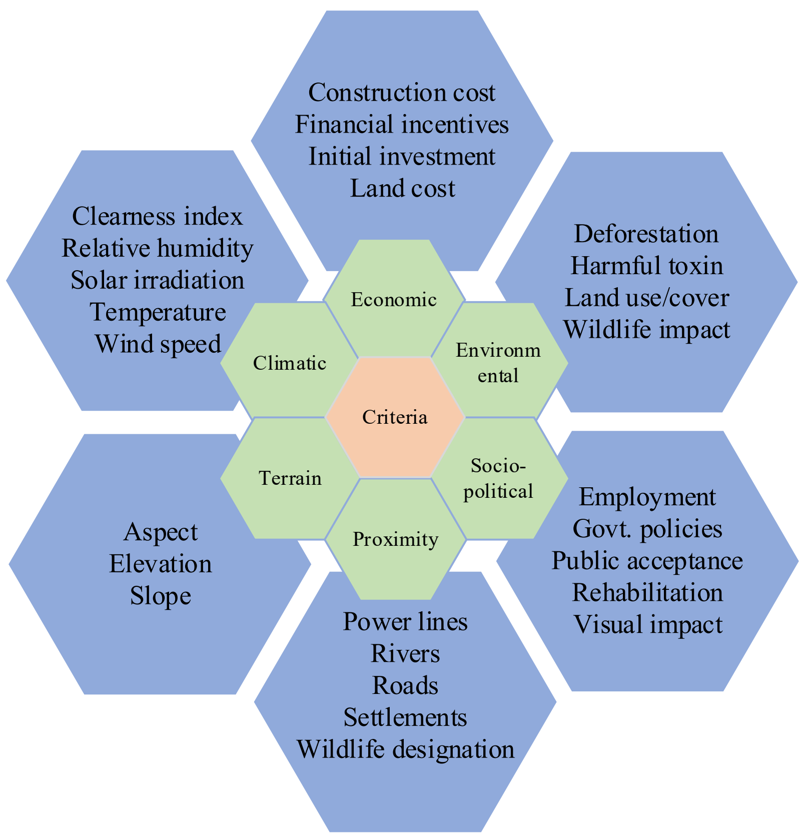

Figure 4.1: Criteria and their sub-criteria for evaluating the potential sites.

4.1.1. Methodology: Site selection

The importance of the criteria can vary depending on the specific region under examination. Additionally, the consideration of supplementary criteria or sub-criteria might become necessary due to variations in social, geographical, and environmental factors. For smaller study areas, the initial step involves conducting a site survey. Subsequently, evaluation criteria are established considering factors such as terrain, environmental consequences, societal approval, and proximity to relevant landmarks. Throughout the process of site visits, interviews, and meetings, the significance of these criteria is communicated to local communities and representatives. Multiple potential sites are then put forth, emphasizing minimal impact on the environment and human aspects, while also ensuring cost-effectiveness and energy efficiency. The identified criteria are subsequently compared in a pairwise manner and input into the software tool. This tool, constructed using the FAHP technique, is designed to determine the optimal installation sites for SPVWPS.

Fuzzy AHP method

In the FAHP method, the preferences are established using PCMs, which utilize a discrete nine-point scale (1 – 9) as depicted in Figure 4.2. To capture the uncertainty in the information of the PCMs, the criteria preferences are subsequently converted into triangular fuzzy integers ranging from 1 to 9.

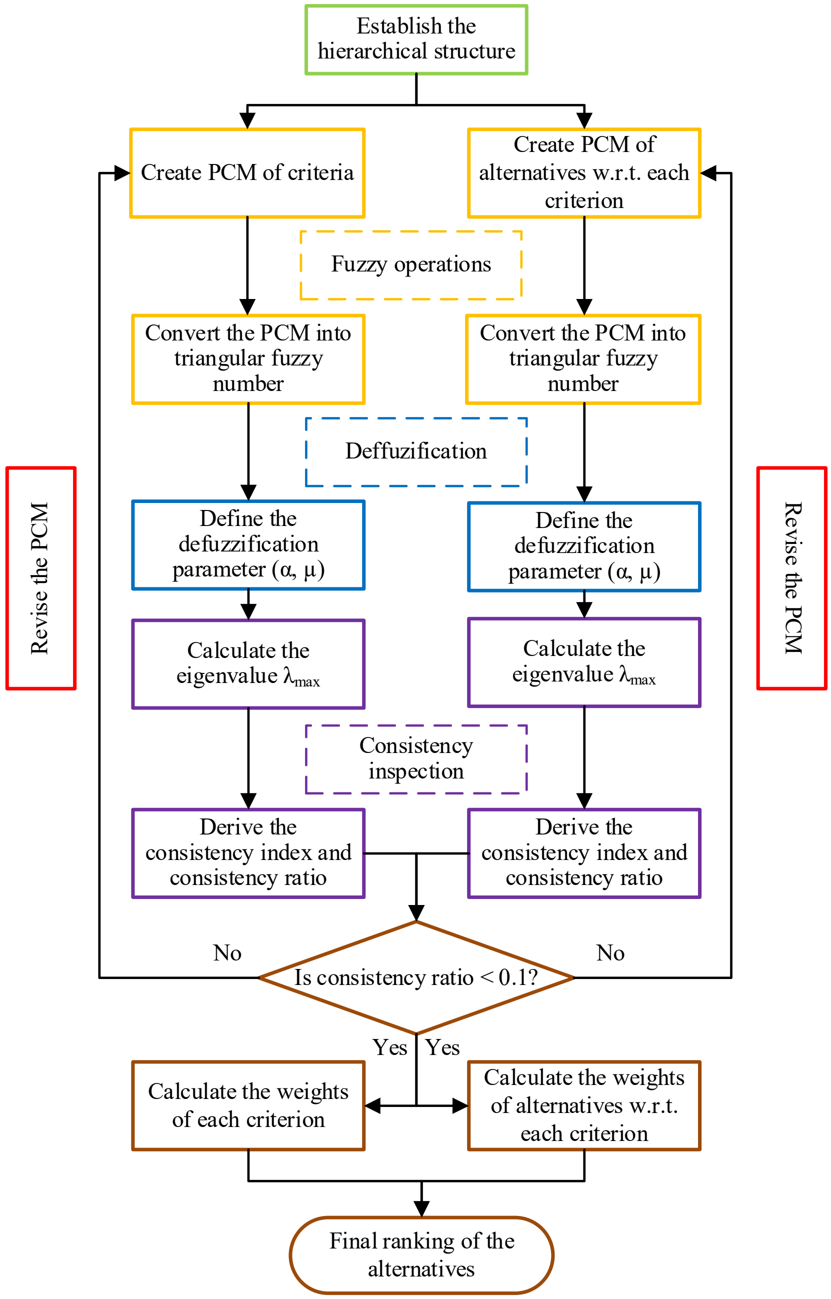

Figure 4.2: Flowchart of the FAHP

The structured approach ensures a systematic and consistent evaluation of criteria and alternatives, enabling robust decision-making. Triangular fuzzy numbers (TFN) are employed to calculate eigenvectors in the PCM for both criteria and alternatives. These TFNs represent the imprecise nature of expert judgments. To ascertain the consistency of judgments, we calculate consistency ratios for each criterion in the PCM for both criteria and alternatives. For each of the "b" criteria, a PCM denoted as $\tilde{A}$ (b, b) is established. This matrix compares one criterion "i" to a second criterion "j" based on Saaty's scale. In this matrix, diagonal coefficients are set to 1, reflecting that a criterion is compared to itself. The other coefficients within the PCM are determined as the inverses of their respective sub-diagonals, as illustrated in (4.1).

$$\tilde{A} = \begin{bmatrix} 1 & \tilde{a}_{12} & \dots & \tilde{a}_{1b} \\ \tilde{a}_{21} & 1 & \dots & \tilde{a}_{2b} \\ \vdots & \vdots & \vdots & \vdots \\ \tilde{a}_{b1} & \tilde{a}_{b2} & \dots & 1 \end{bmatrix} \tag{4.1}$$

a_{ij}^{k}represents the comparing of criteria i and j by an expert k where i is more significant than j.
Therefore, as shown in (4.2),

$$a_{ij}^{k} = \frac{1}{a_{ji}^{k}} \tag{4.2}$$

For $i \neq j$, $\tilde{a}_{ij}$ = 1, 3, 5, 7, 9 or 1^{-1}, 3^{-1}, 5^{-1}, 7^{-1}, 9^{-1}.
The PCM is then converted into a TFN as shown in (4.3).

$$\tilde{A} = \tilde{a}_{ij} = \begin{bmatrix} 1,1,1 & l_{12}, m_{12}, u_{12} & \dots & l_{1m}, m_{1m}, u_{1m} \\ l_{21}, m_{21}, u_{21} & 1,1,1 & \dots & l_{2m}, m_{2m}, u_{2m} \\ \vdots & \vdots & \vdots & \vdots \\ \vdots & \vdots & \vdots & \vdots \\ l_{m1}, m_{m1}, u_{m1} & l_{m2}, m_{m2}, u_{m2} & \dots & 1,1,1 \end{bmatrix} \tag{4.3}$$

where l_{ij}, m_{ij}, u_{ij} ∈ [1/9, 9], the lower, middle, and upper values of the TFN respectively.
When dealing with judgments from multiple experts, the Buckley method is applied for their consolidation. In this context, TFN are employed, comprising the lower, middle, and upper limits. These bounds are established by considering the minimum, geometric mean, and maximum preferences, respectively, among the judgments provided by multiple experts. Specifically, the values l_{ij}, m_{ij}, and u_{ij}, corresponding to the minimum, geometric mean, and maximum values, respectively, are computed for each a_{ij}^{k} (where "k" represents the expert index from 1 to n), as demonstrated in (4.4). This process effectively combines the insights of multiple experts to arrive at a more comprehensive evaluation.

$$l_{ij} = min\, a_{ij}^{k} \tag{4.4}$$

$$m_{ij} = \sqrt[n]{\prod_{k=1}^{n} a_{ij}^{k}} \tag{4.5}$$

$$u_{ij} = max\, a_{ij}^{k} \tag{4.6}$$

For all i, j =1,…n

The parameters α (uncertainty index of judgement matrix Ã) and μ (optimism degree of judgement matrix Ã) are put forward for defuzzification of fuzzy PCM, where 0 ≤ α ≤ 1 and α+μ=1. Higher values of α and lower μ are more suitable. Here, α and μ, both are assumed as 0.5, while advanced users could determine it in the developed software tool.

A function of $g_{\alpha,\mu}(\tilde{a}_{ij})$ was defined based on l_{ij} and u_{ij} in [38], as shown in (4.7) and (4.8).

$$g_{\alpha,\mu}(\tilde{a}_{ij}) = [\mu. f_\alpha(l_{ij}) + (1-\mu). f_\alpha(u_{ij})], \quad 0 \le \alpha, \mu \le 1 \tag{4.7}$$

$$g_{\alpha,\mu}(\tilde{a}_{ij}) = \frac{1}{g_{\alpha,\mu}(\tilde{a}_{ij})} \quad 0 \le \alpha, \mu \le 1: \quad i > j \qquad (4.8$$

where,

$$f_\alpha(l_{ij}) = (m_{ij} - l_{ij}) \times \alpha + l_{ij}$$
$$f_\alpha(u_{ij}) = u_{ij} - (u_{ij} - m_{ij}) \times \alpha$$

α = Stability condition index

μ = Expert judgement pessimism index

To assess the consistency of the opinions of the expert/s, the consistency ratio (CR) is employed, represented by (4.11). The process of evaluating consistency consisted of three sequential steps. First, the software computes the maximum eigenvalue (λ_{max}) of the PCM ($g_{\alpha,\mu}$ (Ã)), as determined by (4.9), corresponding to the highest root of the polynomial.

$$det(\, g_{\alpha,\mu}(\tilde{A}) - \lambda_{max} \tag{4.9}$$

(4.10) presents the consistency index (CI) of matrix Ã.

$$CI = \frac{\lambda_{max}}{b-1} \tag{4.10}$$

where b is the matrix size (criteria numbers).
Ultimately, the CR is calculated from the random index (RI) using the standard consistency indices as shown in Table 4.1.

$$CR = \frac{CI}{RI} \tag{4.11}$$

Table 4.1: Values for Consistency Index based on Number of Criteria

Matrix size (b)	1	2	3	4	5	6	7	8	9	10	11	12	13	14	15
Random index (RI)	0	0	0.58	0.9	1.12	1.24	1.32	1.41	1.45	1.49	1.51	1.54	1.56	1.57	1.58

To ensure consistency with the PCM-derived results, the CR should not exceed 0.10. If it exceeds this threshold, a reassessment of the expert opinion is necessary. Ultimately, the determination of alternative rankings is based on the sum of the product of attribute and alternative weights for each criterion. The weighted evaluation for alternative t is shown by (4.12).

$$\text{Overall alternative rating} = \sum_{i=1}^{b}(attribute\ weight_i\ \times evaluation\ rating_{it}) \tag{4.12}$$

For i = 1, 2, …, b (b: total number of criteria)

4.1.2. Tool Description & Case Study

This section outlines the development of a software tool designed for the optimal selection and sizing of SPVWPS. The methodological steps for site selection, as discussed earlier in the methodology section, have been translated into a MATLAB program using the App Designer module, as demonstrated in Figure 4.3. The resulting SPVWPS tool can be applied to any MCDM problem. Specifically, if you are involved in the installation of SPVWPS, this tool assists you in the initial stage of site selection. For the site selection process, users are required to input site-specific data, such as the Pairwise Comparison Matrix (PCM) for evaluation criteria and the PCM for alternatives, into Excel files (.xlsx) through an intuitive data-driven user interface. The PCM can be filled in both directions without considering the hierarchical arrangement of criteria or alternatives. The first criterion input by the user into the PCM, situated at position (1, 1) in the initial row and column, will be identified as the primary criterion in the tool's interface. Following that, the second criterion, located at (1, 2) in the initial row and second column, will be assigned as the secondary criterion, and so forth. The alternatives will be assigned sequential numbers, corresponding to their order in the PCM. It is crucial for users to keep this order in mind when evaluating the consistency of the alternative PCMs. Additionally, the tool supports both single and multi-expert PCMs for the criteria and single expert PCMs for the alternatives. Advanced users also have the option to specify the degree of uncertainty (α-cut) to align with their preferences. Nevertheless, if left unspecified, the default value of 0.5 will be used for calculations.

After inputting the PCM criteria and specifying the degree of uncertainty within the tool, users can easily obtain the results for criterion weights and rankings by clicking the 'CALCULATE' button. In scenarios involving site selection with multiple alternatives, the tool will then prompt users to provide input for alternative PCMs. Should the matrices submitted by the user be deemed inconsistent, the tool will advise users to review their assessments and recreate the PCMs accordingly.

To evaluate the tool's performance, the best site was selected, and the appropriate system size was chosen. Then, the results were compared with those obtained using a traditional MATLAB program and cross-checked with on-site data. The outcomes from these evaluations showed clear resemblances to the actual on-site data. The tool's flexibility permits the generation of multiple solutions that align with the input data and user preferences. Furthermore, it can be employed to generate similar results for any location worldwide by incorporating location-specific input data.

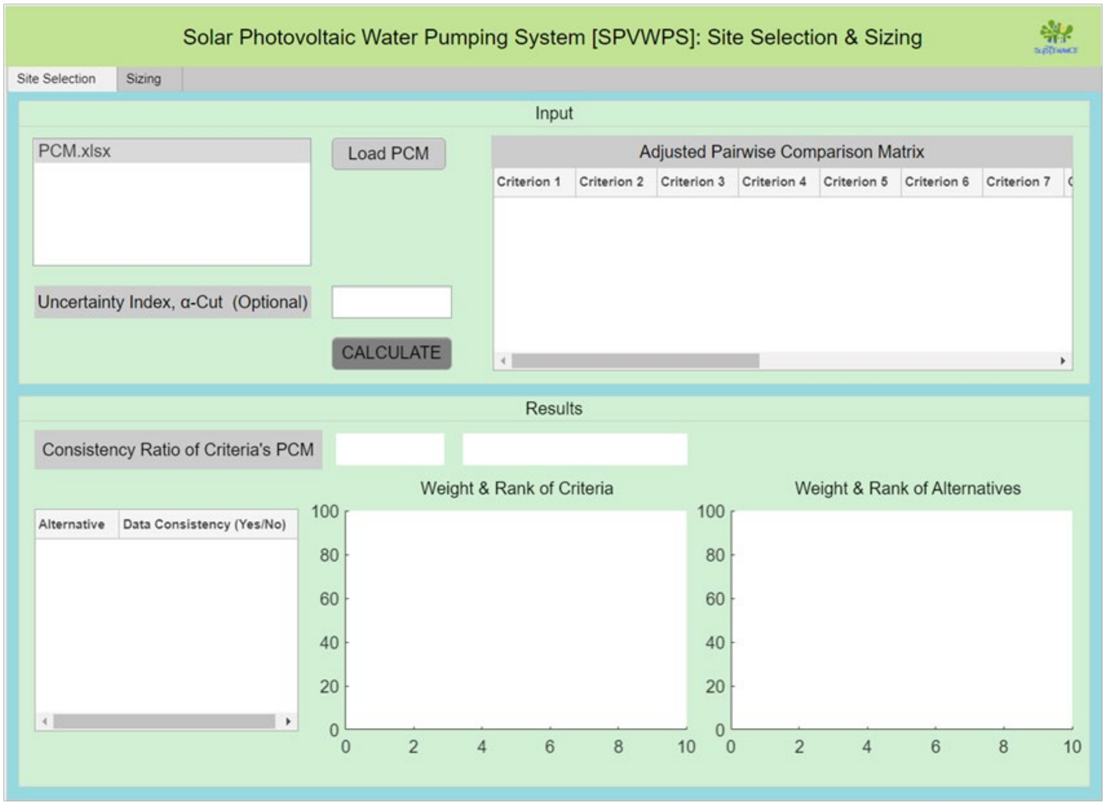

Figure 4.3: Interface of the devised tool: Tab for system site selection

Barubeda, a village located at the intersection of Hazaribagh and Ranchi districts in the state of Jharkhand in India, has been selected as the study site with numerous clusters of houses sharing the district boundaries (Figure 4.4). It is characterized by a low population and covers a total area of 1.09 km^2. The region is deprived of basic amenities such as electricity and water, while being characterized by undulating terrain, which is challenging for any developmental work.

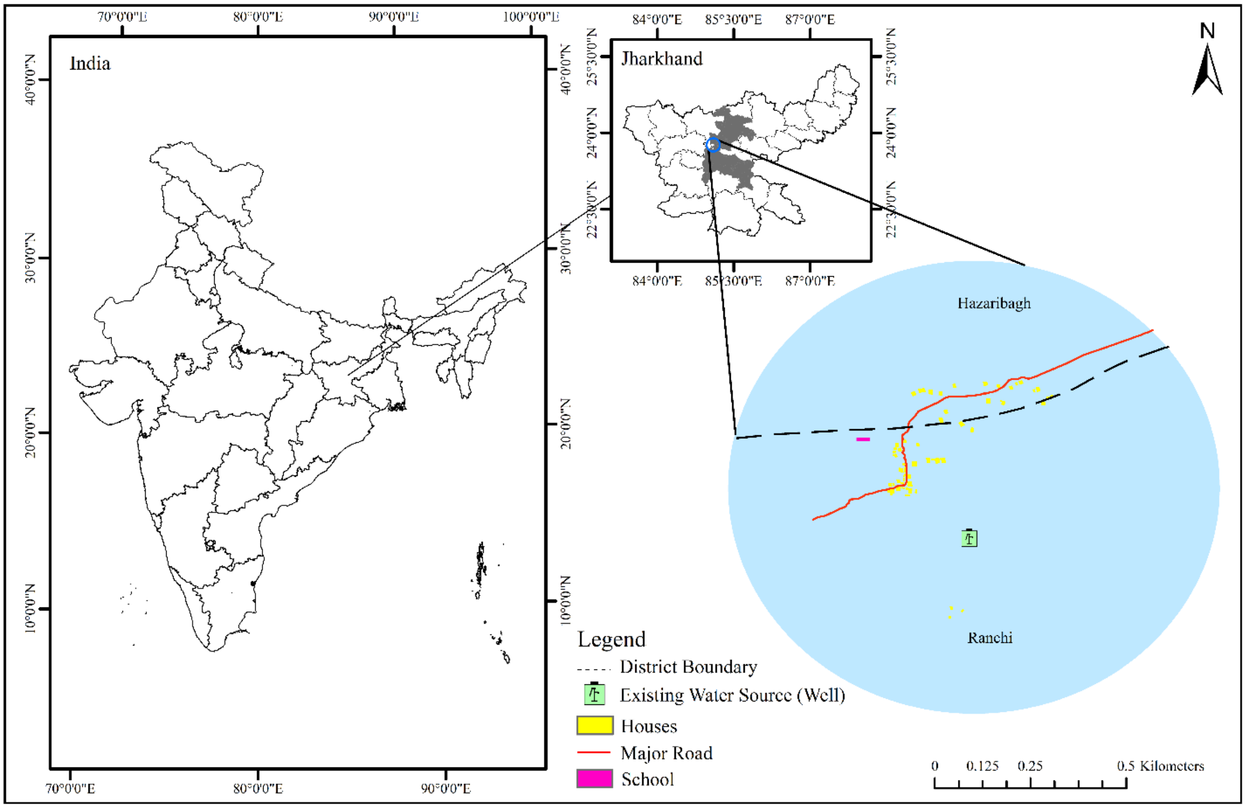

Figure 4.4: Location of the study site on the Indian map

Site selection

An extensive site visit and analysis were conducted to assess the project deployment site's terrain characteristics, land usage, proximity factors, environmental implications, and community acceptance. Following the acquisition of survey data and considering project objectives, spatial scale, and data availability, a range of evaluation criteria were identified and subsequently incorporated into Table 4.2. Due to the limitations posed by barren land availability and the complex terrain, it became impractical to house all components of the SPVWPS in a single location. Consequently, individual sites were carefully chosen for the installation of components such as borewells, PV panels, and water storage tanks.

During the site visits, the significance of each criterion was communicated to local communities and village representatives. Subsequently, alternative potential plots, as depicted in Figure 4.5, were selected for the project components. The selection process considered criteria aimed at minimizing environmental and human impact, all while ensuring cost-effectiveness and energy efficiency. The evaluation of available land is of paramount importance in solar energy projects, given the substantial land requirements of PV power plants, which can have profound effects on local communities and the environment. Therefore, the allocation of plots deliberately excluded forested areas, built-up regions, and agricultural lands. Preference was given to barren or poorly vegetated lands.

Moreover, large-scale PV plants in rural areas often encounter resistance due to their extensive land requirements resulting in the need for deforestation and ensuing social conflicts. Recognizing the potential repercussions, the project factored in environmental impact and social acceptance criteria when allocating alternative potential sites, guaranteeing that all the selected plots garnered environmental and societal approval. Economic viability stands as a critical determinant of the project's success but was not considered in isolation from other criteria. These criteria are interconnected, with each one directly or indirectly influencing construction and maintenance costs.

Table 4.2: Accounting of evaluation criteria for the deployment sites of SPVWPS

Criterion	Description	Description of the alternative plots	Used for site selection of
Aspect (C1)	In terms of the orientation of the terrain's incline, the most favorable aspects are southern slopes in northern regions and flat terrain, as they receive the highest amount of sunlight throughout the year.	Plot 1. South Plot 2. East Plot 3. East Plot 4. Southeast Plot 5. Southeast	Solar PV panel
Availability of water source (C2)	It is feasible to drill wells for extracting water from aquifers in various locations, but the expense and level of challenge are contingent on the type of surface rock. Consequently, it is more economically efficient to bore a well in an already established water source.	Plot 1. Unavailable Plot 2. Available Plot 3. Unavailable Plot 4. Unavailable Plot 5. Unavailable	Borewell
Elevation (C3)	Constructing solar power facilities in mountainous and high-altitude regions presents greater challenges and costs; however, these areas receive increased solar irradiation. Consequently, the selection of the elevation depends on the specific location of the project.	Plot 1. 438 m Plot 2. 445 m Plot 3. 455 m Plot 4. 449 m Plot 5. 448 m	Borewell Storage tank Solar PV panel
Proximity to borewell (C4)	Because the components of the SPVWPS are interdependent, it makes economic sense to construct them in close proximity to each other.	Plot 1. 107.22 m Plot 2. 0 m Plot 3. 60.43 m Plot 4. 141.38 m Plot 5.168.33 m	Storage tank Solar PV panel
Proximity to the centre of the villages (C5)	In this study, the SPVWPS emphasizes the significance of proximity to the settlement, specifically targeting the central locations within villages to ensure convenient access for all residents during stand-post delivery.	Plot 1. 80 m Plot 2. 54.18 m Plot 3. 42.71 m Plot 4. 186.79 m Plot 5. 217.82	Borewell Storage tank Solar PV panel

Proximity to road (C6)	Proximity to the transportation network not only lowers the expenses associated with transporting construction materials but also helps prevent environmental damage and the costs of road construction. Furthermore, it simplifies access for plant operations and maintenance in the event of technical issues.	Plot 1. 26.32 m Plot 2. 35.00 m Plot 3. 25.00 m Plot 4. 62.00 m Plot 5. 60.00 m	Borewell Storage tank Solar PV panel
Slope (C7)	Usually, flat terrain is considered most favorable for solar installations since the design and installation of PV panels on sloping surfaces are more challenging and costly. Steep slopes can pose difficulties related to erosion, drainage, and the stability of foundations.	Plot 1. 6.22º Plot 2. 5.84º Plot 3. 4.05º Plot 4. 4.63º Plot 5. 5.46º	Borewell Storage tank Solar PV panel

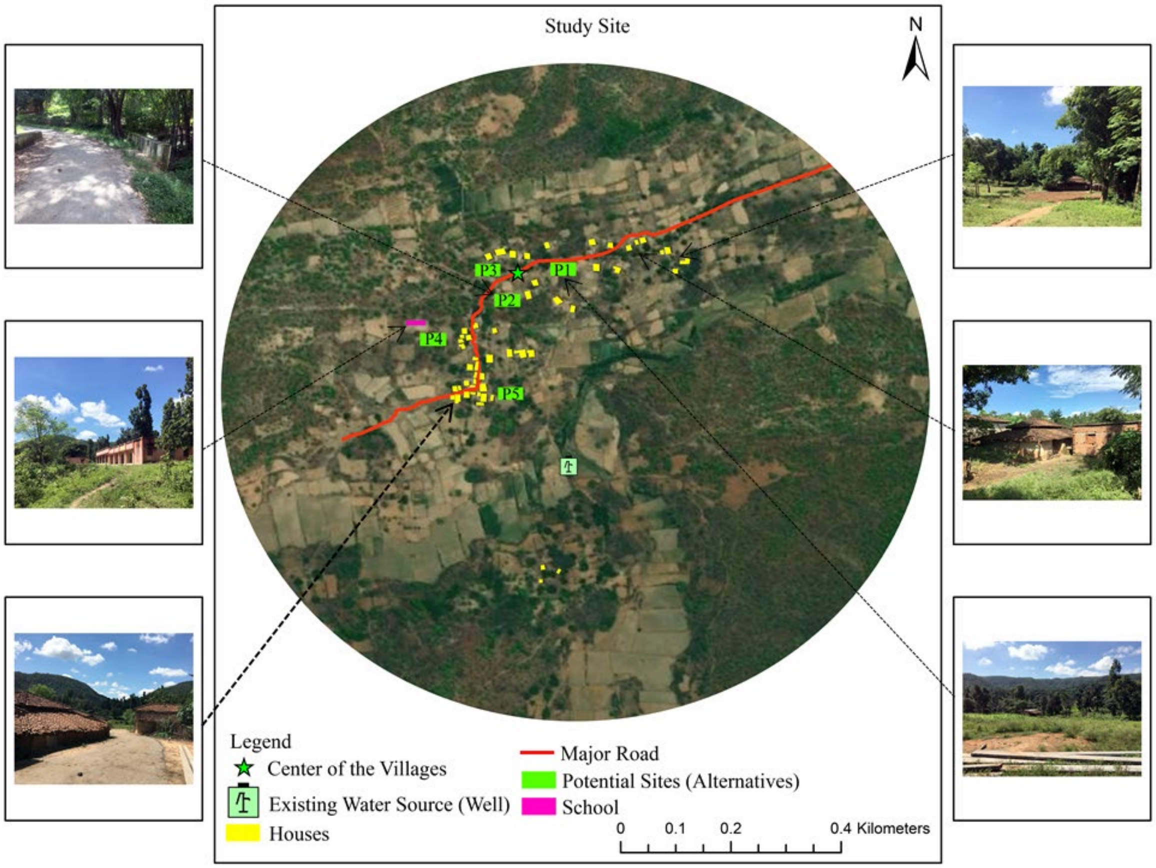

Figure 4.5: Alternative plots of land allocated for the installation of the system components.

The comparison and quantification of the selected evaluation criteria using a well-defined rating scale ranging from 1 to 9, utilizing the PCM method. This rigorous assessment aimed to identify the site that best aligns with the economic, environmental, social, and technical goals outlined in the study. When assessing the criteria for borewell construction, all factors were taken into account except for aspect and proximity to their designated location (i.e., proximity to borewell), as outlined in Table 4.3. Following the ranking of criteria for selecting the borewell site based on the PCM results, the PCMs of the alternative options (found in Table 4.4) were input into the software to rank potential plots. Subsequently, the software tool ranked potential locations for the five designated sites designated for borewell construction, as depicted in Figure 4.6.

Table 4.3: PCM for criteria accounted for the borewell site selection.

Criteria	C2	C3	C5	C6	C7
C2	1	2	9	8	7
C3	0.14	1	8	7	6
C5	0.11	0.33	1	0.5	0.33
C6	0.2	3	5	1	0.5

C7	0.14	3	3	0	1

Table 4.4: PCM for alternatives of borewell construction concerning proximity to the road.

Alternative plot	Plot 1	Plot 2	Plot 3	Plot 4	Plot 5
Plot 1	1	3	0.25	5	4
Plot 2	0.33	1	0.2	4	3
Plot 3	4	5	1	7	6
Plot 4	0.20	0.25	0.14	1	0.33
Plot 5	0.25	0.33	3	3	1

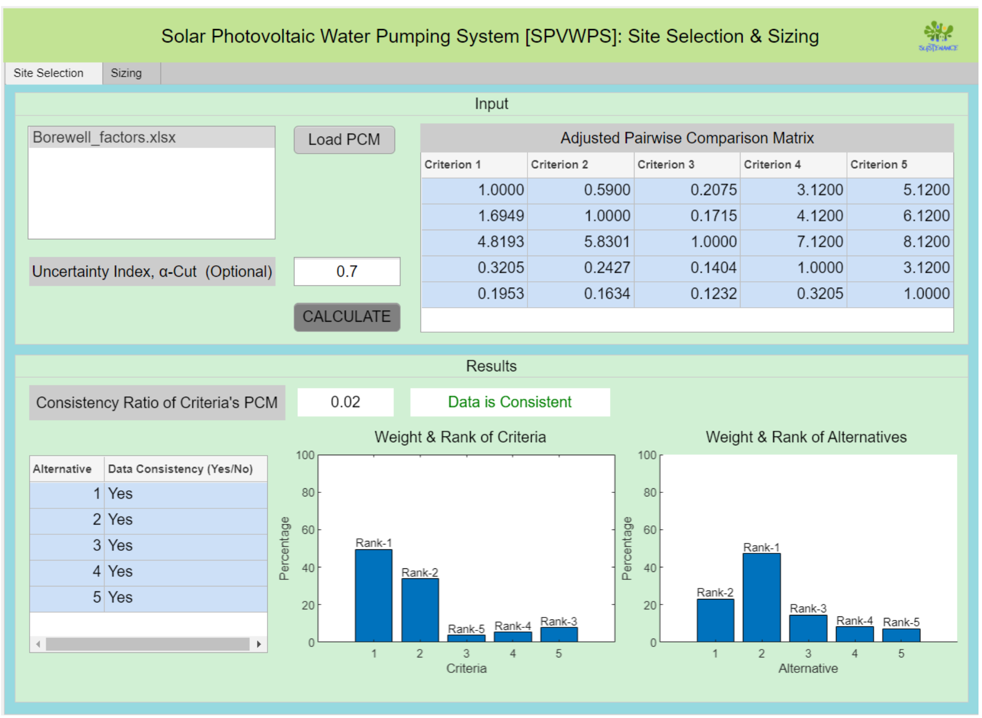

Figure 4.6: SPVWPS tool illustrating the calculated weight, criterion rank and potential alternatives for the borewell site selection.

Similarly, the software received PCM data for the water storage tank, including not only the tank itself but also the water delivery stand post, as specified in Table 4.6. Comprehensive PCM data pertaining to various alternatives related to each evaluation criterion can be found in the attached Annexure. The software assigned the highest priority to the proximity of the site to the center of the villages as the primary criterion for selecting the water storage tank's location. Furthermore, it ranked proximity to the road as the second most crucial factor, greatly contributing to easy accessibility for all residents. This ranking was established based on all criteria, excluding aspect and water source availability. A visual representation of this ranking is presented in Figure 4.7.

Table 4.5: PCM for criteria accounted for the water storage tank site selection.

Criteria	C3	C4	C5	C6	C7
C3	1	3	0.2	0.2	0.33
C4	0.33	1	0.14	0.2	0.2
C5	5	7	1	3	5
C6	5	5	0.33	1	3
C7	3	5	0.2	0.33	1

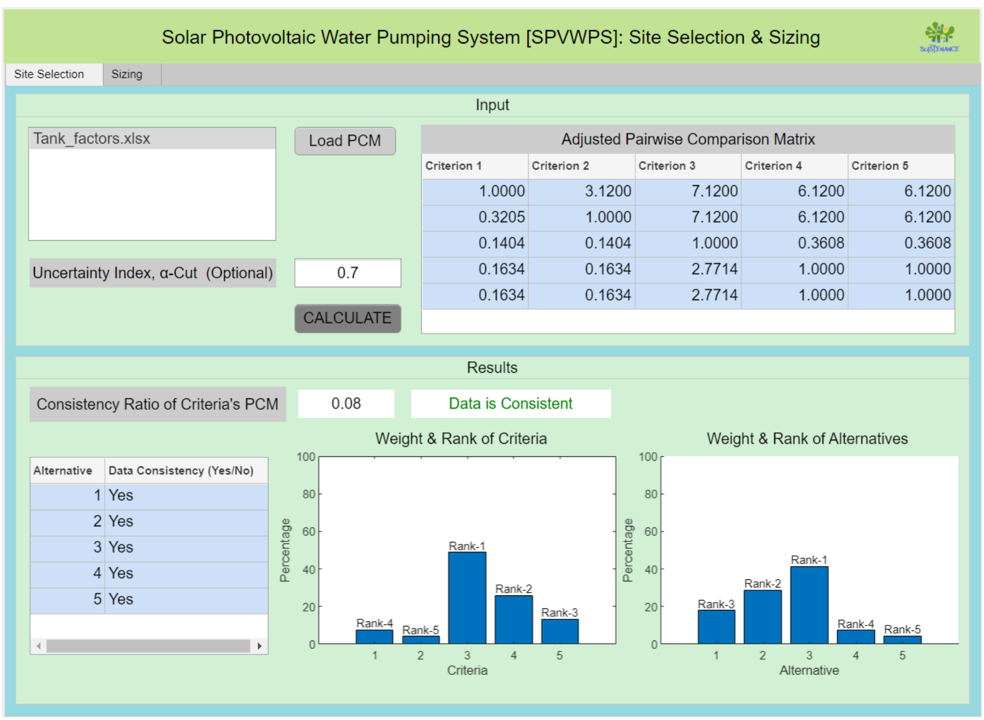

Figure 4.7: Interface of the SPVWPS tool displays the calculated weight and rank of the criterion and alternative for the water storage tank site selection.

In order to achieve peak efficiency, it is imperative that the PV panel receives maximum sunlight exposure, making the aspect criterion the paramount consideration. Additionally, factors like elevation, proximity to roads, and slope contribute to assessing the economic feasibility and ease of construction and maintenance. The software leverages the PCM encompassing these criteria (detailed in Table 4.6) to establish a ranking for the alternative potential sites, as visually represented in Figure 4.8.

Table 4.6: PCM for criteria accounted for the solar PV panel site selection.

Criteria	C1	C3	C4	C5	C6	C7
C1	1	2	8	9	3	7
C3	0.5	1	7	8	2	6
C4	0.13	0.14	1	2	0.17	0.5
C5	0.11	0.13	0.5	1	0.14	0.33
C6	0.33	0.5	7	7	1	5
C7	0.14	0.17	2	3	0.2	1

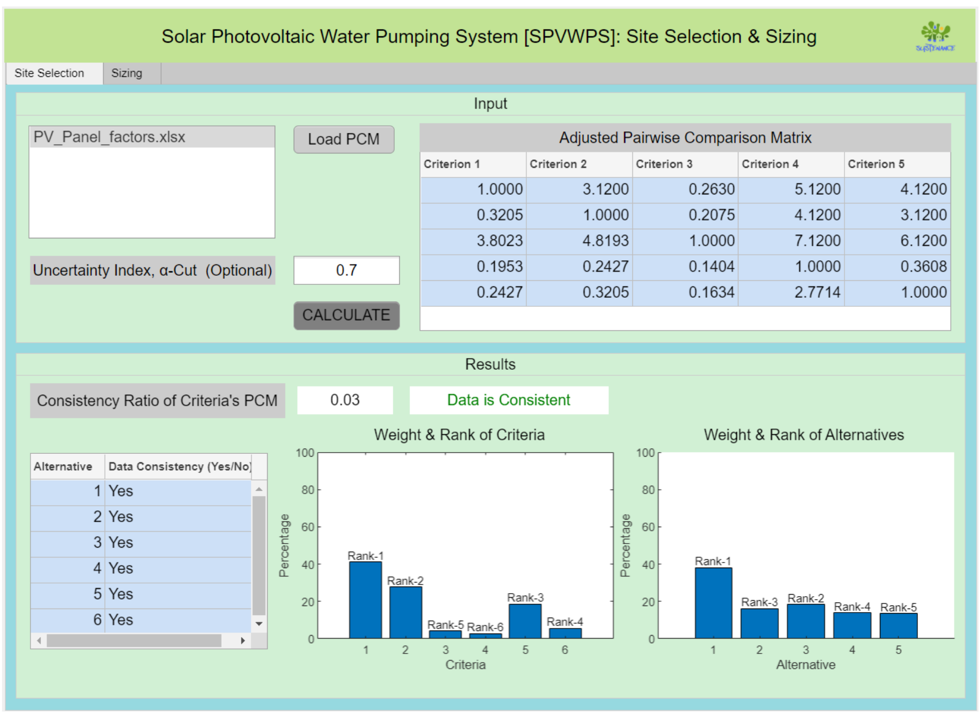

Figure 4.8: SPVWPS tool's interface showcasing the computed weight and ranking of both the criteria and alternatives for selecting the water storage tank site.

Considering their suitability for each of the three components and their respective preferred criteria, three out of the five designated potential plots were singled out for deployment, as illustrated in Figure 4.9. Plot 1 emerged as the most suitable location for PV panel installation due to its optimal south-facing aspect (the highest-priority criterion), proximity to the road, and its adjacency to the borewell site. Plot 2, being the sole allocated plot equipped with a water source, was chosen as the ideal site for borewell construction, with a majority of preferences centered around the criterion of water source availability. Lastly, plot 3, situated closest to the village center and the road, ensuring convenient access to all households from the delivery point, was selected as the prime site for the water storage tank installation.

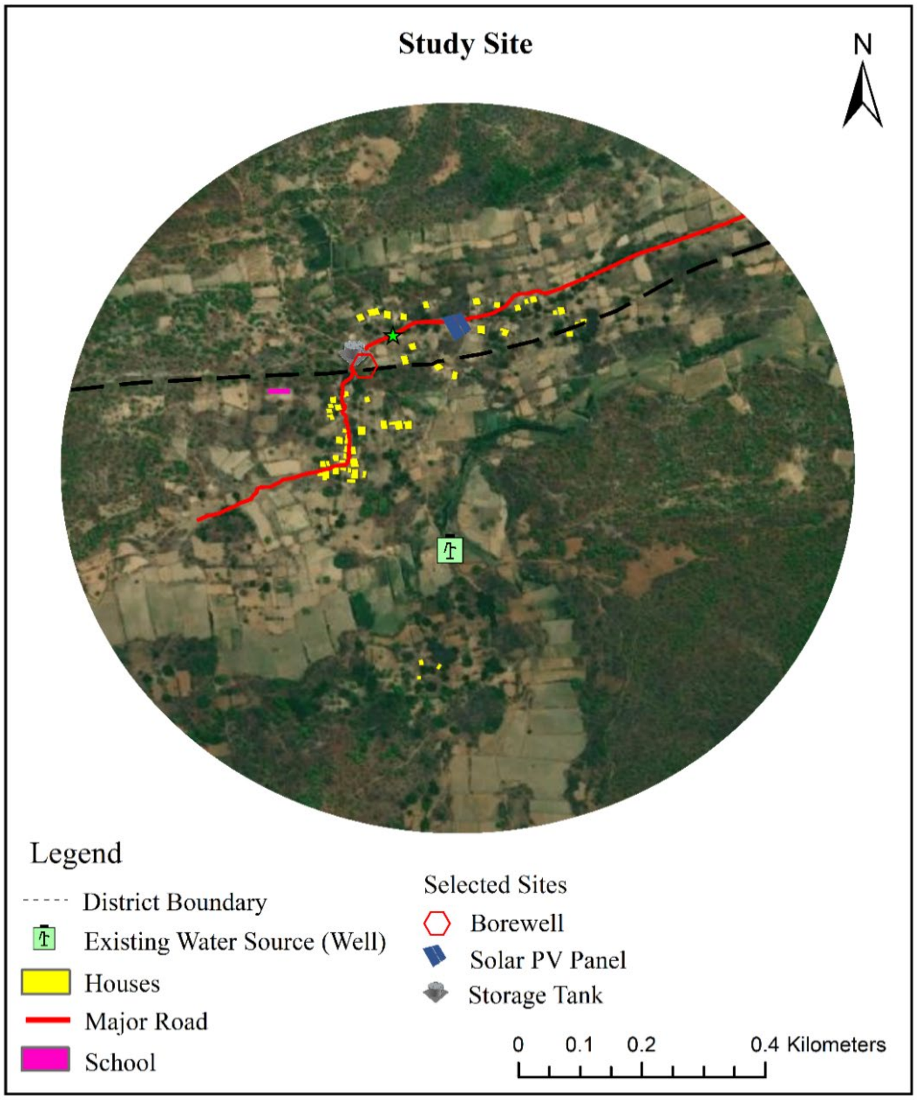

Figure 4.9: Chosen sites for deploying the SPVWPS.

4.2. A software tool for design, sizing, and optimization of solar photovoltaic water pumping systems (SPVWPS) water pumping system

After the site selection process, the subsequent critical phase involves sizing or determining the system dimensions. This begins with the precise estimation of location-specific information, such as water consumption patterns and solar irradiation levels, among other factors. A well-optimized solar pumping system is appropriately sized to meet the specific demands of its intended task. Since there are numerous design options available for various applications, technical design and comprehensive analysis are essential to prevent potential issues like system underperformance or unnecessary cost increases. It's worth noting that while a significantly larger pump can still fulfill the water requirements, it would require a larger PV generator and inverter, inevitably leading to higher overall system expenses. Moreover, operating pumps at a fraction of their capacity can reduce their operational lifespan and jeopardize the borehole's durability, ultimately leading to higher initial and maintenance costs [127], [128]. Achieving the objective of satisfying water demand with minimal capital and operational expenses necessitates the development of an efficient SPVWPS design with precise component sizing.

4.2.1. Methodology: Sizing of SPVWPS

The successful implementation of SPVWPS necessitates careful sizing and optimization of several critical components, including the PV array, electric motor, total dynamic head (TDH), and storage tank volume. These sizing considerations must be customized to fit the specific conditions of the site, taking into account factors such as the availability of solar energy and the quality and quantity of accessible water resources. In the absence of battery storage, the amount of water pumped by the SPVWPS is contingent on the solar irradiation available during a given time period. Pumping operations will coincide with peak sun hours (PSH) when no energy storage is incorporated. However, if storage is integrated, pumping hours will vary based on the battery capacity and PV panel size. Accurate site information is essential, encompassing daily water demand, water source characteristics, solar radiation levels, and TDH requirements.

Empirical relation for the basic parameters:

Daily water requirement: The primary objective when designing and implementing an SPVWPS is to ensure an adequate water supply for all intended users, including humans, livestock, and agricultural needs. To accomplish this, the sizing process begins with a precise assessment of the water demands within the specified area.

Solar insolation: The total solar energy available over a specific period determines the quantity of water that an SPVWPS can pump during that duration. Variations in sunlight intensity, influenced by weather and climate conditions, typically peak around midday when the sun reaches its zenith. In India, solar insolation levels typically range from 3 to 7.5 kWh/m^2/day, indicating the potential energy yield for a given day [39].

Flow rate: The flow rate, or pumping rate (Q), refers to the volume of water that an SPVWPS can pump within a defined time period. It relies on both the size of the array and the solar irradiance. To calculate the water flow rate without batteries, the daily water requirement (DW_{req}) and PSH [132] is considered.

$$Q = \frac{DW_{req}}{PSH} \tag{4.13}$$

Total dynamic head (TDH): Calculating TDH involves considering both the vertical distance water needs to be raised (referred to as static head) and the effective head resulting from pumping a specific volume of water per unit of time through the actual length and diameter of the pipe (known as frictional head). This pipe transports the water to its final destination, usually a water tank as depicted in Figure 4.10. The static head (S_{hd}) can be determined as follows:

$$S_{hd} = h_1 + h_2 + h_3 \tag{4.14}$$

where, h_1 = depth of the well, h_2 = elevation between well and tank, h_3 = height up to tank inlet + staging height

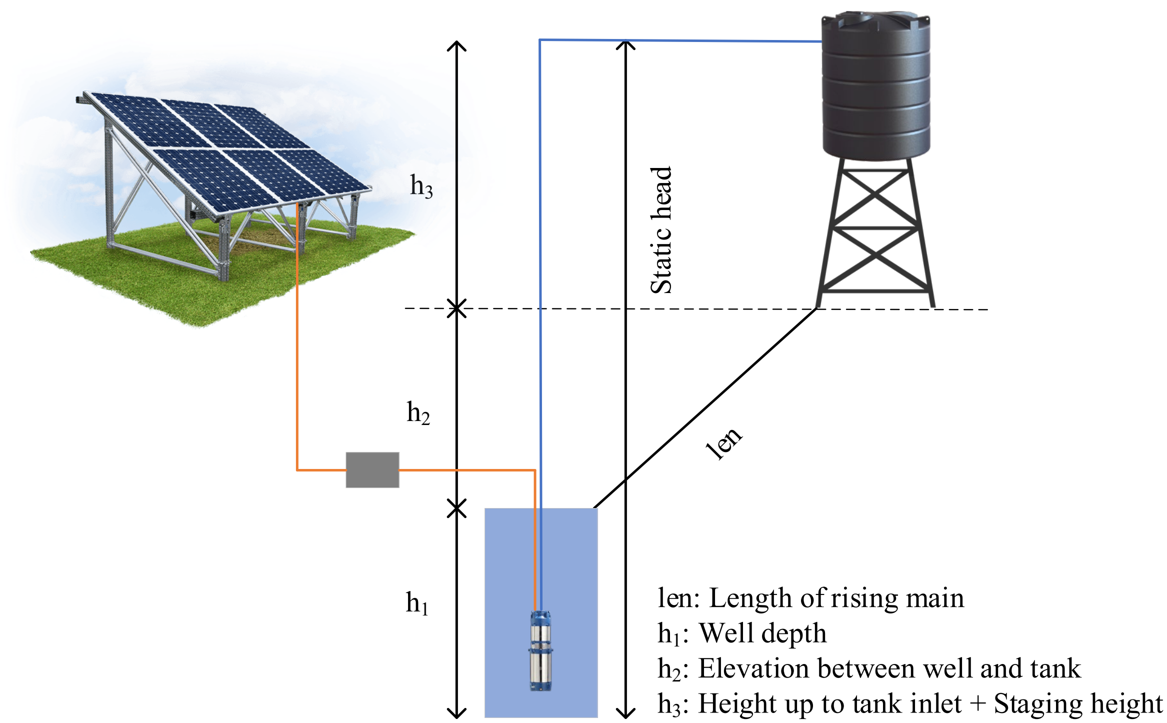

Figure 4.10: A schematic of a traditional well representing the various associated heads.

By quantifying the frictional head losses, the piping system can be optimized for optimal efficiency and ascertain the required pump size to overcome these losses and achieve the desired flow rate. The determination of frictional losses and pressure drops involves the application of different formulae or equations discussed here [133].

The Hazen William frictional loss equation, empirical by nature, represented by hf utilizes a coefficient (c) that varies with the roughness of each specific pipe material. This relationship can be expressed as follows:

$$hf = 1000 \times \left(\frac{v}{4.567 \times 0.001 \times c \times d^{0.63}}\right)^{1/0.54} \tag{4.15}$$

where v denotes the velocity (m/s), c is the roughness coefficient, and d is the diameter of the pipe (mm).

$$v = \frac{Q}{1000 * 0.7855 * d^2} \tag{4.16}$$

where Q equals rate of pumping (L/s) and d, the pipe diameter (m) of the rising main.

Utilizing the frictional head loss from the type of the pipe, its length, and the expected flow rate (hf), the total frictional loss (Tf_l) can be calculated as,

$$T_{fl} = \frac{len \times hf}{1000} \tag{4.17}$$

where len is the length of the rising main (m).

Aside from the frictional losses due to pipe length and material, the fitting components, such as bends and valves also add to the pressure loss, leading to the inclusion of an additional 10% losses for fittings.

$$\text{Total frictional head, } T_{fhd} = T_{fl} + (0.1 \times T_{fl}) \tag{4.18}$$

Finally, TDH or total head on the pump could be determined using the equation as shown below,

$$TDH = S_{hd} + T_{fhd} + v_{hd} \tag{4.19}$$

Where v_{hd} is the velocity head given as,

$$v_{hd} = \frac{v^2}{2g} \tag{4.20}$$

Hydraulic pumping power: It depends on the design flow rate of the system (Q in m^3/s) and the TDH (m) [134]–[136]. Hence, the hydraulic power needed to pump the daily water requirement would be:

$$P_h(kW) = \frac{\rho \times g \times Q \times TDH}{3.6 \times 10^6} \tag{4.21}$$

Where, ρ = water density (kg/m^3), g = acceleration due to gravity (9.81 m/s^2), Q = Rate of pumping (m^3/h), and TDH (m), which is the sum of static head and frictional losses. Furthermore, the motor's efficiency determines the proportion of electrical power it receives that is converted into mechanical power. Consequently, considering the motor efficiency in the calculation of hydraulic pumping power provides more precise sizing [135]. The power required by a motor (P_m) can therefore be determined as:

$$P_m(kW) = \frac{P_h}{\eta_m} \tag{4.22}$$

Where η_m = Efficiency of motor

PV array sizing: Power losses other than those resulting from motor inefficiency contribute to overall system inefficiency. Consequently, the power needed from the array to operate the system is [135]:

$$P_m(kW) = \frac{P_h}{\eta_m} \tag{4.23}$$

Where η_m = Efficiency of motor

The total power required from the PV array in a day to meet the daily water requirement can then be calculated as:

$$TP_{pv} = P_{pv} \times PP_{hr} \tag{4.24}$$

Where PP_{hr} = Pumping hour

The solar panel's peak watt rating (Wr) denotes the highest power output it can generate under optimal conditions, including direct sunlight and no shading. This rating is a crucial parameter for calculating the solar panel's total power output and is measured in watts (W).

$$W_r = \frac{TP_{pv}}{PSH} \tag{4.25}$$

Once the total daily energy demand of the system has been established, the rated power output of an individual module (P_o) can be computed to ascertain the number of PV modules needed (n_{mod}).

$$n \frac{W_r}{P_{O_{mod}}} \tag{4.26}$$

where, $P_O = V_{dc} \times I_{dc}$, and V_{dc}= DC operating voltage, I_{dc}= DC operating current

4.2.2. *Tool Description & Case Study*

The empirical relationships governing the components of the SPVWPS are integrated to achieve the optimal sizing of the system. These relationships are then translated into equations and subsequently implemented into a user-friendly and openly accessible software. Figure 4.11 illustrates the developed tool designed for sizing SPVWPS.

Determining the size or dimensions of the SPVWPS for the study site, as with any other water pumping system, necessitates a comprehensive understanding of water consumption patterns. In this context, conflicting information in existing literature prompted an investigation into the water usage habits of the villagers. This investigation validated the requirement for a stand-post water supply of 70 liters per person per day to meet their domestic needs.

In addition to catering to human consumption, the villagers must also provide water for their livestock, specifically cattle. The water requirements for livestock vary depending on factors such as the animal's weight, feeding conditions, and lactation status. For dairy cows and buffaloes, the estimated water requirement typically ranges from 30 to 35 liters per capita per day (lpcd) under standard feeding conditions. However, lactating cows may require a higher daily intake of 50 to 60 liters, while feedlot cattle may need up to 80 lpcd during the summer months. Grazing cattle, on the other hand, may require up to 48 lpcd [137]–[141]. Considering the dynamic nature of cattle water needs, a confirmed water supply of 60 lpcd is deemed necessary. This decision is based on the fact that not all cattle lactate simultaneously, and there are also oxen among the livestock that naturally do not lactate.

Water consumption profile

- For 400 people, 400*70 = 28,000 liter per day
- For 200 cattle, 200*60 = 12,000 liter per day
- Total water requirement per day = 40,000 litres per day

For assessing the site-specific availability of solar insolation, the data can be gathered from various sources, including Meteonorm (https://meteonorm.com/en/), POWER project by NASA (https://power.larc.nasa.gov/data-access-viewer/), Solargis (https://solargis.com/), NREL's PVWatts calculator (https://pvwatts.nrel.gov/), or utilize solar radiometers like pyranometers and pyrheliometers, which measure solar irradiance at the specific site. The daily PSH can be computed based on the available data, representing the approximate number of hours in a day where the total solar energy received equals an irradiance of 1000 W/m2 [142]. In technical terms, PSH indicates the daily operational hours a PV generator would experience under its rated conditions.

The study area experiences a range of solar irradiance, with peaks at 8.08 kWh (in May 2005) and lows at 2.17 kWh (in December 2021). When examining the solar irradiance data obtained from NASA's POWER project, it was determined that, on average, the site received 5.68 kWh/m2/day between 1990 and 2021. December and January exhibit the lowest solar irradiance, while May, June, and July consistently receive the highest solar irradiance, as illustrated in Figure 4.12. Throughout the 1990-2021 period, the number of days with solar irradiance below 3 kWh/m2/day varies between 0 and 10 days annually. As a result, a PSH threshold of 3 kWh/m2/day was chosen for dimensioning calculations at the site.

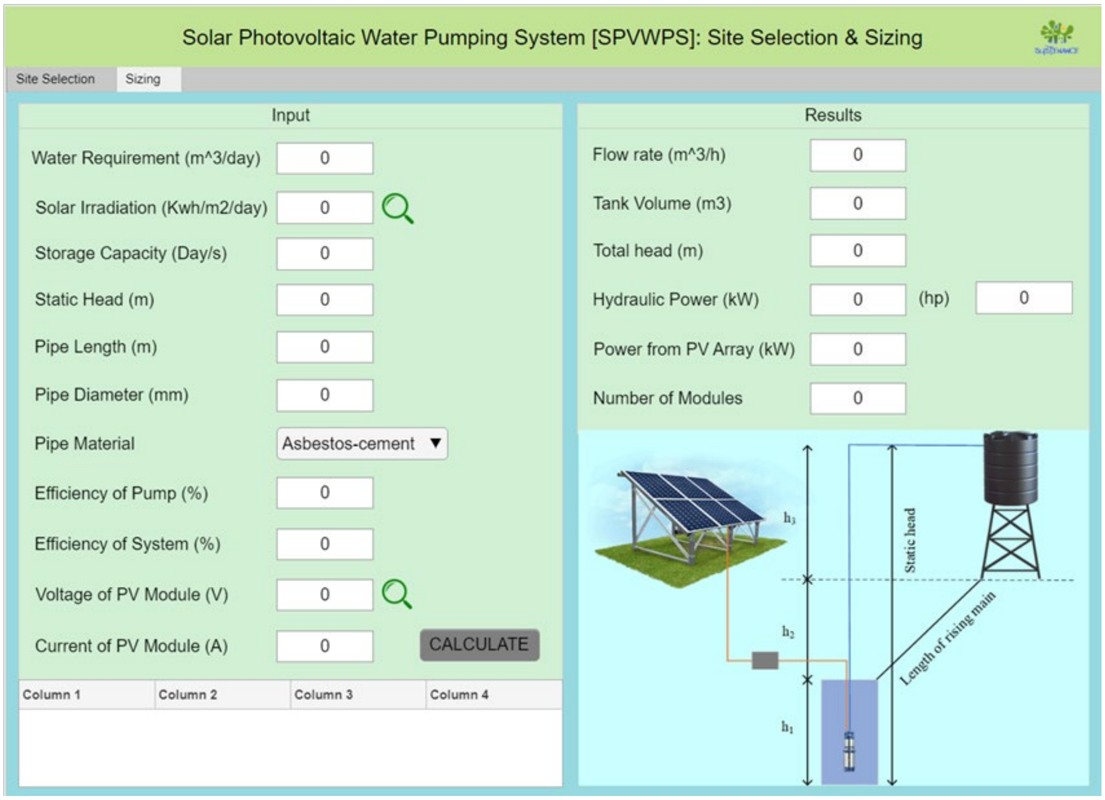

Figure 4.11: A snapshot of the interface of the devised tool showing the tab for system sizing.

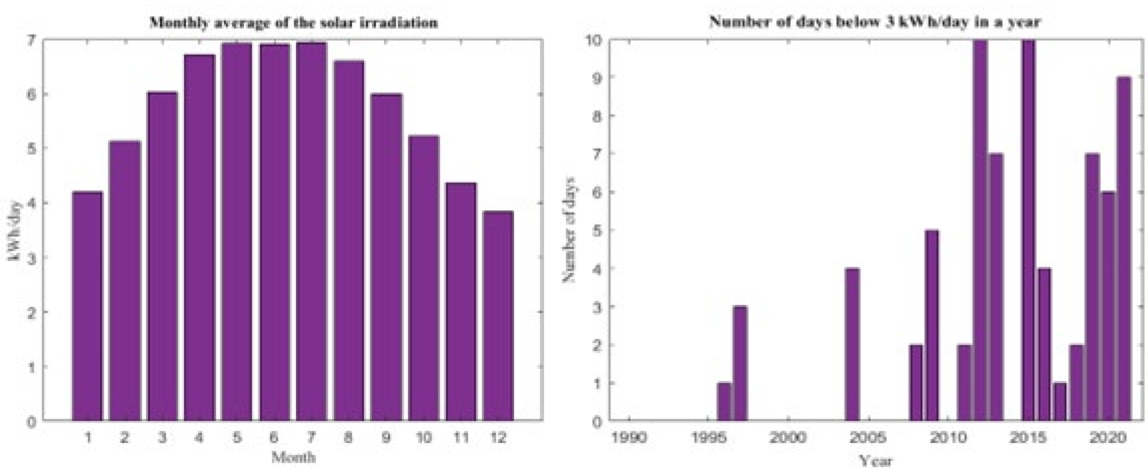

Figure 4.12: Monthly average figures for solar irradiance and the number of days where it is below 3kWh/day in a year.

Based on the profile for water consumption, available PSH at the location, static head, and system efficiencies, the software performs calculations for flow rate, total head, and the energy needed by the motor, as depicted in Figure 4.13. number of PV modules is then calculated based on the tool's provided peak wattage value. This tool relies on input data drawn from field studies and existing literature to establish the ideal dimensions for the components of the SPVWPS, which significantly influence project costs [118], [131], [143].

Using the data collected from the field, which encompass daily water requirements (40 m^3), solar irradiation data (3 kWh), water storage duration (2 days), system and pump efficiencies (each at 60%), required pipe length (65 meters), and static head (60 meters), the optimal sizes for the SPVWPS components were computed. The system, comprising a 5 hp motor and 17 PV modules, has the capacity to meet the villagers' daily water demand, as illustrated in Figure 4.13. The storage tank's volume (80 m^3) and power requirement (6.11 kW or 6110 W) for daily operation, in conjunction with an optimal flow rate, ensure the fulfilment of daily water needs. This calculation ultimately promotes the efficient utilization of energy and water resources, leading to a more precise estimation of project expenditures.

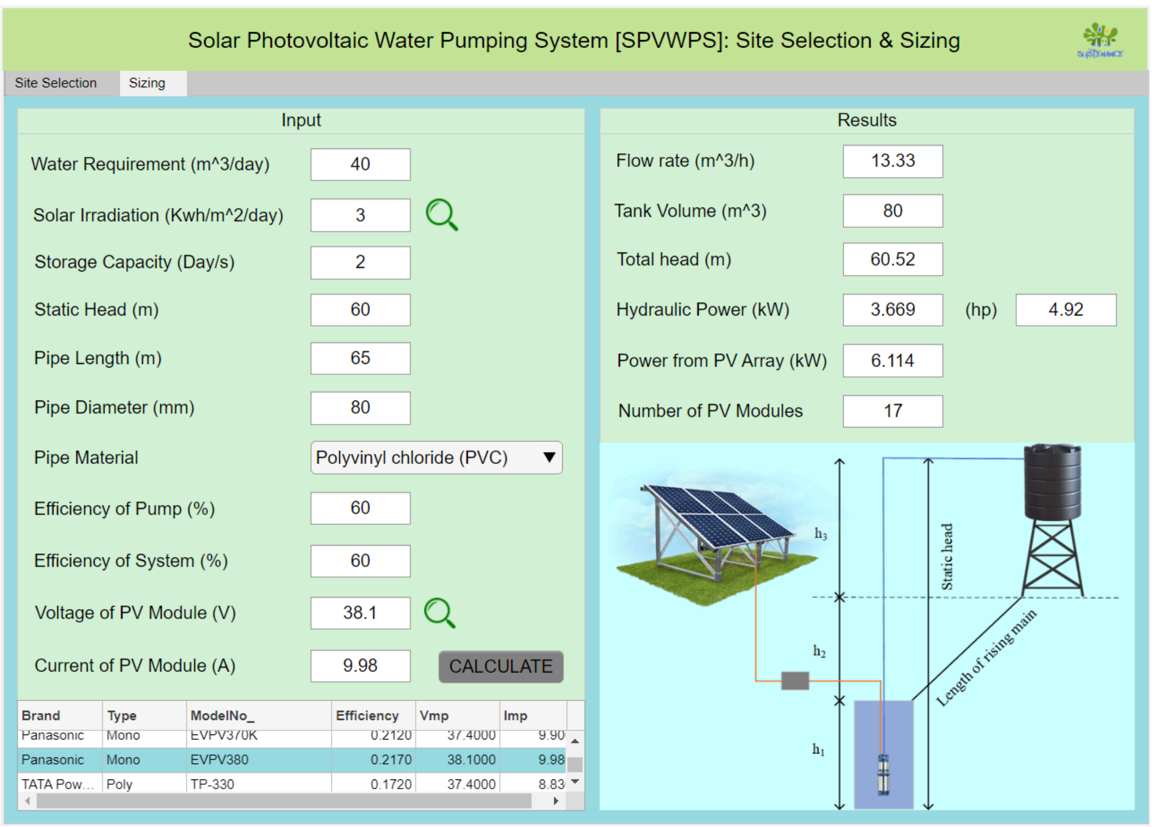

Figure 4.13: Site-specific input and resultant output of the parameters of SPVWPS in the tool.

The methodology outlined in the study presents a comprehensive strategy for identifying suitable deployment sites for solar projects, especially in constrained locations and offers an end-to-end solution for deploying SPVWPS. The resulting tool enhances the efficiency of site selection, optimizes the utilization of energy and water resources.

Traditional site selection typically involves classifying regions into suitable and unsuitable zones instead of pinpointing a specific deployment location. To tackle this challenge, alternatives that consider site evaluation factors are extracted. Concurrently, it resolves the issue of limited high-resolution data for small and uneven sites. The computational complexity in most site selection stages, caused by numerous criteria and alternatives in MCDM approaches, is eased by a user-friendly software tool. This tool automates FAHP calculations, including processes like converting crisp comparisons to fuzzy numbers, solving fuzzy eigenvalues, normalizing weights, computing consistency indices, and determining priority weights and rankings for criteria and alternatives. The results are presented in a user-friendly format for easy interpretation and download. Incorporating input from multiple experts and adjusting criteria weights based on their expertise enhances the efficient identification of highly suitable sites. The tool simplifies and speeds up MCDM calculations for users with limited process knowledge, although familiarity with FAHP or MCDM basics is advisable.

4.3. Benefits of SPVWPS

The implementation of SPVWPS offers a sustainable and cost-effective means of providing clean water access, particularly benefiting marginalized communities. Site selection and sizing tools play a pivotal role in ensuring optimal system placement and sizing to meet community water needs. In the case study's underprivileged villages, the installation of SPVWPS would deliver tangible advantages to the local population, enhancing their access to clean water. The benefits of utilizing SPVWPS and its corresponding sizing tool include:

Cost-effectiveness: Proper site selection and sizing can result in long-term cost savings by reducing initial investment and maintenance expenses.

Increased reliability: Correct sizing and location can enhance system reliability by identifying potential failure sources, such as shading or water source depletion. The system's reliability can be increased by proper size and site guaranteeing optimum performance.

Improved water access: SPVWPS can provide reliable water sources, improving health and well-being.

Reduced workload: Proper system placement reduces the burden of water collection, especially for women, which can be a physically taxing and time-consuming activity. Installing SPVWPS at an optimal location can reduce the workload of collecting water as a daily activity.

Education opportunities: Frequently, girls are prevented from attending school to help with domestic tasks, such as fetching water. By reducing the time and effort required for water collection through strategic system placement, we can potentially enhance girls' access to education. Simplifying water collection could significantly improve educational opportunities, particularly for girls.

Economic benefits: Assured access to water is vital for agriculture, a primary source of income for many rural communities. SPVWPS can allow the villagers to grow crops and increase their income, improving the economic prospects of the whole community. Additionally, money can also be saved on fuel or energy costs for pumping water.

Environmental impact: RE use reduces environmental footprint by lowering the need for fossil fuels which subsequently lowers greenhouse gas emissions and can further lessen the system's negative environmental effects.

In general, the tools used for selecting sites and determining sizes for SPVWPS can have a significant influence on decision-makers. It offers a straightforward solution enabling decision-makers to promote such projects, ultimately leading to improvements in the well-being of individuals and entire communities. This approach proves effective in identifying different categories of site suitability that are both comprehensive and applicable in various regions. While the case study focuses on a site-specific evaluation of the step-by-step programmed methodology for deploying SPVWPS, the open-access software makes it easy to replicate and rely on this methodology.

4.4. Conclusion

In conclusion, the developed tool stands as a versatile and accurate solution for strategically planning the deployment of SPVWPS. Functioning as a comprehensive aid, akin to a solar energy recipe, it streamlines the SPVWPS deployment process. The tool's global applicability necessitates location-specific data inputs. This study addresses the intricate decision-making involved in RE and offers a scientific framework to curtail costs through optimal SPVWPS sizing at suitable sites. Such an approach not only instills confidence in the investors but also fosters a reduced dependence on fossil fuels, aligning with broader global sustainability objectives.

One primary challenge is disseminating knowledge on these systems and tools. Currently, only a small fraction of communities is aware of the affordability and reliability of solutions like SPVWPS, often misunderstanding their benefits due to perceived complexities and expenses. Despite these misconceptions, solar water pumps play a pivotal role in both commercial and residential contexts, particularly in regions with inadequate electricity and water infrastructure. Their cost-effectiveness, minimal environmental impact, and adaptability to varying geographical conditions make them indispensable. This study serves as a foundation for RE plant site selection and optimal SPVWPS sizing.

Anticipating the future, the International Energy Agency predicts that renewables will constitute over 90% of global electricity capacity in the coming years. This growth is propelled by existing policies and the introduction of new strategies to address the global energy crisis. In this light, this research harmoniously aligns with the strategy of promoting RE utilization. Moreover, it directly contributes to achieving sustainable development goals such as affordable and clean energy, access to clean water and sanitation, and indirectly supports climate action, sustainable communities, and urban development. The findings of this study thus hold significance not only in the realm of renewable energy but also in the broader context of sustainable global progress.

Bibliography

[1] L. Nuffel, *Sector coupling: how can it be enhanced in the EU to foster grid stability and decarbonise?* Belgium: European Parliament Brussels, 2018.

[2] A. Orths, "Flexibility from energy systems integration: Supporting syner- gies among sectors," *IEEE Power Energy Mag.*, vol. 17, no. 6, pp. 67–78, 2019.

[3] G. Shahgholian, "A brief review on microgrids: Operation, applications, modeling, and control," *Int. Trans. Electr. Energy Syst.*, vol. 31, no. 6, p. e12885, 2021, doi: 10.1002/2050-7038.12885.

[4] G. Fridgen, R. Keller, M.-F. Körner, and M. Schöpf, "A holistic view on sector coupling," *Energy Policy*, vol. 147, p. 111913, Dec. 2020, doi: 10.1016/j.enpol.2020.111913.

[5] S. M. Dawoud, X. Lin, and M. I. Okba, "Hybrid renewable microgrid optimization techniques: A review," *Renew. Sustain. Energy Rev.*, vol. 82, pp. 2039–2052, 2018.

[6] P. Shanthi, G. Uma, and M. S. Keerthana, "Effective power transfer scheme for a grid connected hybrid wind/photovoltaic system," *IET Renew. Power Gener.*, vol. 11, no. 7, pp. 1005–1017, 2017.

[7] R. K. N. Pragya Nema and S. Rangnekar, "A current and future state of art development of hybrid energy system using wind and PV-solar: A review," *Renew. Sustain. Energy Rev.*, vol. 13, no. 8, pp. 2096–2103, 2009.

[8] J. B. Holm-Nielsen, T. A. Seadi, and P. Oleskowicz-Popiel, "The future of anaerobic digestion and biogas utilization," *Bioresour. Technol.*, vol. 100, no. 22, pp. 5478–5484, 2009.

[9] B. Yan, P. B. Luh, G. Warner, and P. Zhang, "Operation and Design Optimization of Microgrids With Renewables," *IEEE Trans. Autom. Sci. Eng.*, vol. 14, no. 2, pp. 573–585, Apr. 2017, doi: 10.1109/TASE.2016.2645761.

[10] B. Zhao, X. Zhang, J. Chen, C. Wang, and L. Guo, "Operation Optimization of Standalone Microgrids Considering Lifetime Characteristics of Battery Energy Storage System," *IEEE Trans. Sustain. Energy*, vol. 4, no. 4, pp. 934–943, Oct. 2013, doi: 10.1109/TSTE.2013.2248400.

[11] H. Wang and J. Huang, "Joint Investment and Operation of Microgrid," *IEEE Trans. Smart Grid*, vol. 8, no. 2, pp. 833–845, Mar. 2017, doi: 10.1109/TSG.2015.2501818.

[12] M. Alramlawi and P. Li, "Design optimization of a residential PV-battery microgrid with a detailed battery lifetime estimation model," *IEEE Trans. Ind. Appl.*, vol. 56, no. 2, 2020.

[13] Sk. A. Shezan *et al.*, "Effective dispatch strategies assortment according to the effect of the operation for an islanded hybrid microgrid," *Energy Convers. Manag. X*, vol. 14, p. 100192, May 2022, doi: 10.1016/j.ecmx.2022.100192.

[14] S. Y. Derakhshandeh, A. S. Masoum, S. Deilami, M. A. S. Masoum, and M. E. Hamedani Golshan, "Coordination of Generation Scheduling with PEVs Charging in Industrial Microgrids," *IEEE Trans. Power Syst.*, vol. 28, no. 3, pp. 3451–3461, Aug. 2013, doi: 10.1109/TPWRS.2013.2257184.

[15] C. Gamarra and J. M. Guerrero, "Computational optimization techniques applied to microgrids planning: A review," *Renew. Sustain. Energy Rev.*, vol. 48, pp. 413–424, 2015.

[16] K. Tripathi and S. Shrivastava, "FLC Technique in Smart Grid for Demand Side Management," in *Applications of Artificial Intelligence in Electrical Engineer- ing. IGI Global*, 2020, pp. 107–121.

[17] J. C. Fuller, K. P. Schneider, and D. Chassin, "Analysis of residential demand response and double-auction markets," in *2011 IEEE power and energy society general meeting. IEEE*, 2011, pp. 1–7.

[18] R. Billinton and R. N. Allan, *Reliability Evaluation of Power Systems*. Boston, MA: Springer US, 1996. doi: 10.1007/978-1-4899-1860-4.

[19] EIA, "Levelized Costs of New Generation Resources in the Annual Energy Outlook 2022," U.S. Energy Information Administration, 2022.

[20] J. Thakur and B. Chakraborty, "Demand side management in developing nations: A mitigating tool for energy imbalance and peak load management," *Energy*, vol. 114, pp. 895–912, Nov. 2016, doi: 10.1016/j.energy.2016.08.030.

[21] V. Gevorgian, Y. Zhang, and E. Ela, "Investigating the Impacts of Wind Generation Participation in Interconnection Frequency Response," *IEEE Trans. Sustain. Energy*, vol. 6, no. 3, pp. 1004–1012, Jul. 2015, doi: 10.1109/TSTE.2014.2343836.

[22] R. Doherty, G. Lalor, and M. O'Malley, "Frequency Control in Competitive Electricity Market Dispatch," *IEEE Trans. Power Syst.*, vol. 20, no. 3, pp. 1588–1596, Aug. 2005, doi: 10.1109/TPWRS.2005.852146.

[23] EirGrid, "RoCoF Alternative & Complementary Solutions Project - Phase 2 Study Report," Mar. 2016. [Online]. Available: https://www.eirgridgroup.com/site-files/library/EirGrid/RoCoF-Alternative-Solutions-Project-Phase-2-Report-Final.pdf

[24] Grid-India, IIT Bombay, "Report on Assessment of Inertia in Indian Power System," Grid Controller of India Ltd. (formerly POSOCO) and Indian Institute of Technology Bombay, 2022. [Online]. Available: https://posoco.in/wp-content/uploads/2022/01/Assessment-of-Inertia-in-Indian-Power-System.pdf.

[25] T. Inoue, H. Taniguchi, Y. Ikeguchi, and K. Yoshida, "Estimation of power system inertia constant and capacity of spinning-reserve support generators using measured frequency transients," *IEEE Trans. Power Syst.*, vol. 12, no. 1, pp. 136–143, Feb. 1997, doi: 10.1109/59.574933.

[26] P. K. Dhara and Z. H. Rather, "Non-synchronous Inertia Estimation in a Renewable Energy Integrated Power System With Reduced Number of Monitoring Nodes," *IEEE Trans. Sustain. Energy*, vol. 14, no. 2, pp. 864–875, Apr. 2023, doi: 10.1109/TSTE.2022.3227603.

[27] Z. H. Rather, Z. Chen, P. Thøgersen, and P. Lund, "Dynamic Reactive Power Compensation of Large-Scale Wind Integrated Power System," *IEEE Trans. Power Syst.*, vol. 30, no. 5, pp. 2516–2526, Sep. 2015, doi: 10.1109/TPWRS.2014.2365632.

[28] Y. G. Rebours, D. S. Kirschen, M. Trotignon, and S. Rossignol, "A Survey of Frequency and Voltage Control Ancillary Services—Part I: Technical Features," *IEEE Trans. Power Syst.*, vol. 22, no. 1, pp. 350–357, Feb. 2007, doi: 10.1109/TPWRS.2006.888963.

[29] H. Karbouj, Z. H. Rather, and B. C. Pal, "Adaptive Voltage Control for Large Scale Solar PV Power Plant Considering Real Life Factors," *IEEE Trans. Sustain. Energy*, vol. 12, no. 2, pp. 990-998, Apr. 2021, doi: 10.1109/TSTE.2020.3029102.

[30] C. Loutan *et al.*, "Demonstration of Essential Reliability Services by a 300-MW Solar Photovoltaic Power Plant," NREL/TP--5D00-67799, 1349211, Mar. 2017. doi: 10.2172/1349211.

[31] D. Sera, R. Teodorescu, and P. Rodriguez, "PV panel model based on datasheet values," *IEEE Int. Symp. Ind. Electron.*, pp. 2392-2396, 2007, doi: 10.1109/ISIE.2007.4374981.

[32] M. van E. Z. en Klimaat and R. O. en M. Ministerie van Volkshuisvesting, "Government promotes solar energy growth - Rijksoverheid.nl," Jan. 27, 2017. https://www.rijksoverheid.nl/onderwerpen/duurzame-energie/zonne-energie (accessed Aug. 13, 2023).

[33] EMILIANO BELLINI, "Netherlands posts another record year for residential PV in 2022," *PV Magazine International*, 2023. https://www.pv-magazine.com/2023/01/31/netherlands-posts-another-record-year-for-residential-pv-in-2022/

[34] REPowerEU, "Affordable, secure and sustainable energy for EU." [Online]. Available: https://commission.europa.eu/strategy-and-policy/priorities-2019-2024/european-green-deal/repowereu-affordable-secure-and-sustainable-energy-europe_en

[35] Yusuf Latief, "Gridlock: how the Netherlands hit capacity | Enlit World," *Enlit*, Feb. 09, 2023. https://www.enlit.world/smart-grids/grid-management-monitoring/gridlock-how-the-netherlands-hit-capacity/ (accessed Aug. 13, 2023).

[36] "Capaciteitskaart invoeding elektriciteitsnet." https://capaciteitskaart.netbeheernederland.nl (accessed Aug. 13, 2023).

[37] "Watts Up: Dutch electric grid is at capacity." [Online]. Available: https://www.dutchnews.nl/2021/09/watts-up-dutch-electric-grid-is-at-capacity/

[38] "Flashing lights or even a power failure: Alliander warns of a full power grid." [Online]. Available: https://nos.nl/artikel/2466776-knipperende-lampen-of-zelfs-uitval-alliander-waarschuwt-voor-vol-stroomnet

[39] W. USEF, "An Introduction to EU Market-based Congestion Management Models." [Online]. Available: https://www.usef.energy/news-events/publications/

[40] L. Guilly *et al.*, "An Energy Flexibility Framework on the Internet of Things," in *The Success of European Projects using New Information and Communication Technologies*, S. Hamrioui, Ed., pp. 17-37,. [Online]. Available: http://www.scitepress.org/documents/EPS_Colmar_2015.pdf

[41] E. Valsomatzis, K. Hose, T. B. Pedersen, and L. Šikšnys, "Measuring and Comparing Energy Flexibilities," in *Proceedings of the EBDT/ICDT Workshops, 2015, CEUR WS proceedings*, [Online]. Available: http://ceur-ws.org/Vol-1330/paper-14.pdf

[42] "FlexOffers: Unified generalized modelling and management of flexibility in electricity demand and supply – Daisy." https://www.daisy.aau.dk/projects/flexoffers/ (accessed Sep. 16, 2023).

[43] L. Šikšnys, E. Valsomatzis, K. Hose, and T. B. Pedersen, "Aggregating and Disaggregating Flexibility Objects," *IEEE Trans. Knowl. Data Eng.*, vol. 27, no. 11, pp. 2893-2906, Nov. 2015, doi: 10.1109/TKDE.2015.2445755.

[44] "Wat is GOPACS?," *GOPACS*. https://www.gopacs.eu/wat-is-gopacs/ (accessed Sep. 16, 2023).

[45] "Published Program Guides using OpenADR." https://www.openadr.org/dr-program-guide (accessed Sep. 16, 2023).

[46] S. OpenTherm, "What is OpenTherm?," *Opentherm Association*. https://www.opentherm.eu/opentherm-protocol/what-is-opentherm/ (accessed Sep. 16, 2023).

[47] J. S. Vardakas, N. Zorba, and C. V. Verikoukis, "A survey on demand response programs in smart grids: Pricing methods and optimization algorithms," *IEEE Commun. Surv. Tutor.*, vol. 17, no. 1, pp. 152–178, 2014.

[48] R. Palma-Behnke, "A microgrid energy management system based on the rolling horizon strategy," *IEEE Trans. Smart Grid*, vol. 4, no. 2, pp. 996–1006, 2013.

[49] H. Mehrjerdi and R. Hemmati, "Modeling and optimal scheduling of battery energy storage systems in electric power distribution networks," *J. Clean. Prod.*, vol. 234, pp. 810–821, 2019.

[50] J. Gondzio, P. González-Brevis, and P. Munari, "Large-scale optimization with the primal-dual column generation method," *Math. Program. Comput.*, vol. 8, pp. 47–82, 2016.

[51] S. S. Reddy, V. Sandeep, and C.-M. Jung, "Review of stochastic optimization methods for smart grid," *Front. Energy*, vol. 11, pp. 197–209, 2017.

[52] X. Hao, "Smart meter deployment optimization for efficient electrical appliance state monitoring," in *2012 IEEE Third International Conference on Smart Grid Communications (SmartGridComm*, IEEE, 2012.

[53] B. Ahmadi, "A multi-objective decentralized optimization for voltage regulators and energy storage devices in active distribution systems," *Int. J. Electr. Power Energy Syst.*, vol. 153, p. 109330, 2023.

[54] B. Ahmadi, O. Ceylan, and A. Ozdemir, "Distributed energy resource allocation using multi-objective grasshopper optimization algorithm," *Electr. Power Syst. Res.*, vol. 201, p. 107564, 2021.

[55] K. M. Tan, V. K. Ramachandaramurthy, and J. Y. Yong, "Integration of electric vehicles in smart grid: A review on vehicle to grid technologies and optimization techniques," *Renew. Sustain. Energy Rev.*, vol. 53, pp. 720–732, 2016.

[56] V. Jayadev and K. S. Swarup, "Optimization of microgrid with demand side management using Genetic Algorithm." pp. 1–12, 2013.

[57] M. S. Alam, "Energy management in DC microgrid with an efficient voltage compensation mechanism," *Electr. Power Syst. Res.*, vol. 214, p. 108842, 2023.

[58] M. H. Nehrir and B. J. LaMeres, "A multiple-block fuzzy logic-based electric water heater demand-side management strategy for leveling distribution feeder demand profile," *Electr. Power Syst. Res.*, vol. 56, no. 3, pp. 225–230, 2000.

[59] M. E. T. Gerards, "Demand side management using profile steering," in *2015 IEEE Eindhoven PowerTech*, IEEE, 2015.

[60] N. Aguiar, A. Dubey, and V. Gupta, "Network-constrained Stackelberg game for pricing demand flexibility in power distribution systems," *IEEE Trans. Smart Grid*, vol. 12, no. 5, pp. 4049–4058, 2021.

[61] A. Loni and F.-A. Parand, "A survey of game theory approach in smart grid with emphasis on cooperative games," in *2017 IEEE International Conference on Smart Grid and Smart Cities (ICSGSC*, IEEE, 2017.

[62] W. Tushar, "A motivational game-theoretic approach for peer-to-peer energy trading in the smart grid," *Appl. Energy*, vol. 243, pp. 10–20, 2019.

[63] D. Srinivasan, "Game-Theory based dynamic pricing strategies for demand side management in smart grids," *Energy*, vol. 126, pp. 132–143, 2017.

[64] D. Zhang, X. Han, and C. Deng, "Review on the research and practice of deep learning and reinforcement learning in smart grids," *CSEE J. Power Energy Syst.*, vol. 4, no. 3, pp. 362–370, 2018.

[65] M. Ozay, "Machine learning methods for attack detection in the smart grid," *IEEE Trans. Neural Netw. Learn. Syst.*, vol. 27, no. 8, pp. 1773–1786, 2015.

[66] A. Pappu, G. Hoogsteen, and J. L. Hurink, "Distributed Co-operative Demand Side Management for Energy Communities," in *2022 IEEE PES Innovative Smart Grid Technologies Conference Europe (ISGT-Europe*, Novi Sad, Serbia, 2022, pp. 1-5,. doi: 10.1109/ISGT-Europe54678.2022.9960572.

[67] D. E. Olivares, C. A. Cañizares, and M. Kazerani, "A centralized energy management system for isolated microgrids," *IEEE Trans. Smart Grid*, vol. 5, no. 4, pp. 1864–1875, 2014.

[68] T. Logenthiran, D. Srinivasan, and T. Z. Shun, "Demand side management in smart grid using heuristic optimization," *IEEE Trans. Smart Grid*, vol. 3, no. 3, pp. 1244–1252, 2012.

[69] Y. Sabri, N. E. Kamoun, and F. Lakrami, "A survey: Centralized, decentralized, and distributed control scheme in smart grid systems," in *2019 7th mediterranean congress of telecommunications (CMT*, IEEE, 2019.

[70] X. Kou, "A scalable and distributed algorithm for managing residential demand response programs using alternating direction method of multipliers (ADMM," *IEEE Trans. Smart Grid*, vol. 11, no. 6, pp. 4871–4882, 2020.

[71] R. B. Hiremath, S. Shikha, and N. H. Ravindranath, "Decentralized energy planning; modeling and application—a review," *Renew. Sustain. Energy Rev.*, vol. 11, no. 5, pp. 729–752, 2007.

[72] P. Kofinas, A. I. Dounis, and G. A. Vouros, "Fuzzy Q-Learning for multi-agent decentralized energy management in microgrids," *Appl. Energy*, vol. 219, pp. 53–67, 2018.

[73] L. Meng, "Microgrid supervisory controllers and energy management systems: A literature review," *Renew. Sustain. Energy Rev.*, vol. 60, pp. 1263–1273, 2016.

[74] B. Ahmadi, "Congestion Management in Distribution Systems Based on Decentralized and Finite Flexibility Offers," in *Power Systems Computation Conference 2024*, Paris, France, 2024.

[75] G. Hoogsteen, "A Cyber-Physical Systems Perspective on Decentralized Energy Management," [PhD Thesis - Research UT, graduation UT, University of Twente]. University of Twente, 2017. doi: 10.3990/1.9789036544320.

[76] GridWise, "Transactive Energy Framework Version 1.0." [Online]. Available: http://www.gridwiseac.org/pdfs/te_framework_report_pnnl-22946.pdf

[77] K. Kok, "Dynamic pricing by scalable energy management systems — Field experiences and simulation results using PowerMatcher," in *2012 IEEE Power and Energy Society General Meeting*, San Diego, CA, USA, 2012, pp. 1-8,. doi: 10.1109/PESGM.2012.6345058.

[78] V. B. Molderink, J. L. Hurink, and G. J. M. Smit, “Comparing demand side management approaches,” in *2012 3rd IEEE PES Innovative Smart Grid Technologies Europe (ISGT Europe*, 2012, pp. 1-8,. doi: 10.1109/ISGTEurope.2012.6465699.

[79] V. B. A.Molderink, J. L. Hurink, and G. J. M. Smit, “On indirect controlled cost function based dsm strategies,” in *2013 IEEE Grenoble Conference*, Jun. 2013, pp. 1-6,. doi: 10.1109/PTC.2013.6652464.

[80] J. K. Kok, “The PowerMatcher: Smart Coordination for the Smart Electricity Grid,” [PhD-Thesis - Research and graduation internal, Vrije Universiteit Amsterdam, 2013.

[81] “PowerMatcher Under the Hood.” [Online]. Available: http://flexiblepower.github.io/technology/powermatcher/

[82] *BDEW Bundesverband für Energie- und Wasserwirtschaft e.V., Smart Grids Ampelkonzept: Ausgestaltung der gelben Phase*. Berlin: BDEW, 2015.

[83] B. Homan, G. Hoogsteen, S. Nebiolo, J. L. Hurink, and G. J. M. Smit, “Maximizing the degree of autarky of a 16 house neighbourhood by locally produced energy and smart control,” *Sustain. Energy Grids Netw.*, vol. 20, no. N, p. 100270, Oct. 2019, doi: 10.1016/j.segan.2019.100270.

[84] M. Prasad, Z. H. Rather, R. Razzaghi, and S. Doolla, “Real-Time Reduced Model of Active Distribution Networks for Grid Support Applications,” *IEEE Trans. Power Deliv.*, pp. 1–10, 2023, doi: 10.1109/TPWRD.2023.3293791.

[85] Z. Rather, R. Banerjee, A. P. Nath, and P. Dahiwale, “Fundamentals of Electric Vehicle Charging Technology and its Grid Integration.” GIZ, 2021. [Online]. Available: http://www.niti.gov.in/sites/default/files/2021-09/Report1-Fundamentals-ofElectricVehicleChargingTechnology-and-its-Grid-Integration_GIZ-IITB.pdf

[86] B. Borlaug *et al.*, “Heavy-duty truck electrification and the impacts of depot charging on electricity distribution systems,” *Nat. Energy*, vol. 6, no. 6, Art. no. 6, Jun. 2021, doi: 10.1038/s41560-021-00855-0.

[87] Y. Xiang, Z. Jiang, C. Gu, F. Teng, X. Wei, and Y. Wang, “Electric vehicle charging in smart grid: A spatial-temporal simulation method,” *Energy*, vol. 189, p. 116221, Dec. 2019, doi: 10.1016/j.energy.2019.116221.

[88] I. M. Z. Rather and D. L. P. Dahiwale, “Smart Charging Strategies and Technologies for Electric Vehicles,” *NDC Transp. Initiat. Asia*, p. 16, 2021.

[89] J.-M. Clairand, J. Rodríguez-García, and C. Álvarez-Bel, “Smart Charging for Electric Vehicle Aggregators Considering Users’ Preferences,” *IEEE Access*, vol. 6, pp. 54624-54635, 2018, doi: 10.1109/ACCESS.2018.2872725.

[90] P. V. Dahiwale and Z. H. Rather, “Centralized Multi-objective Framework for Smart EV Charging in Distribution System,” in *2023 IEEE PES Conference on Innovative Smart Grid Technologies - Middle East (ISGT Middle East), Mar*, 2023, pp. 1–5. doi: 10.1109/ISGTMiddleEast56437.2023.10078604.

[91] I. I. T. Bombay, R. Z, D. P, L. D, and H. A, “A Critical Review: Smart Charging Strategies and Technologies for Electric Vehicles.” 2021. [Online]. Available: https://greenmobility-library.org/public/index.php/single-resource/QlBDRnJiUnRSb0lmaGxGaFJNM0xuUT09

[92] K. Knezović, S. Martinenas, P. B. Andersen, A. Zecchino, and M. Marinelli, “Enhancing the Role of Electric Vehicles in the Power Grid: Field Validation of Multiple Ancillary Services,” *IEEE Trans Transp Electrification*, vol. 3, no. 1, pp. 201-209, Mar. 2017, doi: 10.1109/TTE.2016.2616864.

[93] X. Xi and R. Sioshansi, “Using Price-Based Signals to Control Plug-in Electric Vehicle Fleet Charging,” *IEEE Trans Smart Grid*, vol. 5, no. 3, pp. 1451-1464, May 2014, doi: 10.1109/TSG.2014.2301931.

[94] H. K. Nguyen, J. B. Song, and Z. Han, “Demand side management to reduce Peak-to-Average Ratio using game theory in smart grid,” in *2012 Proceedings IEEE INFOCOM Workshops*, Mar. 2012, pp. 91–96. doi: 10.1109/INFCOMW.2012.6193526.

[95] N. I. Nimalsiri, E. L. Ratnam, D. B. Smith, C. P. Mediwaththe, and S. K. Halgamuge, "Coordinated Charge and Discharge Scheduling of Electric Vehicles for Load Curve Shaping," *IEEE Trans Intell Transp Syst*, vol. 23, no. 7, pp. 7653-7665, Jul. 2022, doi: 10.1109/TITS.2021.3071686.

[96] M. Uddin, M. F. Romlie, M. F. Abdullah, S. A. Halim, A. H. A. Bakar, and T. C. Kwang, "A review on peak load shaving strategies," *Renew Sustain Energy Rev*, vol. 82, pp. 3323-3332, Feb. 2018, doi: 10.1016/j.rser.2017.10.056.

[97] A. Malhotra, G. Binetti, A. Davoudi, and I. D. Schizas, "Distributed Power Profile Tracking for Heterogeneous Charging of Electric Vehicles," *IEEE Trans Smart Grid*, vol. 8, no. 5, pp. 2090-2099, Sep. 2017, doi: 10.1109/TSG.2016.2515616.

[98] A. Ghosh and V. Aggarwal, "Menu-Based Pricing for Charging of Electric Vehicles With Vehicle-to-Grid Service," *IEEE Trans Veh Technol*, vol. 67, no. 11, pp. 10268-10280, Nov. 2018, doi: 10.1109/TVT.2018.2865706.

[99] Z. Wu and B. Chen, "Distributed Electric Vehicle Charging Scheduling with Transactive Energy Management," *Energies*, vol. 15, no. 1, Art. no. 1, Jan. 2022, doi: 10.3390/en15010163.

[100] C. Cao, L. Wang, and B. Chen, "Mitigation of the Impact of High Plug-in Electric Vehicle Penetration on Residential Distribution Grid Using Smart Charging Strategies," *Energies*, vol. 9, no. 12, Art. no. 12, Dec. 2016, doi: 10.3390/en9121024.

[101] B. Uzum, A. Onen, H. M. Hasanien, and S. M. Muyeen, "Rooftop Solar PV Penetration Impacts on Distribution Network and Further Growth Factors—A Comprehensive Review," *Electronics*, vol. 10, no. 1, Art. no. 1, Jan. 2021, doi: 10.3390/electronics10010055.

[102] C.-H. Lo and N. Ansari, "Alleviating Solar Energy Congestion in the Distribution Grid via Smart Metering Communications," *IEEE Trans Parallel Distrib Syst*, vol. 23, no. 9, pp. 1607-1620, Sep. 2012, doi: 10.1109/TPDS.2012.125.

[103] J. Zhao, Y. Wang, G. Song, P. Li, C. Wang, and J. Wu, "Congestion Management Method of Low-Voltage Active Distribution Networks Based on Distribution Locational Marginal Price," *IEEE Access*, vol. 7, pp. 32240-32255, 2019, doi: 10.1109/ACCESS.2019.2903210.

[104] P. Dahiwale and Z. Rather, "Congestion Management in High Solar PV Penetrated Distribution System using Smart Charging of Electric Vehicles," in *ISES Sol. World Congr. SWC 2023 Accept*, Publ.

[105] S. H. Dolatabadi, M. Ghorbanian, P. Siano, and N. D. Hatziargyriou, "An Enhanced IEEE 33 Bus Benchmark Test System for Distribution System Studies," *IEEE Trans Power Syst*, vol. 36, no. 3, pp. 2565-2572, May 2021, doi: 10.1109/TPWRS.2020.3038030.

[106] A. P. Nath and Z. Rather, "Design of Adaptive Control Scheme for Provision of Frequency Regulation Service from Electric Vehicle Fleet." IEEE, Grenoble, France.

[107] A. P. Nath and Z. Rather, "Application of Electric Vehicle Charging Station for Power Factor Correction of Industrial Load," in *7th E-Mobility Power System Integration Symposium (Accpeted for publication*, Copenhagen, Denmark: IEEE, 2023.

[108] UNESCO World Water Assessment Programme, "UN World Water Development Report 2022: Groundwater - Making the invisible visible," United Nations Educational, Scientific and Cultural Organization (UNESCO), 2022. Accessed: Aug. 13, 2023. [Online]. Available: https://unesdoc.unesco.org/ark:/48223/pf0000380721

[109] WHO, "Drinking-water," *World Healh Organization*, Mar. 21, 2022. https://www.who.int/news-room/fact-sheets/detail/drinking-water (accessed Aug. 13, 2023).

[110] "Sustainable Development Goals, Water and Sanitation." 2023. [Online]. Available: https://sdgs.un.org/goals/goal6,

[111] T. R. Lunel and D. R. Rousse, "PV pumping system: A Python package for modeling and sizing photovoltaic water pumping systems," *J. Open Source Softw.*, vol. 5, no. 54, p. 2637, 2020, doi: 10.21105/joss.02637.

[112] M. Aliyu, G. Hassan, S. A. Said, M. U. Siddiqui, A. T. Alawami, and I. M. Elamin, “A review of solar-powered water pumping systems,” *Renew. Sustain. Energy Rev.*, vol. 87, pp. 61–76, 2018, doi: 10.1016/j.rser.2018.02.010.
[113] A. Allouhi *et al.*, “PV water pumping systems for domestic uses in remote areas: Sizing process, simulation and economic evaluation,” *Renew. Energy*, vol. 132, pp. 798–812, 2019, doi: 10.1016/j.renene.2018.08.019.
[114] A. W. Kiprono and A. I. Llario, *Solar Pumping for Water Supply: Harnessing solar power in humanitarian and development*. Rugby, UK: Practical Action Publishing, 2020.
[115] E. Mboumboue and D. Njomo, “Potential contribution of renewables to the improvement of living conditions of poor rural households in developing countries: Cameroon’s case study,” *Renew. Sustain. Energy Rev.*, vol. 61, pp. 266–279, 2016, doi: 10.1016/j.rser.2016.04.003.
[116] S. Meunier *et al.*, “A validated model of a photovoltaic water pumping system for off-grid rural communities,” *Appl. Energy*, vol. 241, pp. 580–591, 2019, doi: 10.1016/j.apenergy.2019.03.035.
[117] S. R. Mantri, R. S. Kasibhatla, and V. K. B. Chennapragada, “Grid-connected vs. off-grid solar water pumping systems for agriculture in India: A comparative study,” in *Energy Sources, Part A: Recovery, Utilization, and Environmental Effects*, 2020, pp. 1–15. doi: 10.1080/15567036.2020.1745957.
[118] S. S. Chandel, M. N. Naik, and R. Chandel, “Review of solar photovoltaic water pumping system technology for irrigation and community drinking water supplies,” *Renew. Sustain. Energy Rev.*, vol. 49, pp. 1084–1099, 2015, doi: 10.1016/j.rser.2015.04.083.
[119] T. D. Short and M. A. Mueller, “Solar powered water pumps: problems, pitfalls and potential,” *2002 Int. Conf. Power Electron. Mach. Drives Conf Publ*, no. 487, pp. 280–285, Jun. 2002.
[120] B. H. Chowdhury, S. Ula, and K. Stokes, “Photovoltaic-powered water pumping-design, and implementation: case studies in Wyoming,” *IEEE Trans. Energy Convers.*, vol. 8, no. 4, pp. 646–652, 1993, doi: 10.1109/60.260976.
[121] A. Frenjo, A. Wogasso, and R. Rajesh, “Designing and developing solar energy operated water pump for small scale irrigation,” *Int J Chem Sci*, vol. 15, no. 4, p. 194, 2017.
[122] J. Brewer, D. P. Ames, D. Solan, R. Lee, and J. Carlisle, “Using GIS analytics and social preference data to evaluate utility-scale solar power site suitability,” *Renew. Energy*, vol. 81, pp. 825–836, 2015, doi: 10.1016/j.renene.2015.04.017.
[123] J. A. Prieto-Amparán, A. Pinedo-Alvarez, C. R. Morales-Nieto, M. C. Valles-Aragón, A. Álvarez-Holguín, and F. Villarreal-Guerrero, “A regional GIS-assisted multi-criteria evaluation of site-suitability for the development of solar farms,” *Land*, vol. 10, no. 2, p. 217, 2021, doi: 10.3390/land10020217.
[124] S. K. Saraswat, A. K. Digalwar, S. S. Yadav, and G. Kumar, “MCDM and GIS based modelling technique for assessment of solar and wind farm locations in India,” *Renew. Energy*, vol. 169, pp. 865–884, 2021, doi: 10.1016/j.renene.2021.01.056.
[125] S. Gualteros and D. R. Rousse, “Solar water pumping systems: A tool to assist in sizing and optimization,” *Sol. Energy*, vol. 225, pp. 382–398, 2021, doi: 10.1016/j.solener.2021.06.053.
[126] A. Mazloumi, A. Poolad, M. S. Mokhtari, M. B. Altman, A. Y. Abdelaziz, and M. Elsisi, “Optimal Sizing of a Photovoltaic Pumping System Integrated with Water Storage Tank Considering Cost/Reliability Assessment Using Enhanced Artificial Rabbits Optimization: A Case Study,” *Mathematics*, vol. 11, no. 2, p. 463, 2023, doi: 10.3390/math11020463.
[127] N. Argaw, R. Foster, and A. Ellis, “Renewable Energy for Water Pumping Applications In Rural Villages; Period of Performance.” 2003. doi: 10.2172/15004054.
[128] J. Sass and A. Hahn, *Solar Powered Irrigation Systems (SPIS*, Impacts. Economy: Technology, 2020.
[129] “Online Output, Fuzzy AHP Software.” 2023. [Online]. Available: http://www.onlineoutput.com/fuzzy-ahp-software/,

[130] M. Tahri *et al.*, “New Fuzzy-AHP Matlab based graphical user interface (GUI) for a broad range of users: Sample applications in the environmental field,” *Comput. Geosci.*, vol. 158, p. 104951, 2022, doi: 10.1016/j.cageo.2021.104951.
[131] V. C. Sontake and V. R. Kalamkar, “Solar photovoltaic water pumping system-A comprehensive review,” *Renew. Sustain. Energy Rev.*, vol. 59, pp. 1038–1067, 2016, doi: 10.1016/j.rser.2016.01.021.
[132] “Solar PV based Drinking Water Pumping Systems: Case Studies from Jawhar and Mokhada, Technology and Development Solutions Cell.” Center for Technology Alternatives for Rural Areas, Indian Institute of Technology Bombay, 2019. [Online]. Available: https://www.ctara.iitb.ac.in/en/system/files/A%20Case%20Study%20of%20Solar%20Powered%20Drinking%20Water%20Pumping%20Systems%20.pdf,
[133] G. S. Birdie and J. S. Birdie, *Water supply and sanitary engineering*. Dhanpat Rai, 2018.
[134] M. Abu-Aligah, “Design of Photovoltaic Water Pumping System and Compare it with Diesel Powered Pump,” *Jordan J. Mech. Ind. Eng.*, vol. 5, no. 3, 2011.
[135] S. M. Ibrahim, H. H. El-Ghetany, and A. G. Shabak, “Comprehensive design tool for sizing solar water pumping system in Egypt,” *Appl. Sol. Energy*, vol. 56, pp. 18–29, 2020, doi: 10.3103/S0003701X20010053.
[136] R. Sharma, S. Sharma, and S. Tiwari, “Design optimization of solar PV water pumping system,” *Mater. Today Proc.*, vol. 21, pp. 1673–1679, 2020, doi: 10.1016/j.matpr.2019.11.322.
[137] T. Kumari, L. Priyadarshini, A. Kumari, and R. K. Choudhary, “Water Requirement of Dairy Cattle,” *Indian Farmer*, vol. 3, no. 9, pp. 618–622, 2016.
[138] S. J. Phansalkar, “Livestock-water interaction: status and issues.” Vallabh Vidyanagar, Gujarat, India, 2006. [Online]. Available: https://publications.iwmi.org/pdf/H043949.pdf,
[139] J. J. Wagner and T. E. Engle, “Invited Review: Water consumption, and drinking behavior of beef cattle, and effects of water quality,” *Appl. Anim. Sci.*, vol. 37, no. 4, pp. 418–435, 2021, doi: 10.15232/aas.2021-02136.
[140] J. K. Paul and K. J. Clark, “Water quality and requirements for dairy cattle,” *Neb. Ext Anim*, 2017, [Online]. Available: https://extensionpublications.unl.edu/assets/html/g2292/build/g2292.htm,
[141] *Nutrient Requirements of Beef Cattle, 8th Revised Edition*. Washington, D.C.: National Academies Press, 2015. doi: 10.17226/19014.
[142] Z. Sen, *Solar energy fundamentals and modeling techniques: atmosphere, environment, climate change and renewable energy*. Springer Science & Business Media, 2008.
[143] S. Verma *et al.*, “Solar PV powered water pumping system–A review,” *Mater. Today Proc.*, vol. 46, pp. 5601–5606, 2021, doi: 10.1016/j.matpr.2020.09.434.